Indoor Localization of UHF RFID Tags

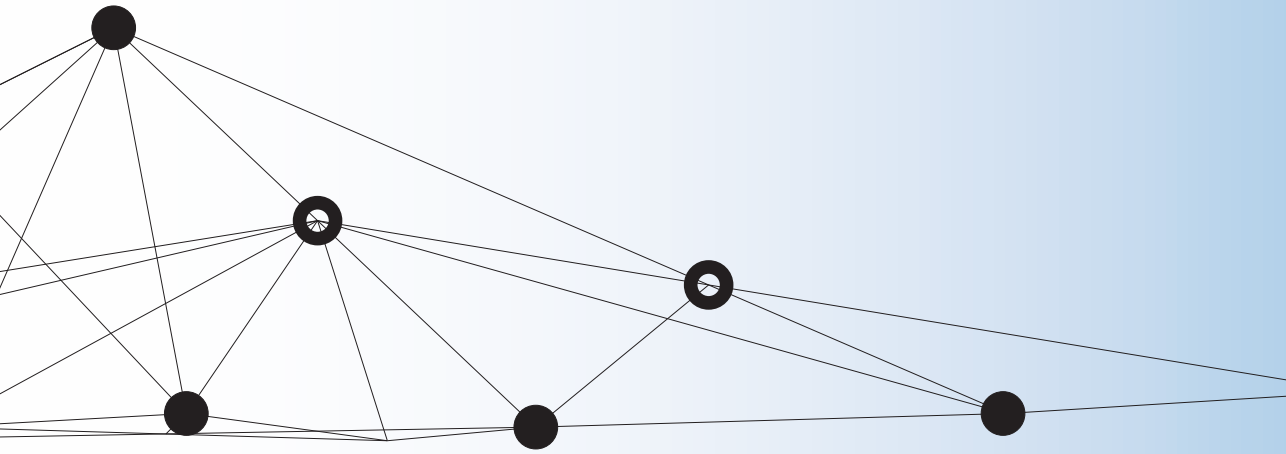

Jordy Huiting

Graduation committee:

Prof. dr. ir.	G. J. M. Smit	University of Twente (promotor)
Dr. ir.	A. B. J. Kokkeler	University of Twente (assistent-promotor)
Dr. ir.	M. J. Bentum	University of Twente
Prof. dr. ir.	R. N. J. Veldhuis	University of Twente
Prof. dr.	K. G. Langendoen	Delft University of Technology
Prof. dr. ir.	S. M. Heemstra de Groot	Eindhoven University of Technology
Dr.	P. J. Compaijen	Nedap N.V.
Prof. dr.	P. M. G. Apers	University of Twente (chairman and secretary)

UNIVERSITY OF TWENTE.

Faculty of Electrical Engineering, Mathematics and Computer Science, Computer Architecture for Embedded Systems (CAES) group

CTIT

CTIT Ph.D. Thesis Series No. 16-412
Centre for Telematics and Information Technology
PO Box 217, 7500 AE Enschede, The Netherlands

Gelderland & Overijssel
Gebundelde Innovatiekracht

The presented work was supported by the Dutch TSP project. The project has joint funding from the European Regional Developement Fund and the Dutch provinces of Gelderland and Overijssel.

This thesis was typeset using LaTeX, Ti*k*Z, and Inkscape.
Printed by Gildeprint, The Netherlands.

ISBN 978-90-365-4250-0
ISSN 1381-3617; CTIT Ph.D. Thesis Series No. 16-412
DOI 10.3990/1.9789036542500

INDOOR LOCALIZATION OF UHF RFID TAGS

Proefschrift

ter verkrijging van
de graad van doctor aan de Universiteit Twente,
op gezag van de rector magnificus,
prof. dr. T. T. M Palstra,
volgens besluit van het College voor Promoties
in het openbaar te verdedigen
op vrijdag 30 juni 2017 om 14.45 uur

door

Jordy Huiting

geboren op 6 oktober 1987
te Doetinchem

Dit proefschrift is goedgekeurd door:

Prof. dr. ir. G. J. M. Smit (promotor)
Dr. ir. A. B. J. Kokkeler (co-promotor)

ISBN 978-90-365-4250-0

Abstract

For many commercial applications it is of interest to identify and localize objects. The most traditional way of identifying objects is to use labels with a printed barcode and attach them to the objects of interest. However, these barcodes need direct line-of-sight between label and scanner, which can be a burden for some applications, for example when labeled products are packaged or the labels are integrated into objects.

When a Radio Frequency *(RF)* transceiver is attached to the object, identification can be done with the help of a wireless communication system and does not require line-of-sight. Technology that uses RF to identify objects is known as Radio Frequency Identification *(RFID)* and the objects are labeled with so-called RFID tags. Equipping tags with fully functional transceivers requires a lot of energy and therefore batteries, increasing size and cost. Technological advances have made it possible to produce tags without batteries, so-called passive tags, which can harvest energy from an incoming RF signal. The RF signal from the reader can also be used to transmit information from reader to tag. To communicate back to the reader, these passive RFID tags use backscattering. The antenna of a tag reflects a certain amount of the energy it receives. By modulating this reflection, tags are able to transmit information.

Many RFID systems have been developed. Long range (typically a couple of meters) and battery-less tags are best supported in the Ultra High Frequency *(UHF)* band. The industry standard protocol for passive UHF RFID tags became known as EPCglobal Class 1 Generation 2. Over the years, these Generation 2 tags have become very cheap (less than 10 cents) and are currently used commercially for a wide range of applications. These applications range from identifying cars that enter a parking garage to individual item level tracking of clothes in a retail supply chain, from the manufacturer right up to the counter of a shop. The advantage of non line-of-sight identification of tags can also be a disadvantage as tagged objects can be anywhere within the read range of the reader. For logistics companies tracking a parcel between distribution hubs, this coarse localization is not a problem. However, when tracking items that are moved from a storage room inside a shop to the shop floor, the ill-defined read range becomes problematic. The read range is difficult to model and to measure as UHF signals are susceptible to reflections, especially within an indoor environment with a lot of reflecting objects. A lot of research has been performed to determine the exact location of a tag, based on different signal characteristics like signal strength and phase.

This thesis describes possible solutions to the localization problem. By measuring the phase difference between the transmitted continuous wave and the received backscatter from the tag at different frequencies, it is possible to estimate the distance between the reader and the tag. By measuring the distance to three readers it is possible to determine the location of a tag with the help of trilateration. The locations of the readers have to be known and any error in the distance measurement influences the location estimate. To overcome the influence of the environment on the distance estimate, this thesis suggests the use of reference tags and the k-Nearest Neighbors *(KNN)* algorithm to derive a location. A localization experiment is done and our phase-based algorithm is compared with a KNN algorithm based on received signal strength. The results in terms of average localization error are similar, about 0.4 m. Furthermore, some experiments are used to determine whether the use of phase measurements for the detection of a moving tag in a portal application is viable. The results show that with state-of-the-art readers tags moving at walking speed cannot be read fast enough to track the phase. However, with improved readers that can scan the phase at least two times faster, tags that move at walking speed can be detected.

Multiple readers and reference tags are expensive to install in a commercial environment. Another approach is to use an array of multiple antennas, a so-called phased array. When a signal is received by two different antennas there will be a time delay between the signals dependent on the Direction of Arrival *(DOA)* of the signal. If we assume that the signals under investigation are narrowband, this time difference becomes a phase difference, hence the name phased array. So, by measuring the phase differences between antennas, the DOA can be determined. In case of two antennas the phase difference translates directly into a DOA. For an array with more antennas the MUSIC or ESPRIT algorithm can be used to estimate the DOA. The observation that a tag is within the near field of a phased array leads to the fact that there is an extra phase difference depending on the distance of the tag to the array. This distance can be estimated with the help of 2-dimensional estimation algorithms. Experiments are used to validate this approach in a real environment. An average angle error of 3 to 4 degrees and a range error in the order of 0.3 m is measured. This range error is comparable to the 0.4 m achieved by the setup described before. Differences with measurements in an anechoic room show that the performance of the system heavily depends on the environment, as the average errors decrease to 1 degree and 0.2 m, respectively.

By combining DOA measurements from multiple phased arrays and the help of trilateration, a location estimate can be made. To decrease the energy consumption of a multi-array system, this thesis explores the use of heavily quantized signals instead of the high resolution signals used in the near field experiments. The DOA estimation algorithms are based on correlations between the different array channels. By using single bit quantized signals, errors are introduced in these correlations, which can be corrected by making some assumptions about the shape of the received signals. Experiments in an anechoic room show that the suggested correction can decrease the average error of single-bit quantized signals from 4 de-

grees back to the unquantized average error of 1 degree. Experiments in a realistic environment show that by using single-bit quantized signals, the DOA estimation degrades from 4 to 6 degrees. If this increase in error is permissible for the application, it is possible to construct an array to estimate the DOA without the need for high resolution Analog-to-Digital Converters *(ADCs)*, which saves on computational cost and power.

Overall, this thesis shows that there are many options to localize Generation 2 tags. However, due to the complex environment with severe multipath effects, localization of Generation 2 tags still remains an open problem.

Samenvatting

Het is voor commerciële toepassingen interessant om objecten te kunnen identificeren en lokaliseren. De meest traditionele manier om objecten te labelen is met stickers die voorzien zijn van een streepjescode. Deze streepjescodes hebben echter het nadeel dat een lezer onbelemmerd zicht op de code moet hebben om deze te kunnen lezen. Dit kan voor sommige toepassingen erg onhandig zijn.

Wanneer een draadloze communicatiemodule bevestigd wordt aan een object, kan dit object geïdentificeerd worden met behulp van draadloze communicatie. Het is dan niet langer nodig om een directe zichtlijn te hebben. Identificatie met behulp van radiogolven (Radio Frequency *(RF)*) is ook wel bekend onder de naam Radio Frequency Identification *(RFID)*. En de labels die aan een object worden vastgemaakt, worden RFID tags genoemd. Een echte draadloze zender zou veel energie verbruiken en zal daarom een batterij nodig hebben, waardoor een tag relatief groot en kostbaar zal worden. Technologische ontwikkelingen hebben het echter mogelijk gemaakt om tags te ontwikkelen die door het aanwezige elektromagnetische veld dat verzonden wordt door een lezer, voorzien worden van energie. Om informatie van de tag terug te sturen naar de lezer wordt er geen gebruik gemaakt van een zender, maar om energie te besparen wordt het 'backscatter' principe gebruikt. Een tag moduleert de informatie door zijn antenne meer of minder te laten reflecteren. Een lezer kan dit verschil in reflectie opmerken en demoduleren.

Er zijn verschillende RFID systemen ontwikkeld die gebruik maken van verschillende frequenties. Met de huidige technologie kan alleen in de Ultra High Frequency *(UHF)* frequentieband een systeem gemaakt worden dat werkt zonder batterijen en kan communiceren over een aantal meters. De meest gebruikte standaard is EPCglobal Class 1 Generation 2. In de loop der jaren zijn deze tags goedkoper geworden en worden de tags commercieel veel toegepast. Toepassingen zijn onder andere het identificeren van auto's die een parkeergarage binnengaan en het volgen van kleding van de fabrikant tot het moment dat de kleding de toonbank over gaat. Het voordeel dat RFID tags geen zichtlijn nodig hebben kan ook een nadeel zijn. Wanneer een getagged object geïdentificeerd wordt door een lezer, is het bekend dat het object zich ergens binnen het leesgebied bevindt. Voor bedrijven die pakketjes volgen van stad naar stad is dit geen probleem. Echter, dit moelijk te definiëren leesgebied wordt bijvoorbeeld een probleem wanneer een kledingstuk getraceerd moet worden op het moment dat het wordt verplaatst van de opslag in een kledingwinkel naar de winkel zelf. De uitdaging wordt gevormd doordat de UHF signalen goed reflecteren. Er is al veel onderzoek gedaan naar het lokaliseren van RFID tags met behulp van signaaleigenschappen zoals signaalsterkte en fase.

Dit proefschrift beschrijft een aantal mogelijke oplossingen voor dit lokalisatieprobleem. Door op verschillende frequenties de fase te meten tussen het verzonden signaal en de ontvangen backscatter, is het mogelijk om een afstand tussen de lezer en de tag te bepalen. Wanneer een afstand tussen een tag en lezer op drie plekken bepaald kan worden, kan met een standaard driehoeksmeting een locatie worden bepaald. De locaties van deze lezers moeten bekend zijn en elke afwijking in de afstandsbepaling beïnvloedt de uiteindelijke locatiebepaling. Om de invloed van de omgeving tegen te gaan, kunnen referentie tags, samen met het k-Nearest Neighbors *(KNN)* algoritme, gebruikt worden om de locatie te bepalen. Experimenten zijn gedaan en de resultaten worden vergeleken met locatiebepaling op basis van signaalsterkte. De resulaten in termen van gemiddelde lokalisatiefout zijn vergelijkbaar, 0,4 m. Verdere experimenten zijn uitgevoerd om uit te vinden of fase metingen gebruikt kunnen worden om een bewegende tag te detecteren. De resultaten laten zien dat een tag die door een persoon op loopsnelheid bewogen wordt niet snel genoeg gelezen kan worden om de fase te kunnen volgen.

Het gebruik van referentietags is echter onwenselijk, zeker in een commerciële omgeving. Een andere oplossing zou zijn om een zogenaamd phased array te gebruiken. Wanneer een signaal ontvangen wordt door twee verschillende antennes zal er een tijdsverschil ontstaan, doordat de antennes zich op verschillende plekken in de ruimte bevinden. Wanneer we aannemen dat de signalen van een tag een kleine bandbreedte hebben, kunnen deze tijdsverschillen opgevat worden als faseverschillen. In het geval van twee antennes kan een faseverschil direct omgezet worden in een hoekschatting. Voor een antenne array met meerdere antennes kan met bijvoorbeeld het MUSIC of ESPRIT algoritme een hoek worden geschat. Omdat een tag zich al snel in het nabije veld van een array bevindt, zou het mogelijk moeten zijn om niet alleen de hoek, maar ook de afstand ten opzichte van de array te schatten. Experimenten zijn gedaan om deze benadering te onderzoeken en leiden tot een gemiddelde fout in de hoekschatting van 3 tot 4 graden en een gemiddelde van 0,3 m in de afstandsschatting. Metingen in een anechoïsche kamer laten zien dat de omgeving veel invloed heeft op de gemaakte afstandsschattingen. Daarom wordt er gekeken naar een combinatie van meerdere hoekschattingen. Om het energieverbruik van een systeem met meerdere arrays te beperken wordt er gekeken naar het effect van het gebruik van sterk gekwantiseerde in plaats van hoge resolutie signalen. De hoekschattingsalgoritmes zijn gebaseerd op correlaties tussen de verschillende antenne kanalen. Door één-bits kwantisatie toe te passen worden er fouten geïntroduceerd in de correlaties. Deze fouten kunnen gecorrigeerd worden door aannames te doen over binnenkomende signalen. Experimenten tonen aan dat de hoekschatting slechts verslechtert van 4 naar 6 graden, zonder de voorgestelde correctie. Wanneer de toepassing deze verhoging van de gemiddelde fout toestaat, is het mogelijk om een array van antennes te bouwen zonder dat er hoge resolutie analoog-digitaalomzetters nodig zijn.

Concluderend, dit proefschrift laat zien dat er mogelijkheden zijn om Generation 2 tags te lokaliseren. Echter, door de complexe omgeving met sterke reflecties, is de lokalisatie van Generation 2 tags nog een open probleem.

Dankwoord

Na vier en een half jaar ligt hij dan eindelijk voor jullie: mijn proefschrift.

Voor buitenstaanders is het niet altijd duidelijk wat de taak van een promovendus is. Je staat niet voor de klas, en nee, op een universiteit worden ook geen producten gemaakt. Een bijdrage aan de wetenschap, dat is het uiteindelijke resultaat. Ik had dit niet gekund zonder de juiste mensen om mij heen. Graag wil ik iedereen bedanken die mij de afgelopen jaren heeft gesteund.

Allereerst wil ik Gerard en André bedanken voor het eindeloos doorlezen van mijn teksten en aanhoren van ideeën. Wanneer experimenten weer eens compleet andere resultaten gaven dan verwacht, wist Gerard het op onze woensdagochtend meeting altijd anders te bekijken. Deze spontaniteit zit hem in het bloed. Zo herinner ik me een TSP uitje waarbij hij in pak een koeienstal in dook om een kalfje te redden. De discussies met André zorgden vaak voor nieuwe ideeën en hebben er voor gezorgd dat mijn verhaal kloppend werd opgeschreven.

Na vele mooie jaren zit mijn tijd bij CAES er nu echt op. Mijn eerste ervaring met CAES was al tijdens het MDDP project, onder begeleiding van Koen. Met het bouwen van een slecht werkende radio werd mijn interesse voor signaalverwerking gewekt. Daarna heb ik mijn masteronderzoek met betrekking tot onderwater communicatie bij jullie mogen uitvoeren onder begeleiding van Koen en André. Ik wil de hele groep bedanken voor de leuke tijd bij CAES, waar het altijd gezellig is tijdens de koffiepauzes, maar waarvan ik er jammer genoeg de laatste tijd veel heb moeten missen. Verder staat CAES bekend om de traditionele lunchwandeling die altijd doorgaat, zelfs midden in de winter. CAES is natuurlijk niet compleet zonder de secretaresses Marlous, Nicole en Thelma, bedankt voor de hulp met de nodige papierwinkel.

De meeste tijd bij CAES heb ik samen met kamergenoot Tom doorgebracht. Vele onderwerpen hebben we besproken, van onze gedeelde voorliefde voor Duits gereedschap tot de problemen met naamgenoot TOM, het nieuwe onderwijssysteem. Waar ik Tom hielp met het importeren van een kettingzaag uit Australië, stond Tom altijd klaar om te helpen met het compleet strippen van panden in Nieuwegein. After Tom left I was a bit lost, however, my new roommate Siavash put me back on track again. Siavash, I loved the discussions we had about the differences and similarities in our cultures.

Onze kamer hebben we vaak gedeeld met studenten. Mark, Idzard, Jippe, Thomas en Chris, wat hebben jullie toch je best gedaan om een werkende FPGA imple-

mentatie te maken, alhoewel ik nog steeds niet weet of het helemaal gelukt is. De masterstudenten Rembrand en Yoppy waren meer succesvol. De metingen die jullie gedaan hebben, heb ik tot in den treure door Matlab gehaald.

Na zijn master was Rembrand zelfs zo onder de indruk van RFID dat hij er bij Nedap zijn werk van heeft gemaakt. Mede hierdoor zorgden Hubert en Rembrand voor een prettige samenwerking, ook buiten het TSP project om.

Naast mijn promotietraject heb ik aan een aantal hobby projectjes gewerkt. Veelal met sponsoring van Gerard en Jeannette. Vaak hadden jullie geen idee wat ik nu weer bedacht had, maar stonden me toch toe het uit te voeren. Ik wil jullie bedanken voor het vertrouwen. Het heeft misschien (te)veel tijd gekost, maar, ter info Tom, de machine is nu (bijna) af.

Wesley heb ik leren kennen tijdens de introductieweken in 2006. Samen zijn we zwemmend en ontdekkend onze tijd op de universiteit begonnen en goed doorgekomen. Na onze master zijn Wesley en ik beiden gaan promoveren, maar we bleven er heel bescheiden onder. Zo bestonden onze uitjes vaak uit niets meer dan een gratis kopje koffie bij de IKEA. Nu ik naar de andere kant van het land ga, zullen de wekelijkse UT-koffie-momentjes wel gemist worden.

Ik wil mijn ouders bedanken voor de steun in al die jaren. Voor jullie was ik nog steeds aan het studeren, ook al beweerde ik zelf van niet. Hierbij bied ik mijn excuses aan voor al die keren dat ik niet op tijd was voor het eten. Al die jaren hebben jullie voor mij klaar gestaan, ik wil jullie bedanken voor de vrijheid en ondersteuning die jullie altijd geboden hebben. Mijn liefste zusje Esther, op dit moment ben je alweer lang terug van vakantie, of was het toch een reis? Bedankt voor het corrigeren van mijn samenvatting, al mag je het de volgende keer pas lezen wanneer het af is. We lijken totaal niet op elkaar, maar we hebben in ieder geval een ding gemeen: we worden allebei dokter, alleen schrijf je het bij mij iets anders.

Marlies, bedankt voor alle hulp, zeker in de laatste maanden. Nu ziet het er toch echt naar uit dat ook jij moet gaan promoveren, of je zult moeten leren leven met het feit dat ik een extra titel heb. Na 9 jaar gaan we dan eindelijk samenwonen, ik hoop dat ik de grote stad overleef...

Jordy
Enschede, januari 2017

Contents

1 Introduction **1**

1.1 Readers and Tags . . . 1
1.2 History of Backscattering . . . 2
1.2.1 UHF . . . 3
1.3 UHF RFID Standards . . . 4
1.4 Localization of RFID tags . . . 5
1.5 Problem Statement . . . 6
1.6 Outline . . . 6

2 EPCglobal Class 1 Generation 2 UHF RFID Tags **9**

2.1 EPC Generation 2 . . . 10
2.1.1 Reader-to-Tag . . . 10
2.1.2 Tag-to-Reader . . . 11
2.1.3 Narrowband Signal . . . 13
2.1.4 Medium Access Control Protocol . . . 13
2.1.5 Reception of Backscatter . . . 14
2.1.6 Link Budget . . . 17
2.2 Conclusion . . . 19

3 Existing Localization Methods **21**

3.1 Introduction . . . 21
3.2 Distance to a Single Reader . . . 22
3.2.1 Signal Strength . . . 22
3.2.2 Phase . . . 23
3.2.3 Direct Sequence Spread Spectrum . . . 25
3.2.4 Ultra-WideBand . . . 26
3.3 Direction to a Single Reader . . . 27
3.3.1 Phased Array . . . 27
3.4 Multiple Readers . . . 29
3.5 Conclusion . . . 30

4 Multi Reader Localization **33**

4.1 Introduction . . . 33
4.2 Ranging . . . 36
4.3 K-Nearest Neighbors Algorithm . . . 37
4.4 Experiments . . . 39
4.4.1 Distance . . . 39
4.4.2 Location . . . 44
4.5 Movement Detection . . . 47
4.5.1 Simulation . . . 47
4.5.2 Experiment . . . 50
4.6 Conclusion . . . 52

5 Near Field Localization **55**

5.1 Introduction . . . 55
5.2 Phased Array . . . 57
5.3 Signal Model . . . 58
5.4 2D Range and DOA Estimation . . . 61
5.4.1 MUSIC Algorithm . . . 61
5.4.2 ESPRIT Algorithm . . . 62
5.5 Simulations . . . 62
5.5.1 2D ESPRIT . . . 65
5.5.2 Influence of Antenna Pattern . . . 65
5.6 Experiments . . . 68
5.6.1 Automated Test Setup . . . 68
5.6.2 RMSE . . . 70
5.6.3 One- and Two-Dimensional MUSIC . . . 70
5.6.4 Angle-Dependent Calibration . . . 73
5.6.5 2D ESPRIT . . . 78
5.7 Conclusion . . . 80

6 Using Phased Arrays with Low Resolution ADCs **81**

6.1 System Decomposition . . . 83
6.1.1 Proposed System . . . 84
6.2 Far Field Estimation and a Near Field Model . . . 85
6.3 Correlation . . . 86
6.4 Quantization . . . 88
6.5 Quantization of a Square Wave . . . 89
6.5.1 Different Phase . . . 92

6.5.2 *Equal Phase* . . . 93
6.5.3 *Relation to Correlation Coefficient* . . . 93
6.5.4 *Correction* . . . 94
6.6 Simulation . . . 96
6.7 Experiments . . . 96
6.8 2D Localization . . . 101
6.9 Conclusion . . . 103

7 Conclusion and Recommendations 105
7.1 Contributions . . . 107
7.2 Recommendations . . . 107

A (2D) MUSIC 109
A.1 Scanning over the Noise Subspace . . . 111

B (2D) ESPRIT 113

Acronyms 115

Bibliography 117

List of Publications 125

1

Introduction

To know where you are, has always been useful to mankind. Already in Homer's Odyssey the process of using the stars to navigate the oceans is described. The light from the stars is used by sailors to determine their own location. If we fast forward to modern times, we have artificial stars, satellites, to help us navigate the oceans. With these systems, for example the Global Positioning System *(GPS)*, a receiver is able to accurately estimate its own location based on signals coming from the satellites.

In many cases the location of a receiver is used as location estimate for the location of an object. For example, ships, cars or people in case of GPS receivers. A shipping container can for example be tracked by a shipping company with the help of a GPS receiver and some kind of transmitter to send the position information to a central control room. To be able to discriminate between containers, the transmitter does not only transmit a location estimate, but also some identification information. With technological advances it becomes possible to develop smaller receivers which can be attached to smaller objects.

An electronic system that can be attached to an object and used for wireless identification is also known as a Radio Frequency Identification *(RFID)* tag and information transmitted by a tag is received by an RFID reader.

1.1 Readers and Tags

An RFID system is usually used to identify objects. Objects can range from animals to shipping containers. To be able to identify an object, often tags are attached to the object. This can be done via tags containing a barcode, but in the case of RFID we attach so-called RFID tags to the objects to make them identifiable with the help of radio frequency. These tags come in many different types. Tiny glass encapsulated battery-less tags can be implanted and are used for animal identification, while battery-powered tags might be used to track shipping containers. RFID tags consist of antennas and electronics to allow communication and power can be provided by (RF) harvesting or other mechanisms like batteries. Next to the tags,

Figure 1.1 – Passive RFID tag consisting of antenna and IC

we define a reader as the device that is used to receive the identification information from the tag. This device can be connected to other systems that make use of the identification.

Identification over radio frequency can be done with a normal transmitter and receiver. Almost all wireless communication devices have some identification built-in to let the receiving party know who is transmitting. For example, in the case of wifi, a laptop transmits a Medium Access Control *(MAC)* address to the access point which is used as identification. A small wireless radio, often also known as the tag, can be battery powered and attached to an item that needs to be tracked. Such a system is called an active RFID system because the tag is able to (actively) transmit radio waves to a reader.

Besides active transmitting, it is also possible to exchange data by modulating the radio waves reflected by the tag's antenna. This process, called backscattering is described in the following section. With the help of this approach, one is able to save on transmission hardware and power usage. When a tag is battery powered and uses backscattering to communicate with the reader, it is called a semi-passive tag.

Tags can also be constructed to harvest energy from a continuous wave transmitted by the reader. In this case the tag is called passive and does not need batteries. This is a huge advantage, because passive tags can be made small and at low-cost. Passive tags can currently be bought for less than nine Eurocents[1]. Figure 1.1 shows an example passive RFID tag, the size of this UPM web tag is 34 x 54 mm. The largest part of this tag consists of the antenna. In the middle the very small Integrated Circuit *(IC)* can be seen.

1.2 History of Backscattering

As with many commercial technologies, the creation of RFID technology is the result of inventions and challenges in the military domain. Radar systems were invented in the early 1900s and in use by all parties at the start of the second world war. Radar systems operate by transmitting a powerful radio signal into a certain

direction. If the signal reaches a large object, an airplane for example, some of the signal power reflects back. This reflection is received by a ground station and a range is estimated based on the time difference between transmitting the signal and receiving the reflected signal.

The reflection of a signal by an object is often not in one direction. Due to the reflections in multiple directions, the signal is said to be backscattered by the object. Some of the scattered signal is reflected back in the direction of the transmitter and can be received by a receiver attached to the transmitter. RFID tags that are said to use backscatter to communicate with a reader, base their communication on this principle: a transmitted radio signal can be reflected by the antenna of a tag which can be received by a reader. By changing the impedance that is connected to the antenna of a tag, the amount of signal that is reflected can be changed. By modulating the impedance, a tag is able to backscatter information. A sensitive reader might be able to receive this information. In Chapter 2 backscatter communication is presented in more detail.

Not only the backscatter principle of communication finds its origin in radar technology. Also a solution to the need for identification with radio signals originates from radar systems. With the help of radar systems all parties in the second world war were able to detect aircrafts in the sky. However, a radar system does not tell whether a detected aircraft is an enemy fighter or a friendly bomber returning to base. In 1939 an Identification Friend or Foe *(IFF)* system was developed in the United Kingdom to be able to recognize a friendly aircraft. Upon reception of radar waves, a system on board the aircraft would transmit a modulated signal on the same frequency. Because the transmit signal is generated on board, it is relatively strong compared to the radar signal reflected by the aircraft. Therefore the transmitted signal will show up on the screen of the radar operator as a modulation of the signal strength. This modulation is hopefully identified as friendly by an operator[17].

1.2.1 UHF

There are roughly three frequency bands where typical RFID tags operate: LF, HF and UHF. In the Low Frequency *(LF)* band, tags can be found that operate on a frequency of 125 kHz. The read range is usually smaller than 50 cm and this frequency band allows for operation in the vicinity of water and metal. These tags are mainly used for animal identification and (building) access control[24].

In the High Frequency *(HF)* band other access control tags can be found. These systems use a frequency of 13.56 MHz and have a slightly larger read range than LF tags. The main advantage over the LF tags is the increased data rate that is possible due to the increased carrier frequency. Both LF and HF RFID systems make use of inductive coupling between two coils: the reader coil and the tag coil. Such a system can be seen as a transformer where a tag modulates the load on its coil which is immediately seen as a load change on the coil of the reader. Due to the limited range of passive LF and HF tags, these tags are only suitable for short range

localization up to 50 cm. For active tags, these low frequencies can be used for localization by making use of active transmitters[81].

In contrast to the RFID systems that operate in the LF and HF bands, systems in the Ultra High Frequency *(UHF)* band are based on radiative or electromagnetic coupling. In these UHF systems, antennas are matched to the carrier frequency and transmit (or backscatter) electromagnetic waves that can be received by another antenna. In the UHF band, two small frequency bands can be distinguished. In the 2.4 GHz band, tags are usually active and therefore have a large read range, because traditional wireless communication is used instead of backscatter. A typical application is toll collection.

In the lower part of the UHF band tags operate at a frequency of 860-960 MHz. In this range tags can harvest enough energy to create completely passive tags. Furthermore, the read range can be much larger than for HF tags (several meters) and the higher carrier frequency allows for a larger bandwidth which result in a higher data rate, which is useful for identification purposes. Because passive UHF RFID Generation 2 tags are so ubiquitous, this thesis focuses on the localization of these tags.

1.3 UHF RFID Standards

In the lower part of the UHF band, the first passive RFID systems were developed in the early 1990s[56]. At that time, the developed technology could not be commercialized and further research only took off when Intermec acquired the rights and patents in the late 1990s[74].

One of the main foreseen business applications was the use of these passive tags in supply chain management. Products could be tagged once and followed along the entire supply chain. Producers of tags and readers knew that to achieve this goal, interoperability between different brands would be necessary. Therefore, in 1999, several universities and large multinationals setup the so-called Auto-ID Center at the Massachusetts Institute of Technology. In October 2003 this center was replaced by a research network consisting of Auto-ID labs at different universities around the world. The standards these labs developed are managed by an organization called EPCglobal[36]. Several different versions of passive UHF RFID tags were developed by the Auto-ID labs. The most successful version is known as the EPCglobal Class 1 Generation 2 protocol (in short EPC Generation 2).

Today EPC Generation 2 tags are not only used for supply chain management by many large multinationals, but are also used for toll collection and baggage tracking[24]. Due to the UHF band, they have a read range of several meters and can be made entirely passive.

In case of a retail environment, every individual item has a unique tag attached to it in contrast to barcodes, which are often used to describe product groups. Individual identification allows every item to be tracked along the supply chain. Starting

from the manufacturer, an item can be tracked to distribution warehouses where items might be packed together into boxes. Ideally a system can identify all individual items in a box in a split second when they arrive at the warehouse. Upon departure from the warehouse to a retail store all items have to be identified again. A typical retail store has a stockroom where products arrive and have to be identified. From this stockroom multiple items can be moved to the store itself. Then, when a customer wants to buy an item, the tag can be used to identify the individual product. When an item leaves the shop without being sold, the tag could be used as anti-theft measure. To be able to have all kinds of retail items tagged, even items that have a low value, the RFID tags have to be low cost and small in size. To meet all these demands, UHF tags have been developed. To maintain interoperability with all tags available, one of the goals of this thesis is to design a localization system that uses standard Generation 2 tags. In Chapter 2 an overview of the Generation 2 protocol is given.

1.4 Localization of RFID tags

Indoor localization of tagged objects has received considerable research attention and numerous systems have been suggested, Chapter 3 describes work related to localization of passive tags in more depth. In the most basic form, the presence of a tag near a reader can be used as a location estimate. To get a more precise estimate, different signal properties are used to estimate the range or angle of a tag. In general a stronger signal received by a reader is an indication for a closer distance to a reader. Based on the signal strength, attempts are made to determine the range to a tag[25].

Other range estimation techniques make use of a large bandwidth to counteract reflections, which are present in indoor environments. These techniques are known as Ultra-WideBand *(UWB)*[7]. With the help of a large bandwidth reflections can be detected and a time-of-flight can be measured, which is a direct measure for the distance. Furthermore, a distance difference of a tag will lead to a phase difference at the reader, therefore the observed phase of the received signal can be used to make ambiguous range estimations[91].

Next to range estimation, techniques are developed to determine the angle of arrival of the electromagnetic wave between a reader and tag. Rotating antennas can be used to determine the angle where a signal is the strongest[58]. Furthermore, phased arrays can be use to determine an angle[11].

However, these existing systems have serious drawbacks. Some systems use active transmitters which require batteries that have to be replaced and increase cost, certainly when compared with passive tags. Others use UWB techniques which require special hardware, for example antennas and a wideband frontend, to be able to estimate a location. In Chapter 3 an overview of localization techniques is given.

1.5 Problem Statement

The holy grail is to find a long-range localization system that uses low-cost battery-less passive tags. Of course such a system should operate under all conditions and should have only a very small error. The most obvious choice is to use tags that operate in the lower part of the UHF band, because with currently available antennas and IC design techniques, these tags can be designed in such a way that they function without batteries and still have a relatively large read range at low cost.

However, the environment in which these tags operate is not ideal. Reflections from floors, walls and furniture will complicate the localization process. Another complicating factor is that in the UHF frequency band only a very small band is reserved for unlicensed use. Therefore, the localization systems have to operate under these narrowband restrictions set by the regulatory bodies.

EPC Generation 2 tags can be low-cost, battery-less and have a relatively long read range. Therefore, accurate localization systems based on these tags are extensively studied in literature. However, a clear answer has yet to be found. Nevertheless, because the use of EPC Generation 2 tags is widespread, a localization system based on these tags remains attractive.

The goal of this thesis is defined as: *The development of a low-cost localization system for EPC Generation 2 tags, that is able to estimate the location of RFID tags in typical indoor environments.*

Such a system should fulfill the following requirements:

R1	*Accurate*	Localize tags with an accuracy of 50cm.
R2	*Reliable*	Reliable location estimates have to be made, even in difficult indoor environments.
R3	*Low-cost*	Cost should be minimized in terms of hardware, system and computational cost.
R4	*Fast*	The system is able to determine the location of hundreds of tags per second.
R5	*Bandwidth*	The system follows regulatory restrictions on bandwidth and transmitted power.

1.6 Outline

The properties of the EPC Generation 2 protocol that are relevant for a localization system, are explained in Chapter 2. An overview of systems that were developed previously for the localization of EPC Generation 2 tags is given in Chapter 3.

Chapters 4 to 6 each introduce a new localization technique for EPC Generation 2 tags. Based on [JH:1] a multi reader platform is used to localize tags with the help of reference tags within a measurement zone, whereby phase-based ranging is compared with a ranging method where the Received Signal Strength Indicator

(RSSI) is used as input for the localization algorithm. The performance of the proposed phase-based algorithm is similar to the traditional method based on signal strength.

Based on [JH:2], in Chapter 5 we introduce a phased array system and use it to determine the range and direction of a tag and hence the location within a two dimensional plane. This approach is valid because the measurements take place within the near field of the array. Experiments in two normal rooms and an anechoic room show that range estimation is possible, however, the environment introduces a lot of errors.

In Chapter 6, the use of a phased array based on low precision Analog-to-Digital Converters *(ADCs)* is investigated. The results show that extreme (single-bit) quantization increases the average error. However, the increase is relatively small for normal rooms and can be corrected by a correction algorithm[JH:3].

Finally, in Chapter 7, some conclusions are given and recommendations for future work are described.

2

EPCglobal Class 1 Generation 2 UHF RFID Tags

Abstract – *With current technology the only frequency band that can sustain passive, long range RFID tags is the UHF band. Several competing standards have been developed. However, the industry standard known as the EPCGlobal Class 1 Generation 2 protocol has become the dominant protocol. To be able to localize these tags based on the signals, a tag and reader exchange, this chapter investigates the signal transmitted by the reader and the signal that is backscattered by the tag. Besides the link budget, describing the signal levels received by Generation 2 reader, some protocol characteristics are explained, all of which form the basis for localization algorithms.*

The development of passive RFID tags started in the 1980s with the first passive RFID tags that started backscattering their identification code as soon as they received enough power to do so. In these kinds of system, a reader would only have to transmit a continuous wave and listen for tag responses. This setup is also known as 'tag-talks-first'. This system leads immediately to problems when there is more than one tag powered on at the same time. In some circumstances the tags transmit a signal simultaneously causing collisions. The solution to this problem is to have a 'reader-talks-first' setup. In this case, a defined protocol between a reader and tag has to make sure that only a single tag is read at a time. Numerous solutions were developed by different organizations.

A group of universities and organizations like GS1, controlling the distribution of traditional barcodes, foresaw the application of RFID tags to identify products down to an individual item. In 2003 they setup an organization to standardize UHF RFID technology called EPCglobal and introduced the term Electronic Product Code *(EPC)*. This code is meant to be used as an identification code for individual products and can be used on barcodes or stored in RFID tags. This organization

defined the EPCglobal Class 1 Generation 2 protocol for UHF RFID tags, which eventually became an ISO standard: ISO 18000-6C[48].

2.1 EPC Generation 2

The EPC Generation 2 protocol describes the use of the UHF band to communicate with tags. The exact frequency is dependent on the regulatory bodies of countries. Two commonly used frequency bands are 865.6- to 867.6-MHz in European Telecommunications Standards Institute *(ETSI)* territory and 902- to 928-MHz under Federal Communications Commission *(FCC)* regulations. Tags are usually able to operate on all of the globally used frequencies[3]. The bandwidth available, 2 and 26 MHz, for UHF RFID tags is significantly different depending on the location where the system is used. The small bandwidth available in Europe, leads to strict spectral demands for communication protocols.

As mentioned before, a system where multiple tags can be present within the read range of a reader, has to use a 'reader-talks-first' protocol. A scheme that is also implemented by EPC Generation 2 tags. By transmitting a continuous wave the reader powers on all tags within range. The reader transmits data to the tags and (hopefully) a single tag is selected. Which can then respond to further commands from the reader.

A tag has to be low-cost. Therefore, the systems use amplitude modulation of a continuous wave to transmit communication parameters to the tags and start a new round of the defined interrogation protocol. Because a passive tag is also powered by the wave transmitted by a reader, measures have to be taken to prevent the tag from running out of power. Assuming amplitude modulation and modulating a '0' as a low value/off-state, a reader might switch off the continuous wave for multiple symbols in case of many repeating '0's. During this period a tag is not able to harvest power and might run out of power, something which is undesirable as a tag needs power to be able to process the received data. To solve this problem, the protocol ensures that always some power is transmitted. The communication from the reader to tag differs from the communication from tag to reader. Therefore, we examine both in the following sections.

2.1.1 Reader-to-Tag

The reader is able to modulate the amplitude of the continuous wave. This amplitude modulation is used to transit binary data to the tag. Because a tag is depending on the power it can harvest from the same continuous wave, a modulation scheme is used whereby the carrier remains powered on at least half of the time. The data is said to be Pulse-Interval-Encoded *(PIE)*, meaning that the time interval used to transmit data is depending on the data itself. There is no fixed sample period, only a fixed time the continuous wave is switched off or attenuated to signal the end of a bit, known as the Pulsewidth *(PW)* duration. When a binary '0' is to be transmitted the reader switches on the continuous wave for a duration of PW after which the

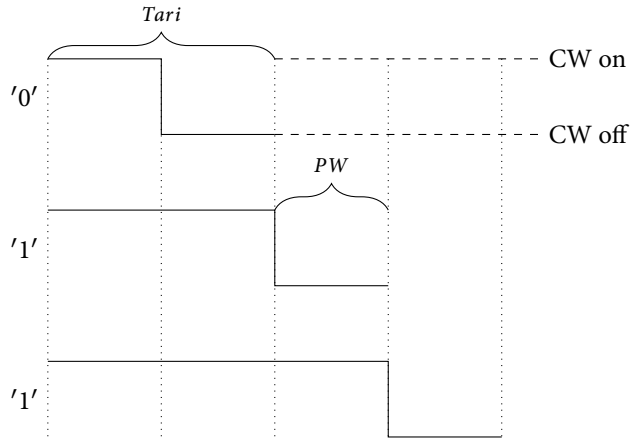

Figure 2.1 – Reader-to-tag protocol

continuous wave is switched off for another duration of PW. The total duration of this transmission is known as the Type A Reference Interval *(Tari)*. During transmission of a binary '1' the reader keeps the continuous wave on for a longer period of time. In the Generation 2 protocol this time is specified as a range between two and three times PW. A reader is free to use any value in between the two and three times PW. In Figure 2.1 the extreme options for transmitting a '1' and '0' are shown.

The duration of the Tari interval is not fixed either, but may be arbitrarily chosen from $6.25\mu s$ to $25\mu s$. Assuming only transmission of zeros, this gives a maximum data rate of $160kbs^{-1}$. Due to spectral demands set by regulator bodies, this data rate may have to be lowered. Furthermore, filtering might be necessary to achieve enough spectral efficiency to allow multiple readers interrogate tags at the same time in different frequency bands. Spectral efficiency is of particular concern in Europe as only four 200 kHz channels are defined in the limited 2 MHz band[32].

2.1.2 Tag-to-Reader

When the reader switches to listening mode it starts transmitting a continuous wave. This wave is received by the tag and used to harvest power. Furthermore, the tag is able to modulate the continuous wave from the reader, for example by switching the antenna from the normal power harvesting state to a shorted state. This changes the impedance of the antenna, which in turn changes the reflection characteristics of the antenna and the amount of signal that is scattered back.

A tag can use two different encoding schemes to transmit data to the reader. These techniques are known as FM0 and Miller-Modulated Subcarrier *(MMS)* encoding and are both based on modulation of a square wave signal with a period called

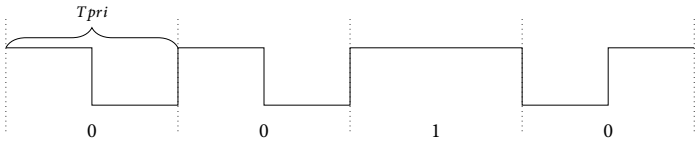

Figure 2.2 – FM0 encoding

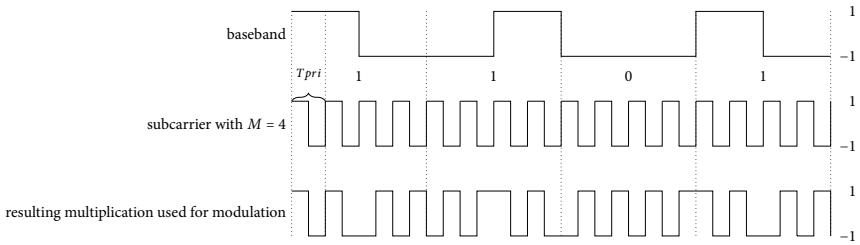

Figure 2.3 – Miller-Modulated Subcarrier (MMS) encoding

Backscatter-link pulse-repetition interval, often defined as Tpri. $\frac{1}{Tpri}$ is known as the Backscatter Link Frequency *(BLF)*. This frequency is set by the reader at the start of the interrogation round with a maximum of 640 kHz.

These encoding schemes are again used to prevent energy starvation of the tag. If the tag would have to transmit only one signal value, which happens to correspond with the short circuit state, the tag would run out of power and would not be able to transmit any more data.

In FM0 encoding, see Figure 2.2, the start of a new bit is marked by a dashed line. The tag always switches state when a new bit is to be transmitted. For a binary '0' the state is also changed in between, during the transmission of '1' symbol the state is kept constant.

The other encoding scheme is known as MMS, which uses the same approach, however, it encodes ones with a state change instead of zeros and vice versa. Furthermore, to limit spectral use, there is no state change when two consecutive ones are transmitted as there is already a state change during this symbol. This data encoding forms a kind of baseband signal that is then multiplied with M cycles of the BLF square wave, also known the as subcarrier. M is set by the reader during initialization and can be 2, 4 or 8. Different combinations of BLF and M can be used to achieve specific spectral properties and/or make a trade-off between data rate and Signal-to-Noise Ratio *(SNR)*, related to a certain Bit Error Rate *(BER)*. In Figure 2.3 a graphical overview of this encoding is shown.

2.1.3 Narrowband Signal

The signal transmitted by a tag has a certain bandwidth due to the chosen communication parameters. The highest BLF of 640 kHz with FM0 modulation gives a bitrate of 640 kb/s. The FM0 modulation differs from standard Binary Phase Shift Keying *(BPSK)*, because one symbol period is longer than the other. However the behavior is similar to standard BPSK; the maximum bitrate leads to an unfiltered spectral mainlobe with a width of 1.2 MHz[41].

If the bandwidth of a signal is small compared to the carrier frequency, the signal is said to be narrowband, a property which is often used for localization principles as time differences can be approximated with phase differences.

By definition, the Fractional Bandwidth *(FB)* is the ratio of the signal bandwidth, BW, to the center carrier frequency (f) as follows:

$$\text{FB} = \frac{\text{BW}}{f} \cdot 100\% \tag{2.1}$$

In case the FB is smaller than 1%, the signal is said to be narrowband[5]. Therefore, the EPC Generation 2 signal can be classified as narrowband as even with maximum data-rate the signal fulfills the definition: $\frac{1.2Mhz}{865Mhz} \cdot 100\% \approx 0.14\%$.

2.1.4 Medium Access Control Protocol

To be able to estimate a location based on a signal transmitted by an RFID tag, it is necessary for the tag to transmit at least something. As explained before, EPC Generation 2 tags do not transmit directly upon receiving power, but need to be instructed by a reader to do so. Furthermore, it is important to have only one tag replying at the same time to avoid collisions. This collision problem is common to (wireless) communication networks and many methods have been developed to counteract these collisions. So-called MAC protocols often require transmitters to be able to receive the signal from other transmitters. In the case of EPC Generation 2 tags, this requirement is not feasible as it would require a very sensitive, power hungry, receive chain to be included in the passive tag. Therefore a MAC protocol is defined in the EPC Generation 2 standard that does not require a tag to be able to receive backscattered signals from other tags.

A tag entering the field of a reader remains in an idle state until the reader signals the start of an inventory round with a command known as $Query$. This command includes some configuration data which is received by all nearby tags. All tags receiving the $Query$ command will generate a random number of 16 bits, denoted $RN16$, and select a random slot number from one of 2^Q available slots. This Q value is initialized during the $Query$ command and can be freely chosen by the reader. The number of tags in the field is of influence on the number of tags selecting the same slot. If there are many tags in the field and a reader issues a small Q value, a lot of collisions will occur due to the fact that a large number of tags select the same

slot number. However, if there are not many tags, but a high Q value is used, a lot of empty slots have to be read leading to a waste in air time and hence bandwidth and power. When power is provided by a fixed reader, wasted power is of less concern. However, the loss is useful airtime directly leads to the unwanted effect that less tags per time-frame can be read. So, depending on the expected number of tags, a reader chooses Q, whereby $0 \leq Q \leq 15$. A lot of research has been done on selecting the optimal Q value[34] [60].

After sending the $Query$ command, all tags decrease their slot-number by one and the tags having selected a slot-number of zero in this slot start backscattering their 16 bit random number, $RN16$. The reader decodes the $RN16$ and transmits this number to the tag, if a tag receives its own random number, the tag knows that it is the only tag that answered in this slot. (Unless in the unlikely event that two tags selected the same slot and 16 bit random number. In this case a collision occurs which is detect by a Cyclic Redundancy Check *(CRC)*)

Upon reception of its own $RN16$ a tag starts backscattering the EPC identifier and a CRC without any further command. The EPC and CRC are received by the reader and with the help of the CRC, a reader is able to detect reception errors. These errors can be introduced by the environment, like other transmitters in the same band, reflection and noise, or the collision of two tags due to a failure in the random number generation. The EPC stored in the tag can be 16 to 496 bits long. A typical EPC Generation 2 passive IC like the Impinj Monza 3, used for some experiments in this thesis, is factory programmed with a 96 bit unique EPC[45].

After the EPC is received, the reader can issue more commands to a tag, for example to read or write data from/to its general purpose memory. If the reader was only interested in the EPC, the next slot is signaled by sending a $QueryRep$ to all tags. All tags decrease their slot counter by one and the tags which now have a slot counter of zero start backscattering their $RN16$. The reader can keep querying until all slots have been passed, after which all tags have hopefully answered without collisions.

In case of many collisions, the reader can increase the Q value and start a new $Query$ round. All tags have to respond again. This behavior might be undesirable in the case of many tags, as no new information is gained by reading a tag again and valuable slots are lost. To exclude some tags from the following round the EPC protocol allows for session flags to be set and have only tags with certain session flags participate in the next query round.

2.1.5 Reception of Backscatter

As explained before, to transmit data, tags change the impedance seen by their antenna. Depending on this impedance the antenna reflects a different amount of the continuous wave it receives; the signal is said to be backscattered. A reader must be able to receive this relatively small backscattered signal.

If only a single antenna is used to transmit the continuous wave and receive the modulated signal from the tag, special measures have to be taken to prevent half of the transmitted power to enter the receive chain. In this case circulators or directional couplers have to be used. These devices make sure that a large portion of the transmitted signal follows the path to the antenna and not into the reception chain.

The modulated wave that is backscattered by a tag can be modeled as a wave with exactly the same carrier frequency as the continuous wave that is transmitted by the reader. Let us assume that the change in impedance only changes the amplitude of the reflected signal, a simple model is given by Equation 2.2.

$$s(t) = \begin{cases} 1 \cdot \cos(2\pi\omega t), & \text{if } x(t) = 1 \\ 0.1 \cdot \cos(2\pi\omega t), & \text{if } x(t) = 0 \end{cases} \tag{2.2}$$

The modulated wave that enters the antenna of the reader might have zero phase difference with the continuous wave, and only an amplitude difference. If, in this case, the received signal is multiplied with the continuous wave, the modulated information appears at baseband. If, for example due to distance, the modulated signal is 90 degrees phase shifted compared to the continuous wave, there appears no signal at baseband.

To be able to observe the baseband signal irrespectively of the phase difference between the continuous wave and the modulated backscattered wave, a common method is to mix the signal to form a complex baseband signal. Multiple methods exist, where the results are mathematically equivalent: a so-called inphase and quadrature component are formed.

A possible method is to down-mix the signal with the transmitted continuous wave and a 90 degrees phase shifted version of this wave in the analog domain. The two resulting signals are filtered to remove the higher frequency components and only keep the baseband signal. Both baseband components can then be sampled and quantized by an ADC. These sampled signals are typically shown in a single figure, with the inphase and quadrature component on the x- and y-axis respectively.

Even if special measures are taken to limit power from the continuous wave into the receive chain, the signal will remain relatively small. This translates into the fact that the baseband signal after down-mixing contains a large Direct Current *(DC)* offset due to leakage. This offset is usually removed in the analog domain before sampling. In Figure 2.4 an IQ plot with leakage is shown. Because two states are used to modulate the data, in the IQ plot two points appear (which will become point clouds for noisy data as shown in Figure 2.5), similar to traditional BPSK. As shown in Figure 2.4, if this DC offset is removed a new origin is formed. In Figure 2.5 an IQ plot based on actual ADC data is shown. Almost no leakage remains visible in this figure, the data points are more or less centered around zero.

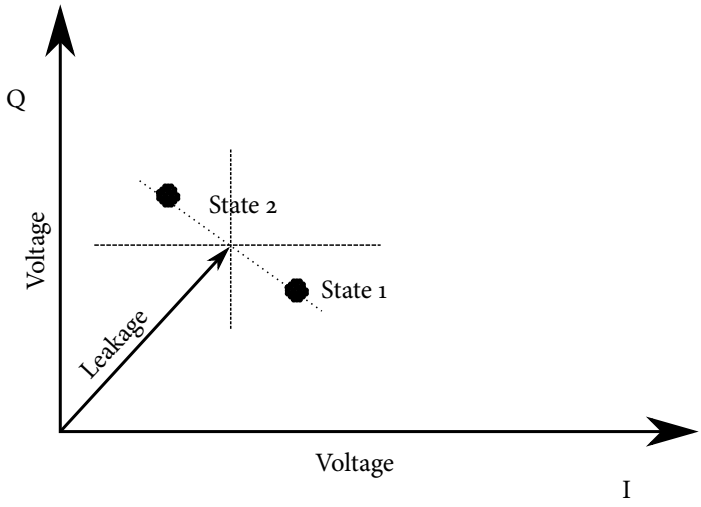

Figure 2.4 – IQ plot including leakage

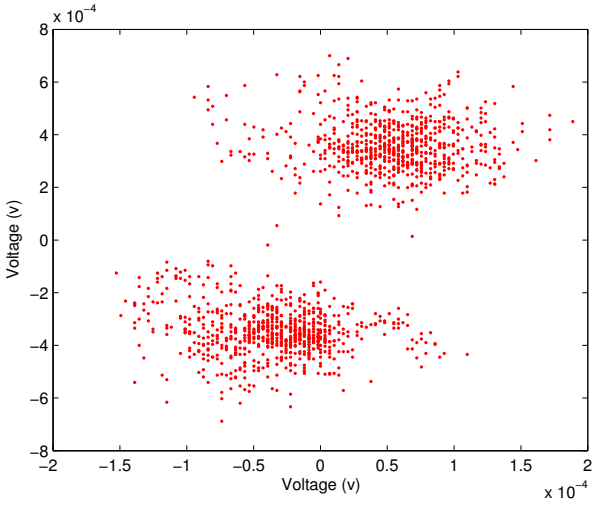

Figure 2.5 – IQ plot from measurements

2.1.6 Link Budget

Only a small portion of the transmitted signal is reflected by the tag. To be able to have enough signal strength in the receiver of the reader, a relatively strong continuous wave is transmitted by the reader. The amount of power that a receiver needs to be able to successfully decode the transmitted or, in this case, backscattered information, is known as the link budget. In the case of backscattering RFID, this link budget is depending on several properties. First of all, the power transmitted by the reader. The ETSI limits the transmission power to 2 W Effective Radiated Power *(ERP)*, which is 33 dBm[32]. Note that this is defined as the power level when a signal leaves the antenna, therefore a directional antenna will not allow for more power to be transmitted. However, a directional antenna will help to increase the signal level in the receive chain of the reader.

The first loss encountered after the transmit antenna is the path loss from reader to tag. In the most simple model the reader antenna can be modeled as a point source. The energy transmitted by this antenna propagates and spreads out over the surface of a sphere. The power received by the tag decreases accordingly with distance. This effect is known as the free space path loss. The power received by the tag, P_r, is a scaled version of the power transmitted, P_t:

$$P_r = P_t \cdot \left(\frac{\lambda}{4\pi r}\right)^2 \tag{2.3}$$

The wavelength, λ, and distance between transmit and receive antennas, r, are used to calculate the received power. The path loss can be calculated as a ratio and expressed in decibels as follows:

$$\frac{P_r}{P_t}(dB) = 20 \cdot \log_{10}\left(\frac{\lambda}{4\pi r}\right) \tag{2.4}$$

For a distance of 1 meter and a carrier frequency of 865MHz this results in a loss of almost 32 dB. Not only the signal transmitted by the reader will be attenuated, but also the signal backscattered by the tag. Therefore this loss will be encountered twice.

In practice a tag will not be able to backscatter all signal power it receives. A couple of dB will be lost by the modulation efficiency. The Impinj Monza 3, used for some experiments in this thesis, is specified to have a modulation efficiency of 0.8 which translates into a loss of about 1 dB.

The orientation of a tag is usually not known in advance. Therefore the antenna gain of UHF RFID tags is usually small. Because a lot of tags are based on dipoles, the gain is in the order of two dB[75]. However, a mismatch in polarization can lead to extra signal attenuation so we assume a zero influence of the tag antenna.

The described gains and losses all add up and should be larger than the sensitivity of the reader. The Impinj R2000 transceiver IC has a sensitivity of -93 dBm[47]. With

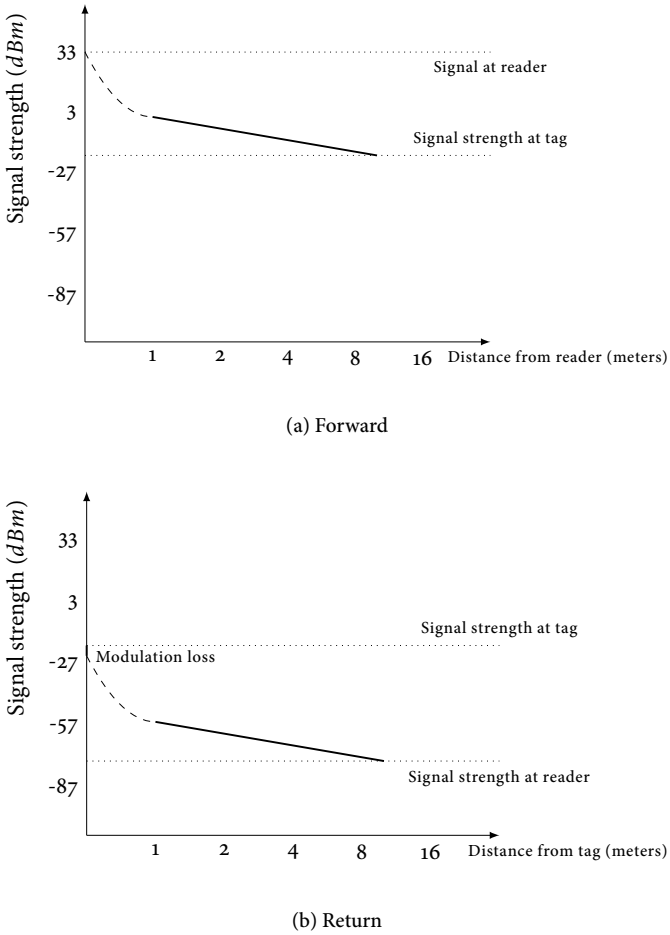

Figure 2.6 – Example link budget, adapted from [31]

a Monza 3 tag at ten meters from a reader, transmitting at maximum power, the received power is: 33 dBm - 51 dB path loss - 1 dB modulation loss - 51 dB path loss + 2dB reader dipole antenna gain = -68 dBm. In Figure 2.6 a graphical overview of this link budget is given, note that the signal level drops as the distance increases. The top graph shows the signal strength dropping over the path from reader to tag. In the bottom graph the return path is shown. As the equation for path loss does not hold in the near field, this first part is shown by a dashed line[31].

In a conventional wireless communication system, communication is possible by having enough signal strength at the receiver. However, in the case of passive RFID tags there is another property to take into account. The tag has to harvest power

and needs a certain signal strength to be able to harvest enough power. In this case, the system is not limited by reader sensitivity, and the system is said to be forward-link limited. If a tag can be made highly energy efficient or has a different power source, for example a battery, the system is ultimately limited by the reader sensitivity, in which case the system is called reverse-link limited. The Monza 3 has a sensitivity of −15 dBm, meaning that the example above is already invalid with a distance between reader and tag of 10 m. The tag cannot harvest enough power to start the communication process, because 33 dBm - 51 dB = −18 dBm signal power received at the reader, which is smaller than the needed sensitivity. With this tag a communication range of 10 meter is not possible and the system is forward-link limited.

By choosing a newer tag like the Monza 6[46], with a sensitivity of −22.1 dBm, according to this simple model, a tag can be powered at 10 meters. However, with a maximum path loss of 55 dB (33 + 22 dB), a tag will most likely still be forward-link limited, even when a reader is transmitting at maximum power of 33 dBm. The resulting signal level of −76 dBm (33 − 55 − 1 − 55 + 2 = −76 dBm) at the reader is well within reach of modern receive chains. Tag designs become more and more sensitive and eventually the system will become reverse-link limited.

The link budget described above is over simplistic and can only be used as a guideline. The free space model certainly does not hold for an indoor radio channel in the 865 MHz band, because the signal will be reflected by objects and surfaces in the environment. Instead of the free space model an option is to use a typical fading channel model[38], ray tracing[55] or a combination of both[9]. Furthermore, the effects of polarization and antenna gains have been largely ignored.

2.2 Conclusion

An overview of the EPC Generation 2 protocol is given in this chapter. A relevant property of these tags is that a tag has to be activated before it will start backscattering data. Based on this backscatter we can localize the tag. Therefore it is relevant to know some characteristics of this signal.

The backscatter signal can be received by an off-the-shelf reader, but it is also possible to receive the tag signal with a separate receive chain. By using coherent demodulation as explained in Section 2.1.5, a sampled baseband signal yields two points in a complex plane.

The link budget described in this chapter shows that the read range of tags is mostly limited by the amount of power the tags can harvest and not by the reader sensitivity.

3

Existing Localization Methods

Abstract – *Traditionally RFID systems couple identification to localization. The fact that a tag is read by a reader indicates that it is close to the reader. For some applications more detailed localization is necessary and localization of EPC Generation 2 tags is therefore an active topic in literature. Numerous localization systems have been developed to localize a tag within the read range of a reader. These systems are based on certain signal properties, for example RSSI and phase. Different approaches have been developed but no accurate localization systems based on UHF RFID tags has been found yet.*

3.1 Introduction

In recent years, localization of objects has gained much attention. Based on certain characteristics of a transmitted signal, a receiver or combination of receivers might be able to estimate a location. These systems are developed to localize objects locally, in contrast to for example GPS, and are known as Real-Time Location Systems *(RTLSs)*. The frequency band used by these localization systems can differ from LF to Infrared *(IR)* and often these systems make use of active transmitters in the tags. As this research focuses on the localization of passive EPC Generation 2 tags, a literature overview of localization methods based on these tags is given and, unless otherwise stated, all cited references are on EPC Generation 2 based localization systems.

The ultimate goal is to localize a tagged object in all dimensions of time and space. If we assume a stationary situation, this becomes localization in the three dimensions of space. Many localization systems assume that the object is located in a 2D plane, reducing the localization to a two dimensional problem.

In this 2D space, usually Cartesian coordinates are used to mark a location relative to a predefined origin. In the case of a single reader, the origin could be the center of the antenna. However, when using a single reader, it makes sense to use a polar

coordinate system. In this case, the two coordinates, range, R, and direction, θ, can be estimated separately. Based on this coarse classification, we discuss different localization approaches in this chapter.

3.2 Distance to a Single Reader

The most coarse approximation of location is the identification process itself. If a reader is able to read the EPC identifier from a tag, we can infer that a tag is located relatively close to the specific reader[1]. The location of the tag is somewhere within the read range of the reader. Although this read range is not well defined in an indoor environment, for some applications this coarse localization is enough. In case of supply chain tracking the knowledge that a tagged object is in a certain warehouse might be enough. On the other hand, one might want to know when a tag is moved into a certain truck, requiring more fine grained localization.

A straightforward approach to narrow the possible location of an observed tag is to limit the read range of the reader. This can be done by lowering the transmitted power of the continuous wave sent out by the reader. Tags close to the reader will be able to respond with lower power levels. Although there exists no hard boundary and there is an intermediate region in which tags sometimes are able to harvest enough energy and sometimes not[25]. A suggested improvement is to include reference tags. These tags have to be located at known positions in the environment of the reader and are used to calibrate the estimation[23]. These reference tags can be fixed permanently to the environment. In this way, changes in the environment after setup can be taken into account. However, if the use of permanent tags in the read zone is unwanted, the calibration can be done only at startup, after which the reference tags can be removed. In both cases knowledge about the exact position of the reference tags is needed, a requirement that is not easily fulfilled, because it requires other, possibly manual, localization techniques. The manual labor required for calibration can be too costly. Furthermore, human positioning of reference tags is prone to errors.

3.2.1 Signal Strength

In the previous chapter, the link budget is explained. The gradual decrease of transmit power can be seen as lowering the total link budget until the tags sensitivity limit is reached. Another option that is remarkably similar, is to measure the power of the returning signal. As described during the analysis of the link budget in Section 2.1.6, the strength of the signal received by the reader is strongly dependent on the distance from the reader. Some off-the-shelf readers are able to provide an RSSI. This can be a true power measurement as is the case for the reader we used in experiments[47] or just an indicator with no defined relation to the received power[30]. Unfortunately the received signal strength is not only affected

[1] The system is vulnerable to cloning/man in the middle attacks, however, the impact is limited because the system is not (yet) used for high security applications[21].

by distance but also by the propagation environment (e.g. reflections) and antenna patterns. Therefore, systems based on RSSI require extensive calibration and/or reference tags[30] [52].

3.2.2 Phase

Measuring the phase of reflected signals at different frequencies is a common way to determine the distance to an object in radar systems[18]. A similar approach can be used for passive backscattering RFID tags[91]. As described in Chapter 2, EPC Generation 2 tags transmit their information with a modulation technique similar to BPSK. The continuous wave that is used to power the tag and is backscattered by a tag is tapped off and used to down-mix the information signal to baseband. In this case, there is no phase drift between the transmitted carrier and the local oscillator as they originate from the same generator. This coherent detection makes it possible to use the phase of the received information signal as measure for distance. The observed phase, ϕ, is modeled by assuming that a sine wave travels to a tag and is scattered back to the reader. Therefore, twice the distance, R, is covered by the signal. For every wavelength, λ, the signal travels the phase increase with 2π, giving:

$$\phi = \frac{R}{\lambda} \cdot 2\pi \cdot 2 \tag{3.1}$$

However, the observed phase, $\hat{\phi}$, will be ambiguous and cannot be used as a direct measure for the distance due to the inherent phase wraps.

$$\hat{\phi} = \frac{R}{\lambda} \cdot 2\pi \cdot 2 \mod 2\pi \tag{3.2}$$

A phase difference can be used to estimate a displacement in case an observed phase change contributes to a change in distance. If all variables in the equation above remain equal, a slight phase change indicates a distance difference. However, as with RSSI measurements, in reality the phase measurements will be affected by other (environmental) effects as well[67].

Time Domain Phase Difference

By measuring the phase of the received signal multiple times and assuming that the observed phase difference is caused only by the movement of the tag, a distance change can be derived. In Equation 3.3 $\Delta\phi$ is the absolute phase difference between two tag observations.

In real systems the absolute phase is unknown. However, phase differences can be measured as long as the change in distance ΔR is not too large compared to the time difference between consecutive samples. ΔR should always remain smaller than the wavelength. Otherwise phase wraps occur that cannot be detected and lead to estimation errors. In case of the used UHF frequencies, the wavelength,

λ, is about 34 cm. Leading to a maximum distance change between consecutive samples of 17 cm.

$$\Delta R = \frac{\Delta\phi \cdot \lambda}{2 \cdot 2\pi} \tag{3.3}$$

To derive the speed of the tag,Δv , the distance difference has to be divided by the time difference,Δt , between the tag observations.

$$\Delta v = \frac{\lambda}{4\pi}\frac{\Delta\phi}{\Delta t} \tag{3.4}$$

If the speed of tag movement is restricted, it is possible to use this speed estimate to calculate a position estimate[19].

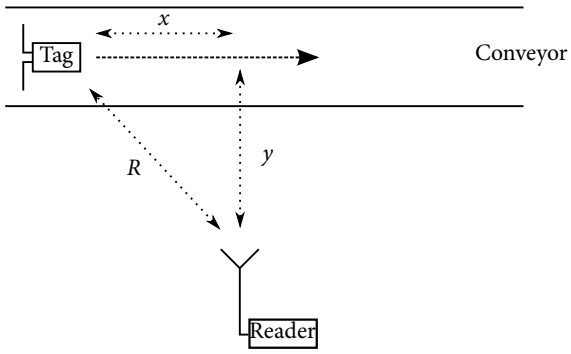

Figure 3.1 – Top view of conveyor system used by [20]

In reference [20], tags are assumed to be on a conveyor belt and move perpendicular to the reader antenna, see Figure 3.1 for a top view of such a setup. The phase is measured multiple times by the reader and stored for offline processing. The distance between the tag and reader has a non-linear relation to the distance from the center of the read antenna. Assume x as the displacement from the center of the reader antenna and y the distance between the center of the reader antenna and the conveyor belt. The distance R between tag and reader is defined as: $R = \sqrt{x^2 + y^2}$. This non-linear relation between the displacement, x, and range, R, also translates to the observed phase. Wrapping of the phase can be undone as long as the reader is able to interrogate the tag fast enough, or in other words the tag moves slowly enough. The gradient or shape of the derived parabolic relation is dependent on the distance between reader and tag. By means of a computationally expensive search, [20] tries to find a model that describes the measurements best. The position of the tag on the conveyor belt is then extracted from the model.

Frequency Domain Phase Difference

As can be seen in Equation 3.1, the wavelength, λ, also has a relation to the distance. Again we are unable to measure absolute phase, but with help of a frequency difference we are able to calculate a distance. By computing the difference of two

different phases, ϕ_1 and ϕ_2, as the result of two frequencies $f_1 = \frac{c}{\lambda_1}$ and $f_2 = \frac{c}{\lambda_2}$, for the distance R, we get:

$$R = \frac{\phi_1 - \phi_2}{\frac{1}{\lambda_1} - \frac{1}{\lambda_2}} \cdot \frac{1}{4\pi} \tag{3.5}$$

Here, λ_1 and λ_2 are the wavelengths of the two different frequencies at which the different phases are measured. Defining the phase difference as $\Delta\phi$ and frequency difference as Δf, the distance is defined as:

$$R = \frac{c \cdot \Delta\phi}{4\pi \cdot \Delta f} \tag{3.6}$$

Due to the ambiguity of the measured phase this distance is not unambiguous unfortunately. This ranging technique is similar to the approach known in the radar field as Frequency-Modulated Continuous-Wave *(FMCW)*. In these radar systems, the carrier wave is usually swept across a certain bandwidth. Another option which is well suited for RFID systems is to step the frequency of the reader and measure the received phase. In the next chapter we use this technique with multiple antennas to achieve 2-dimensional localization. Promising ranging experiments have been done in an anechoic room by [71].

In [57] the dependence of this technique on bandwidth is shown. In an ideal environment the measure $\Delta\phi/\Delta f$ would be constant for every possible frequency difference, Δf, meaning that the propagation channel is not frequency selective. However, the UHF propagation channel is never ideal. Therefore, more information is needed to characterize the channel. If more bandwidth is used to measure the effects of the propagation channel, these systems becomes more like a UWB channel characterization system explained in Section 3.2.4.

3.2.3 Direct Sequence Spread Spectrum

As said in the previous section, a better range estimate could be made by using a larger bandwidth. A suggested approach is to transmit a relatively wideband signal together with the interrogation signal. If the antenna of a tag is able to backscatter the entire transmitted band, it is possible to receive this backscatter and derive a range estimate. In some research, a wideband signal is generated digitally and a carrier wave is added[37].

This technique is called Direct Sequence Spread Spectrum *(DSSS)* to indicate that a wideband signal is created instantaneously, in contrast to frequency hopping or swiping systems. With the help of a custom hardware platform, the authors of [10] are able to estimate the range to a tag with an accuracy of 25 cm up to a range of 4 meters. The authors note that the power of the DSSS signal is kept 40 dB below the level of the interrogation signal. This is allowed according to the spectral mask defined in the EPC Generation 2 standard. The authors propose a bandwidth of 12 MHz and use it for experiments. Assuming a transmit power of 33 dBm, this results in a signal strength of -7 dBm. This amount of power might be allowed

by the standard, but is certainly not allowed by the regulatory agencies. In the Netherlands, outside the appointed RFID bandwidth only -60 dBm is available for unlicensed use in the UHF band[3]. This approach violates our requirement R5 mentioned in Section 1.5 .

3.2.4 Ultra-WideBand

To show that a lot of bandwidth is necessary to achieve reliable ranging in typical UHF RFID application scenarios, the authors of [7], [8] and [9] used an UWB system. In a typical RFID scenario (a gate through which tagged goods are moved) UWB channel characterization experiments have been done. A Vector Network Analyzer *(VNA)* was used in the frequency band from 500 MHz to 1.5 GHz. One of the UWB antennas is fixed at the location of the reader antenna. Another antenna is moved to possible tag locations. At every location, the channel between these two antennas is characterized. To characterize these channels, the analyzer uses 1 MHz steps in the 1 GHz wideband and measures the received phase and amplitude for every step. In this way for every location a frequency response is generated that can be transformed into an impulse response, for example with the help of a Fourier transform.

The channel is assumed to remain constant over time. Therefore, the power delay profile is defined as a squared version of the impulse response. A power delay profile shows the received power after a certain time delay. In an ideal situation all power would arrive at once, after a certain delay depending on the distance between the antennas. However, due to multipath this is not the case. Signals that are reflected against walls for example, have a longer path to follow and therefore arrive later at the receiving antenna. If only discrete reflections would be present and unlimited bandwidth would be available the reflections would show up as identifiable delta functions in the power delay profile. In reality the system uses a bandwidth of 1 GHz and many different reflections exist. Therefore, identifying discrete reflections in the power delay profile proves to be difficult.

Based on numerous of these channel measurements, a stochastic model of the channel is created that is used to build a simulator[6]. Based on the large bandwidth that is used to characterize the channel, the authors provide estimations of the bandwidth that is necessary to achieve a certain accuracy in a gate scenario. Inside the gate a 10 MHz bandwidth gives a maximum range error of 2 meters. In early research, the authors show that UWB ranging requires special antennas to allow a tag to backscatter[7]. Other research tries to combine normal UHF dipole antennas with UWB antennas to solve this problem[33]. With the help of unlimited bandwidth, tags can be localized accurately. However special hardware and antennas have to be added to reader and tag, making a system non-compliant with the EPC Generation 2 standard and a practical implementation cost prohibitive, due to the UWB equipment. Furthermore, with current technologies these systems can not be made passive as the UWB transmitter that has to be included in the tag re-

quires a lot of power. Therefore this approach violates requirement R3 defined in Section 1.5.

3.3 Direction to a Single Reader

A possible approach to estimate the Direction of Arrival *(DOA)* from a tag is to use a rotating reader antenna[58]. In the center of the main beam of the reader antenna the received signal strength of the tag will be the highest. However, an antenna pattern is relatively flat at the top, therefore finding the maximum is sensitive to noise. In Figure 3.2 the antenna pattern for the patch antennas used for the experiments in this thesis are shown. Both the phase and power pattern are shown. From the signal power pattern it is clear that the antenna is most sensitive in the forward direction and gradually decreases towards the edges.

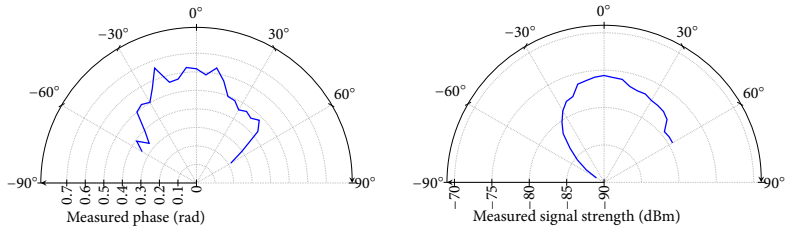

(a) Phase

(b) Signal Power

Figure 3.2 – Radiation Pattern

Another option is to find two similar points on the antenna pattern. In [86] a system is proposed whereby a single reader antenna is rotated with the help of an electric motor. The antenna is not rotated continuously but step wise to allow the reader to interrogate the tag. For every angular step the system records whether it is possible to interrogate the tag. In this way two boundaries are found. Assuming the antenna pattern of the reader is symmetrical, the direction of the tag is exactly in between these two boundaries. The authors of [86] also suggests to use two rotating antennas to find two directions from known antenna positions to enable 2D localization. This approach is also susceptible to conditions in the environment, for example reflections and moving objects. As the reader(s) need(s) to rotate, this adds interrogation time and extra cost to the system, which violates requirements R3 and R4 defined in Section 1.5.

3.3.1 Phased Array

Imagine an array of multiple antennas receiving the backscatter signal from a tag. This signal travels along a different path to every antenna where each path has a

different length. If we assume a narrowband signal, the difference in path length to every antenna is observed as a phase difference in the baseband signal.

If the signal from every antenna is sampled by an ADC, further processing can be done in the digital domain. A straightforward solution is to use traditional beamforming and scan over all angles. This approach does not give a very high resolution and is computationally expensive. Literature suggests numerous other algorithms. A notable high resolution algorithm is known as MUSIC[78]. See Section 5.4.1 for more explanation.

A research group from the Cologne University of Applied Sciences[11] [28] [54] constructed a linear phased array of three antennas. The backscatter signal received by every antenna is converted to baseband by three off-the-shelf reader ICs. The mixers are fed with the same local oscillator to make sure the phase is locked. The baseband signals are digitized to allow for offline digital processing. The traditional ROOT-MUSIC algorithm is used to estimate a DOA. Multiple of these phased arrays are then used to localize within a 3x3 meter grid. Four arrays are located at the corners of a square and are used to estimate four DOAs. Part of their research focuses on the process of combining these estimations to a location estimate within the square. Ranging from basic triangulation to fitting the estimations to a system model.

Other research has been done on circular arrays in a warehouse environment[42] [43] and tagged items on a conveyor belt[20].

Transmit Beamforming

Due to the fact that radio channels are reciprocal, a signal can be directed into a certain angle. When a signal is transmitted by multiple antennas, the signals add up in the receiving tag antenna. Depending on the path lengths between the transmitting antennas and the receiving tag antenna, these signals add up constructively or destructively. A beam pattern shows at which angle the array of antennas emits most power. With traditional phased array techniques this power can be steered to different angles by changing the phase of the transmitted signals at the different antennas.

By changing the angle in which most power is transmitted in steps and recording whether a tag can be interrogated is relatively similar to the rotating antenna approach. In [29], a three antenna transmit array is used which scans over the array by changing the signal phases and transmit power to be able to find the tag. When a tag can be interrogated only in one specific beam direction, at a certain power level, the tag is assumed to be in the middle of that beam. This system is not viable for moving tags or changing environments. The authors state that is takes 1.8 seconds to do a single scan. Because multiple power levels are used, the total time to do a single DOA estimation is even longer. With the help of multiple arrays, the authors are able to estimate a 2D location. Because every array needs to do its own

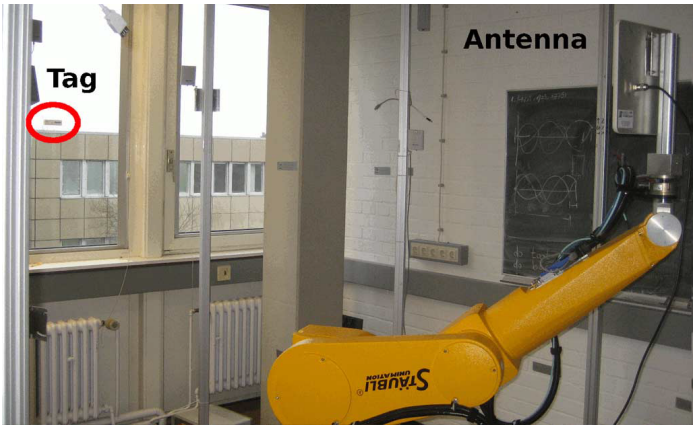

Figure 3.3 – Synthetic Aperture robot arm from [63]

DOA estimate, a long measurement time is needed, in the order of 10 seconds, to get a location estimate.

Synthetic Aperture

A somewhat related approach is to use a single antenna, and then move the antenna in space to synthesize an array, assuming time invariance. In this way, a multi antenna array is synthesized. This technique originates from the field of radar, where it is known as Synthetic Aperture Radar *(SAR)*[4]. The authors of [62] and [63] use a robot arm to move a single reader antenna in a horizontal plane, shown in Figure 3.3. For every discrete position, a phase measurement is taken by interrogating the tag that has to be localized. With the help of offline processing of in total 4141 tag interrogations a single location estimate is derived.

In [59] and [70] a synthetic aperture approach in the case of tagged items on a conveyor belt is described. The conveyor belt is moving with a known speed and tags can only be located within a certain area of the conveyor belt. Therefore the authors are able to exploit the known and predictable movement of a tag instead of the reader antenna as basis for their SAR approach. As these systems use either mechanisms to move the reader, or assume a certain movement of the tags, these approaches cannot be used in our situation.

3.4 Multiple Readers

Although originally not designed for EPC Generation 2 tags, a well-known localization scheme is LANDMARC[64]. It proposes to use multiple reference tags and multiple readers at known locations for the first time. In the original LANDMARC research the system estimates a 2D location of a tag based of the received

signal strength from active reference tags. With the help of the k-nearest neighbors, known as reference tags, a location estimate is made.

Based on the difference in signal strength between the reference tags and the tag with unknown location, the k closest tags are selected. With the help of a weighting algorithm, a location estimate is derived from these neighbors.

Also other localization algorithms using reference tags are based on LANDMARC, for example VIRE[90] and a 3 dimensional optimization in [40]. The VIRE approach interpolates the RSSI values between reference tags to refine the grid. For every reader a so-called proximity map is calculated which stores the interpolated RSSI values. When a reader measures an RSSI value from an unknown tag, it maps the value onto its proximity map. This yields a map with possible locations for the tag. By combining these maps of several readers, the location of an unknown tag can be estimated.

Of course similar approaches can be taken for passive EPC Generation 2 tags[26] [65] and a 3 dimensional localization scheme based on RSSI with passive tags has been done by [51].

A possible solution is to install reference tags permanently, and take continuous reference measurements during operation. A disadvantage is that a lot of time is lost as all readers have to be used to get a measurement from all reference tags and the unknown tag. Another option is to use a prerecorded set of reference measurements, which are then used to get an estimate. In this case only a tag range estimate per reader is necessary.

The described systems are based on RSSI as a signal strength measurement which gives at least an unambiguous range estimate. In contrast to phase measurements, which suffer from ambiguity due to phase wraps. However, if movement is predictable, the measured phases can be mapped to a model for the location of a tag. In [77] the authors use four reader antennas on the corners of an square. This approach tries to locate butterflies and therefore assumes that a tag cannot move very fast. With a model of the system, the authors are able to track a tag based on phase measurements. However, their model based approach needs a correct initial position.

3.5 Conclusion

Based on different properties of the received tag signal, numerous systems have been suggested to estimate the location of EPC Generation 2 tags. Often a range or DOA estimation is made, requiring different receivers to estimate an exact location.

Approaches using extensive bandwidth are not feasible in practice, as the radio spectrum is limited by regulatory bodies. High power wideband systems will interfere with other users and will therefore never be allowed.

Some systems are based on the reception of multiple reader-tag communication sessions. Because the EPC protocol has to be followed, such a system is inherently slow and cannot cope with tag movement during a single location estimate.

Making use of reference tags means that the reference tags have to be read at some point. If this process is done at real time, again multiple tags have to be read which is unwanted in case of tag movements or changing environments.

An ideal system is able to locate a tag based on a single communication session with a tag to allow for moving tags and preserve the normal read rate. In the following chapters we explore methods to localize EPC Generation 2 tags based on this principle.

4

Multi Reader Localization

Abstract – *This chapter presents a 2D localization system for UHF RFID tags. By measuring the phase difference between the transmitted continuous wave and received backscatter from the tag at different frequencies, it is possible to estimate the distance between the reader and tag. By determining distance estimates to three antennas at a fixed location, it is possible to determine the location of a tag with the help of trilateration. Errors in the location of the antennas and in the distance measurement influence the location estimate. Mainly to overcome the expected impact of the environment on the distance estimate, we opt for the use of reference tags with known location and the k-Nearest Neighbors* (KNN) *algorithm to derive a location. An experiment is done and the phase-based results are comparable with a KNN algorithm based on received signal strength. Furthermore, experiments show that in a controlled environment phase measurements could be used to discriminate between moving and stationary tags in a portal application.*

4.1 Introduction

For the localization of RFID tags, some systems use the number of reads per second as a measure for the distance, assuming that a tag is read more often when it is close to a reader. Based on measurements of multiple readers at different locations, a location estimate can be made by combining the different distance measurements. This can also be combined with changing the output power of the reader[89]. In effect, these systems try to measure signal strength, which was not available on the early readers. Later systems started using RSSI as a related measure for range[16] [64].

Large parts of this chapter have been published in [JH:1].

In theory there is a direct relation between the observed signal strength, often indicated by RSSI, and distance. The RSSI is often seen as an indicator, resembling no physical property in contrast to a Receive Signal Strength, which is a true power level. Some external factors influence this measurement, for example the orientation of the tag and manufacturing tolerances in the tag's sensitivity. Furthermore, the environment has a large impact on the observed signal strength. Literature suggests a system based on reference tags to overcome environmental dynamics[64]. These reference tags with known locations are placed in the localization area. Figure 4.1 shows a possible system setup. In this figure the reference tags are indicated by RT and the Commercial Off-The-Shelf *(COTS)* readers are shown at the corners of the grid. RSSI measurements of tags with an unknown location are compared with the measurements of known tags. In the figure a single unknown tag is shown. A possible way to derive the location of an unknown tag is the k-nearest neighbors algorithm as used by the LANDMARC algorithm[64].

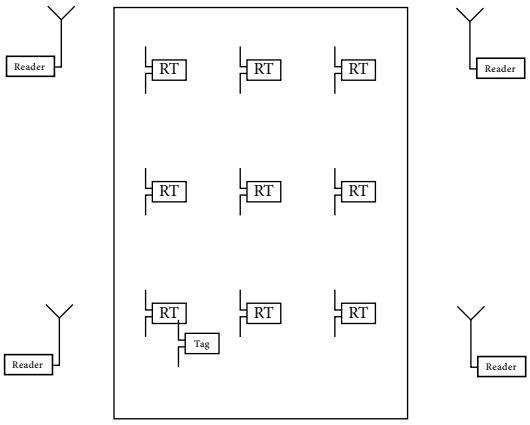

Figure 4.1 – Top view of four readers, unknown tag (Tag) and reference tag (RT) distribution.

Instead of using the RSSI measurements for localization, in this chapter, the use of phase measurements for localization purposes is investigated. According to Chapter 2, a EPC Generation 2 reader can demand a tag to backscatter some information. After giving the order, the reader starts to transmit a continuous wave. The tag modulates the requested information on this wave by changing the impedance that is connected to the antenna, effectively modulating the level of backscattering by the tag. The reader receives this backscatter and demodulates the information.

There is a phase difference between the transmitted continuous wave and the modulated backscattered wave that contains the requested information. This phase difference depends on several factors: the receive and transmit chain of the reader, the impedance of the tag and the distance between the tag and reader.

When measuring phase, there is an inherent ambiguity of 360 degrees. As phase relates to a distance, this phase ambiguity translates into a distance ambiguity that is related to the wavelength. At 865 MHz this translates to a distance ambiguity of 0.34 m. By using phase measurements at multiple frequencies, the unambiguous range can be enlarged.

Determining the distance between a tag and a single reader antenna is not enough to determine the exact location, because the tags might be located anywhere on a circle around the reader. By combining measurements from different readers, in principle it is possible to locate a tag with a trilateration algorithm. As noted in [53], these algorithms rely on an accurate distance measurement. However, the 865 MHz signal used by the UHF RFID system is susceptible to multipath. Especially in an indoor environment with a lot of scattering due to reflections from walls, furniture, people and other objects. A possible solution to this problem is to use reference tags similar to the RSSI based methods. The idea is that a reference tag is subjected to the same kind of scattering as a tag that has to be localized. By combining the measured location with the observed data of a known tag, the location of an unknown tag can be estimated. A closely related term is fingerprinting, whereby the system is calibrated using measurements from tags at known locations during a calibration phase, after which the data is stored and the reference tags are removed. In contrast to a system with always present reference tags, changes to the environment after calibration cannot be overcome by fingerprinting, while measurements from permanent reference tags can be used for every measurement round.

In [77] movement of a tag is tracked with the help of phase measurements from multiple readers. The authors show that the initial position of a tag is needed to initialize the used Kalman filter to track the moving tag. Furthermore, this approach is only able to track moving tags and fails if there is no movement.

In this chapter, the range between a reader and tag is determined based on phase measurements at different frequencies. This process is described in Section 4.2. A localization algorithm using the derived ranges of reference tags is explained in Section 4.3, followed by the result of ranging and localization experiments in Section 4.4. In Section 4.5 the use of phase measurements to discriminate between stationary and moving tags is examined. Finally, Section 4.6 discusses the results.

4.2 Ranging

A wave traveling from the reader antenna to a tag undergoes some phase shift dependent on the distance. The backscattered wave also undergoes the phase shift on its way back and the total distance traveled makes the unambiguous range $\frac{1}{2}\lambda$. Therefore, with the wavelength of a 865 MHz carrier being about 30 centimeters, there is an unambiguous range of 15 cm. An integer number, N, of half wavelengths counts for an unknown offset due to the phase wraps. In the following equation $\hat{R}$, the unambiguous range is defined. R is the true distance between antenna and tag, φ the observed phase and λ the wavelength of the used carrier.

$$\hat{R} = \frac{\varphi\lambda}{4\pi} = R - N\frac{\lambda}{2} \tag{4.1}$$

For this model the frequency-dependent effects and the phase offset created by wires are neglected. A frequency-independent constant phase offset is assumed which can be removed by calibration.

As described in Chapter 3, measuring the phase of reflected signals at different frequencies is a common way to determine the distance of an object in radar systems and can also be used for range estimates of backscatter based RFID tags. Using multiple frequencies at the same time is not supported by the relatively low budget hardware available for RFID. Nor is it possible to sweep over a frequency band, another common ranging technique. It is however possible to time multiplex different frequencies with COTS hardware, in other words, measure the phase at different discrete frequencies sequentially. Hereby we assume that the tag does not move while the phase difference at different frequencies is being measured. The measured phases can be written as:

$$\varphi_i = \left(R - N_i\frac{\lambda_i}{2}\right) \cdot \frac{4\pi}{\lambda_i} \tag{4.2}$$

We now measure the phase at two different frequencies, with wavelengths λ_1 and λ_2, whereby $\lambda_1 \neq \lambda_2$. The observable phase difference can be found by subtracting these two phases.

$$\Delta\varphi = \varphi_2 - \varphi_1 = \left(R - N_2\frac{\lambda_2}{2}\right) \cdot \frac{4\pi}{\lambda_2} - \left(R - N_1\frac{\lambda_1}{2}\right) \cdot \frac{4\pi}{\lambda_1} \tag{4.3}$$

Solving Equation 4.3 for R and substituting the frequency for the wavelength, $\lambda_i = \frac{c}{f_i}$, and assuming no phase wraps, $N_1 = N_2$, gives the following expression for the absolute distance:

$$R = \frac{c(|\varphi_2 - \varphi_1|)}{4\pi(f_2 - f_1)} \tag{4.4}$$

Hereby f_2 has to be defined as the value larger than f_1 to get a positive frequency separation. When $N_1 \neq N_2$, phase wraps occur and an ambiguity is introduced

as it is unknown what the difference is between N_1 and N_2. In effect the unambiguous range is increased by using multiple frequencies. However, an ambiguity will always remain. When this unambiguous range is larger than the possible read range, the ambiguity can be neglected.

This unambiguous range is dependent on the frequency separation and is given by inserting the maximum observable phase, 2π, into Equation 4.4:

$$l_{unamb} = \frac{c(2\pi - 0)}{4\pi(f_2 - f_1)} = \frac{c}{2\Delta f} \tag{4.5}$$

whereby $\Delta f = f_2 - f_1$, the frequency separation[91].

A smaller separation yields a larger unambiguous range. However, this can conflict with phase noise, the random error made in the process of measuring a phase. As the phase translates directly into a distance, phase noise affects the distance measurement. The phase difference is effectively spread out over the observable range, meaning phase is related to resolution. Therefore, as expected, the phase difference between the transmitted and received wave should be measured as accurately as possible. To limit the effect of phase noise in the measurement, a larger frequency difference can be used, which introduces a larger phase difference that can be more easily measured. If also intermediate frequencies are used, the phase can be tracked over phase wraps which would otherwise cause ambiguity. Furthermore, repeated measurements can be used to average out some noise, at the cost of measurement time. Overall, it is most beneficial to take many samples over a large bandwidth to have a large unambiguous range and high resolution.

A measure known as the group delay defines the phase behavior of a channel over multiple frequencies. The proposed ranging method based on measuring phase at multiple frequencies, can be seen as an attempt to measure the group delay and thereby assumes a system with linear phase. However, due to multipath, the channel that is being measured can (and will) have a non-linear phase[35]. To reconstruct the line-of-sight component in a multipath environment it is possible to measure the impulse response over a large bandwidth. This process requires a large bandwidth[7] and is therefore not feasible with EPC Generation 2 tags, as already explained in Chapter 3.

4.3 K-Nearest Neighbors Algorithm

A method to use distance related measures for localization is known as the *k*-Nearest Neighbors *(KNN)* algorithm. In an ideal, reflection-free, environment the received signal strength would fall off in accordance with free-space path loss and can be used as an estimate of true distance. However, the measurement hardware, orientation of antennas and the environment introduce deviations and cause an unclear relation between RSSI and distance. Because it is difficult to relate a measured RSSI to true distance, the traditional KNN algorithm only assumes that tags close to each-other will have similar RSSI. The LANDMARC algorithm[64] uses

reference tags with known location to relate RSSI measurements from these reference tags to RSSI measurements from tags with unknown locations. The same assumption can be made for phase-based range estimates; tags close to each-other will have similar range estimates. Therefore, we investigate the use of phase-based ranging as basis for the KNN algorithm in this chapter. In the following sections, distance related measures are defined: RSSI for the traditional algorithm and a phase-based range estimate for the proposed algorithm. Suppose, there are n readers which can determine a distance related measure to r reference tags and u tags with unknown locations. Note that the n readers can be complete antenna/reader pairs, but also n antennas time-multiplexed to one reader.

The distance related measures of unknown tags, whether they are RSSI measurements, traditionally used, or phase-based range estimates, are stored in vector $\mathbf{U} = (U_{1,1}, ..., U_{n,1}, U_{1,2}, ..., U_{n,2}, ..., U_{n,u})$ whereby $U_{n,u}$ stores the distance related measures of tag u measured by the nth reader. The same can be done for the r reference tags: $\mathbf{R} = (R_{1,1}, R_{2,1}, ...R_{n,r})$ where $R_{n,r}$ stores the distance related measures of reference tag r measured by the nth reader. The distance related measures are not necessarily a distance in meters, as the difference between two RSSI measurements has no direct relation to true distance. When all distance related measures are made, the differences between the known tags and the unknown tag(s) are calculated. There are multiple ways to calculate these differences. LANDMARC uses the traditional Euclidean distance between the different measurements. For every reader the squared differences between the distance related measures of the unknown and reference tags are summed and the root of this sum is called the distance D:

$$\mathbf{D}_{p,q} = \sqrt{\sum_{i=1}^{n} (\mathbf{R}_{i,q} - \mathbf{U}_{i,p})^2} \tag{4.6}$$

where $p = 1, ..., u$ and $q = 1, ..., r$.

For every unknown tag, u, there is a list of r distances D_r. A straight forward method to decide on the position of the unknown tag is to choose the closest reference tag and assume the location of the unknown tag to be the same as the location of the reference tag: a 1-nearest neighbor algorithm. In general the k reference tags with the smallest distances are chosen to estimate a location. To combine the distances from k reference tags into an estimate for the unknown tag, a weighted solution could be used. $(x, y, z)_u = \sum_{i=1}^{k} w_{u,i}(x_i, y_i, z_i)_u$ for a 3 dimensional localization with weight factors $w_{u,i}$ and with $(x, y, z)_u$ the estimated location of tag u. The weights could treat every reference tag equally $w_{u,i} = \frac{1}{k}$ and effectively average the locations estimated with k reference tags. The authors of the LANDMARC algorithm however, make an intuitive assumption that the nearest tag should have the highest weight[64]. Their solution for the weights is:

$$w_{u,r} = \frac{\frac{1}{D_{u,r}^2}}{\sum_{i=1}^{k} (\frac{1}{D_{u,i}^2})} \tag{4.7}$$

4.4 Experiments

A development board made by Impinj based on their Indy R2000 UHF RFID transceiver IC[47] is used in the following experiments in combination with Impinj Monza 3 tags. The R2000 IC is a complete System-on-Chip implementing an entire digital transceiver. A digital transmitter modulates information onto a carrier, after which the signal is passed through a power amplifier. An antenna can be connected to the R2000 without the need for extra components, although an extra power amplifier is present on the development board. Within the receiving part of the transceiver, the R2000 mixes the received signal down with the I and Q version of the generated carrier. A DC offset due to transmitter leakage and constant reflections is easily filtered out. The result is an IQ constellation centered around the origin with two constellation points, see Figure 2.5.

Other EPC Generation 2 transceivers use only the inphase or quadrature component, depending on the highest signal level. The R2000, however, rotates the received signal in the IQ plane to optimize SNR. The amount of phase shift needed for this rotation is written to a register and can be accessed by the control software. Because the protocol modulates the backscatter channel with Miller or $FM0$ encoding as explained in Chapter 2, only transitions contain information, not the absolute phase. A point in the constellation diagram can resemble a zero or one depending on how the signal is received.

The phase correction circuitry only adjusts the phase angle to zero. Imagine a BPSK IQ diagram at the transmitter, where the digital '1's are modulated at -1 and the '0's at 1. Due to the path between transmitter and receiver there is a phase difference, resulting in the same IQ diagram, however, rotated. The receiver has at this stage no knowledge about the '1's and '0's and therefore another 180 degree phase ambiguity is introduced. Further up the processing chain the information stream is decoded. At that moment the introduced ambiguity could be solved by always rotating to have '1's at -1, but the R2000 does not posses this capability.

For every tag that is read, besides a time stamp and the EPC to identify tags, a phase and an RSSI measurement are stored.

4.4.1 Distance

First of all, a distance measurement is performed with a single reader and tag, because experiments reported in literature [71] and [77] in an anechoic room give promising results for phase-based ranging methods[71] [77].

To investigate the performance of the proposed ranging system in a real-life environment, the following experiments are conducted in two different environments, a typical office room of 3x6 meters and a large empty office of 15x15 meters. The typical office room contains a lot of sources of clutter, like computers and persons, that introduce interfering multipath. The empty office room has some stationary objects and walls at a distance of a couple of meters, but not near the measurement

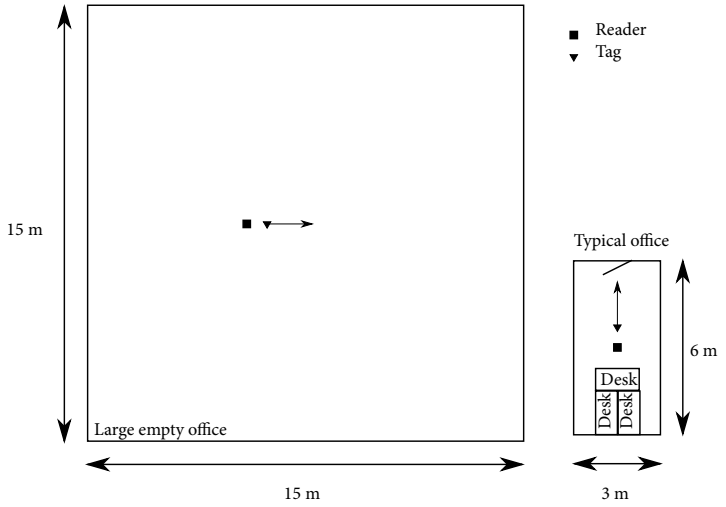

Figure 4.2 – Rooms used for experiments

site. In Figure 4.2 an overview of both situations is shown. In this figure the change in distance between tag and reader is indicated by an arrow. Due to the available antennas, the FCC band from 902 to 928 MHz is used with the reader set at its default hopping behavior known as Frequency-Hopping Spread Spectrum *(FHSS)*.

For every frequency hop, the observed phase is measured multiple times. For each frequency these phase measurements are averaged and the frequency-phase relation is unwrapped. A typical frequency-phase relation used for range estimation is shown in Figure 4.3. For different distances similar figures can be observed.

With the help of offline processing in Matlab, a linear fit is calculated. The slope of this curve is used as measure for the distance following Equation 4.4. This procedure is executed in two different rooms for several distances between tag and reader yielding the results in Figure 4.4 and Figure 4.5. These figures show the true distance together with the mean and standard deviation of several hundred measurements per distance with a minimum of 450 tag reads. Note that the number of measurements within a fixed observation interval is not constant due to the interrogation protocol.

The original LANDMARC algorithm is based on the assumption that nearby tags have similar RSSI, but can in general be used with other measures related to distance. Besides phase, the reader also reports RSSI measurements for every tag read. In Figure 4.6 the average RSSI values of the same experiment as on which Figure 4.5 is based are shown together with the observed standard deviation. The average is calculated over all tag observations at the different frequencies and can explain the relatively large deviations. In this way the shown RSSI is based on the same samples as the phase-frequency measurement. The drop in average signal strength

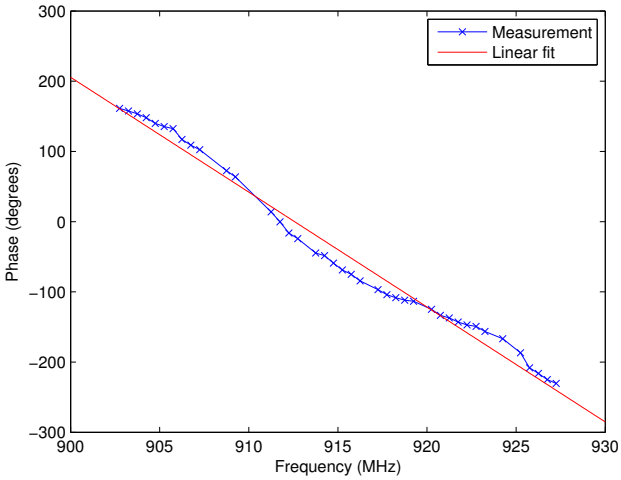

Figure 4.3 – Phase measurement of a tag with a tag-reader distance of 180 cm in the typical office.

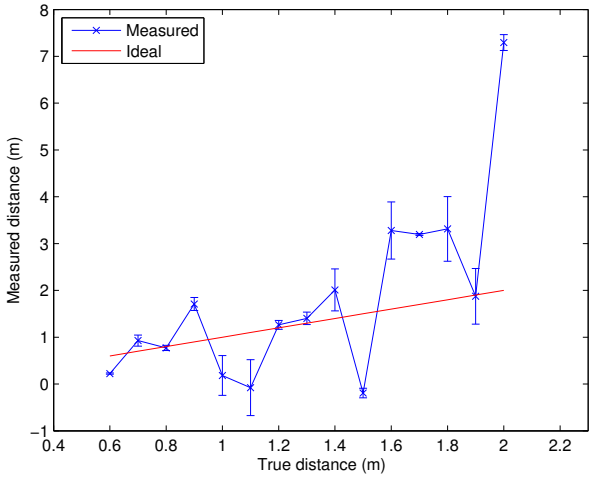

Figure 4.4 – Measured vs True distance - Typical office

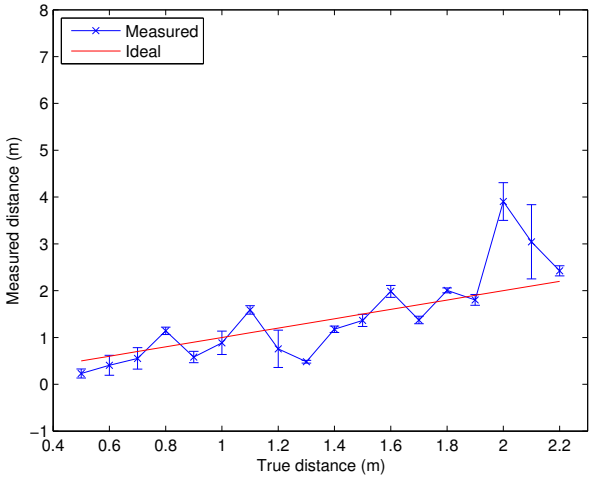

Figure 4.5 – Measured vs True distance - Large empty office

from 0.5 m to 2.2 is 16 dB, which is more than the 12 dB derived from the free-space path loss model. The spherical spreading assumed by a free-space model does not hold near the antenna as shown in Figure 2.6. Furthermore, antenna orientation and polarization effects can have effect on the received signal strength. Reflections also influence the received signal strength. From literature it is known that the free-space path loss model does not hold in an indoor environment[79]. However, Figure 4.6 clearly shows that signal strength decreases when tags are positioned further from the reader and that there is a strong relation between the distance and RSSI and tags close to each-other will have similar RSSI. Although the RSSI does not follow the theoretical model, by curve fitting the measurements a range estimate can be made. An exponential fit of the average RSSI is shown in Figure 4.6. For comparison, this fit can be used to determine a range estimate based on a received RSSI measurement as is done for the ranging experiments.

Discussion of the Results

Figures 4.4 and 4.5 show the existence of errors between the ideal and measured distance. To capture the performance in a single figure, the average of all (absolute) errors is calculated. The Mean Absolute Error *(MAE)* is 1.06 m for the office room and 0.42 m for the large empty office. For some distances multiple measurements contain a large standard deviation indicated by the error bars. In these cases, the phase-frequency relation is disturbed. In Figure 4.7 it can be seen that the phase-frequency relation is not completely linear, a least-squares linear fit is used to match the curve. This effect introduces errors in the final phase-frequency relation used for range estimations as the curve fitting introduces small errors. Other range estimates are shown to have a large error with low standard deviation, for

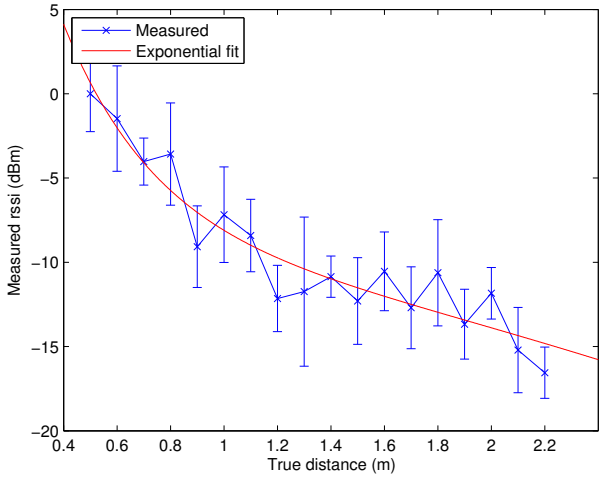

Figure 4.6 – RSSI measurement - Large empty office

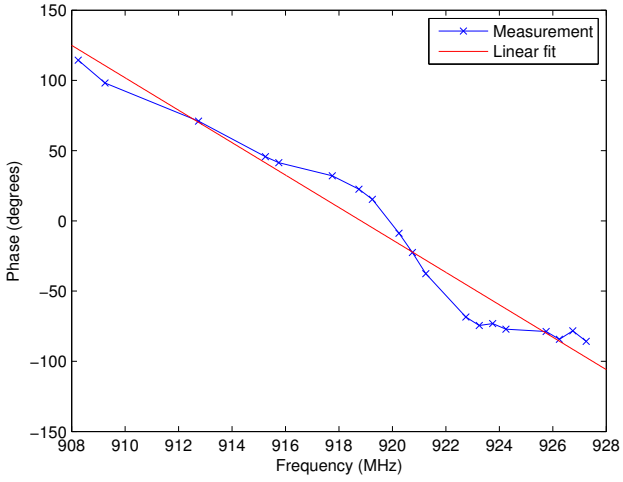

Figure 4.7 – Phase measurement of a tag with a tag-reader distance of 150 cm in the large empty office showing a curved phase-frequency relation

example at 1.7 m in Figure 4.4. These range estimates indicate a severe problem of inaccuracy due to the environment, caused by multipath. Sometimes reflecting surfaces are oriented in such a way that they cause powerful reflections. The effects appear to be time invariant. The measurement at 1.5 m shown in Figure 4.4 exhibits a small standard deviation and a large negative distance estimate. The phase measurements give an almost flat phase-frequency relation due to limited phase-frequency measurements and resulting failed unwrapping. This translates into almost zero distance estimate. Due to the correction for antenna cable length the final distance estimate is below zero.

Figure 4.5 confirms that in a large empty office with less reflections, the measurement results are better than in a typical office room.

For comparison the exponential curve shown in Figure 4.6, which is based on the measurements in the large empty room, is used to do range estimates in the typical office. This gives a MAE of 1.45 m, which is 0.39 m larger than the phase-based ranging in the typical office.

The authors of [71] report a ranging accuracy of 0.14 m in an anechoic room, which is significantly better than the result of 0.42 m obtained in the large empty office. This indicates that the environment has a large influence on the measurement accuracy. Based on RSSI, the authors of [26] are able to determine the distance to an accuracy of 0.33 m with the help of reference tags, which are not needed for distance estimation based on the phase-frequency relation.

4.4.2 Location

To localize a tag in a room, an experiment is done using a hardware setup with multiple readers (of the same type as used in the previous experiments) and reference tags. The readers and reference tags are setup like in Figure 4.1, with a grid spacing between the reference tags of 0.6 meter. These experiments are performed in the large empty office.

As shown in Figure 4.8, the four reader antennas are also aligned on the same grid. The tags are placed on non-conductive supports one meter above the floor. Every reader is used to interrogate the tags present in its field for 32 seconds. During every measurement round, there is only one unknown tag present within the grid of reference tags.

The location estimation error used for the algorithm, is the Euclidean distance between the derived location (x, y) and true location (x_t, y_t).

$$E_{error} = \sqrt{(x - x_t)^2 + (y - y_t)^2} \tag{4.8}$$

During the measurement round of 32 seconds, the reader continuously scans the environment for tags and stores the results. With the help of offline processing, a range is derived from the phase versus frequency curve. This range is then used as input for the KNN algorithm to calculate the location of the unknown tag. In the

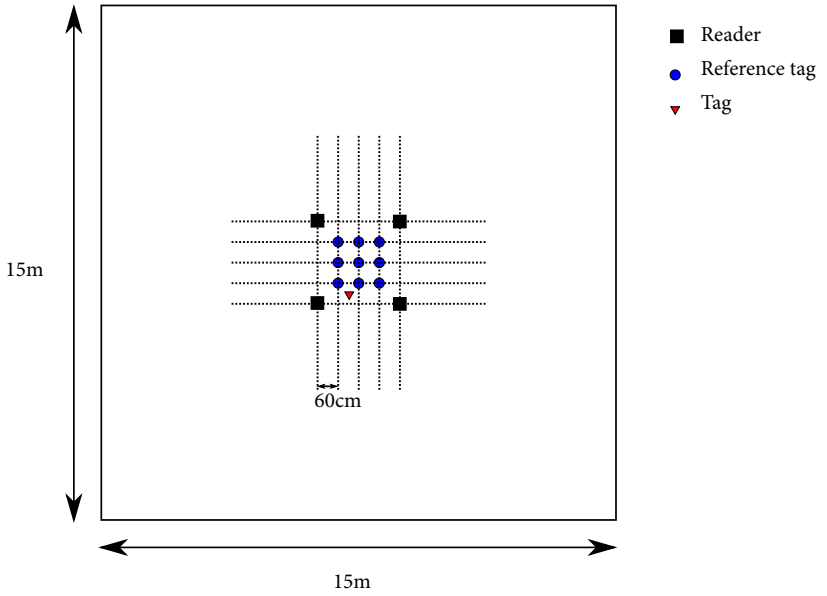

Figure 4.8 – Measurement setup

Table 4.1 – Phase-based average localization error (m) over all possible reader combinations and standard deviation.

k	Number of readers:		
	2	3	4
1	0.60 (0.27)	0.56 (0.29)	0.42 (0.28)
2	0.46 (0.12)	0.47 (0.08)	0.57 (0.11)
3	0.35 (0.09)	0.42 (0.08)	0.44 (0.07)
4	0.35 (0.04)	0.42 (0.05)	0.47 (0.07)
5	0.33 (0.05)	0.28 (0.03)	0.43 (0.04)
6	0.32 (0.05)	0.30 (0.05)	0.45 (0.03)

following results, the number of readers and the number of reference tags, the k in the KNN algorithm, is varied. To select which k reference tags to use, the weighting algorithm of LANDMARC is used. Note that the shown averages in Table 4.1 for different numbers of readers are for all possible combinations of readers, for example for two readers the average is based on the results of six possible combinations of two readers.

In Figure 4.9, results from the localization experiment are given, where the average localization error in meters, for the unknown tag, is given as a function of the k-value. For this measurement the readers were individually used to interrogate all present tags at different frequencies for 32 seconds. This results in about 3500 individual phase and RSSI samples. Based on the phase measurements, a range is

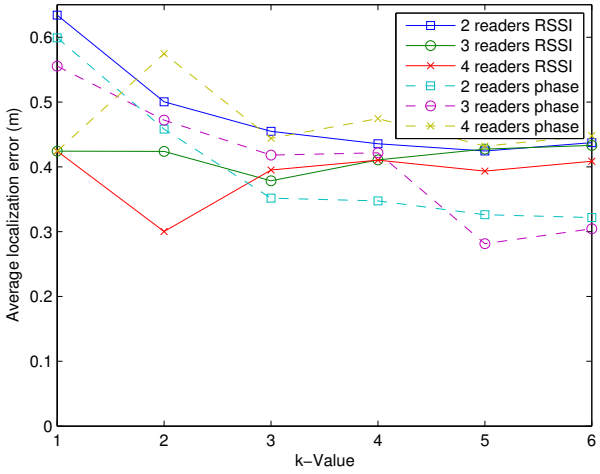

Figure 4.9 – Localization error

calculated, as described in Section 4.2, which is used as distance related measure for the KNN localization algorithm. This process has been repeated six times. Because the reader reports not only phase, but also RSSI for every observed tag, the KNN algorithm is also performed on the RSSI data from the same measurements to compare the results. The RSSI based results can be seen in Figure 4.9 as well. In Table 4.1 the same numbers for phase-based localization are given together with the standard deviation. It has to be noted that the readers were not able to determine a distance measurement for every tag from every reader position. The algorithm skips (reference) tags which are not read by one of the selected readers.

Discussion of the Results

Figure 4.9 shows that the most accurate results are achieved for a system with three readers and k=5 using phase-based measurements. The averages shown for different numbers of readers are for all possible combinations of readers. However, when two opposite readers are used, the results improve. When only two, in the grid oppositely located, readers are used, the error for two readers for $k = 6$ reduces to 0.27 compared to the system using an average of all possible combinations of two readers, with an error of 0.32, showing that using opposite readers yield the best results. Although the exact location of the readers is not needed for the algorithm, it is beneficial to use locations of the readers spaced apart as much as possible, to gain the most diverse information.

The results of the phase-based algorithm are, for some chosen system parameters, better than the RSSI based algorithm. For a k value of 5 this difference is more than 0.1 m, which is a reduction of the average localization error of 25%.

For the phase-based method, using more reader antennas appears to be not beneficial. Environmental changes during measurement can introduce this effect, as the differences are minimal, the exact cause is not investigated further.

Phase-based ranging can have slightly better results with high k values. However, overall these results show that RSSI-based and phase-based localization with the help of reference tags have similar results and an accuracy of about 0.4 meter is to be expected.

Other methods suggested by literature to localize UHF RFID tags based on the KNN algorithm give similar results. The authors of [65] describe an average error 0.83 m, however, the measurement area (4 m) is bigger than in our case. The authors of [27] use sixty reference tags to localize items in a bookshelf. The best average localization error the authors achieve is 0.64 cm. Several extensions to the original KNN exist. The authors of [26] describe different approaches based on the KNN algorithm and achieve an average localization error of 0.33 m with the original algorithm with a range of 4 m, which can be lowered by 34% by using a combination of optimizations.

Furthermore, the effect of multipath and stray readings is profound. A tag located well beyond the normal read range can spontaneously start to backscatter information. In general, these stray reads are known to be problematic in a portal like environment[2]. In such a situation, an attempt is made to limit the read zone to a portal like structure, a door for example. Tags should be read when they move through the door and not when they are located in the shopping-window. This is one of the reasons to investigate fine-grained localization further in the following chapters.

In [67] phase-based measurements of tags moving past a reader show a parabolic relation. In the following section, experiments will be done to evaluate the use of phase measurements to discriminate between stationary and moving tags.

4.5 Movement Detection

The previous sections assumed a stationary situation in which the tag does not move. As described, the observed phase is related to the distance. In the case of movement of a tag relative to the reader, the observed phase will change. This section describes these effects and tries to use phase changes to detect movement.

4.5.1 Simulation

Suppose a person with tagged items is walking underneath an antenna fixed to the ceiling. This person walks at a comfortable speed of 1.5 m/s[15]. This is modeled with a tag moving horizontally at a height of 50 cm and an overhead antenna is positioned 2.5 meters above the floor. This means that the distance, r, between tag

and reader changes according to the following equation:

$$r = \sqrt{x^2 + y^2} \tag{4.9}$$

whereby x is the horizontal changing distance and y the fixed vertical distance.

In Figure 4.10 an overview is given, whereby the axes from Equation 4.9 are indicated by x and y. The origin of the coordinate system is defined as the center of the surface of the (patch) antenna. The tags are simulated to move along the x axis, underneath the antenna. Again the distance between tag and reader can be translated into phase and a 2π ambiguity is included. As the phase measurement is symmetrical around the center of the antenna, phase behavior needs to be determined only in case the tag is moved towards or away from the antenna. The simulated phase of a tag moving away from the center is shown in Figure 4.11. Furthermore, the power of the signal, the RSSI, is also simulated, as can be seen in Figure 4.12.

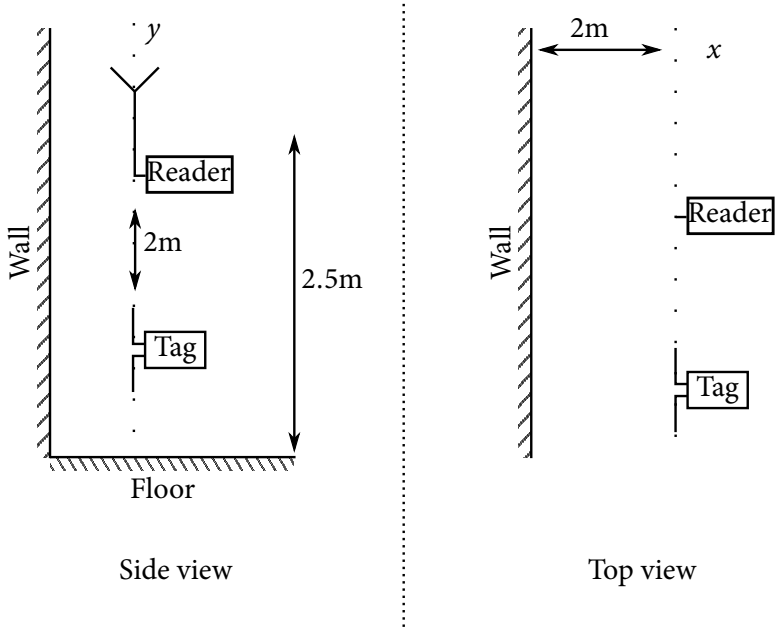

Figure 4.10 – Schematic views of simulation model

Furthermore, reflections from a wall and the floor are modeled. The surfaces in Figure 4.10 are modeled as pure reflective surfaces and a single reflection, namely the reflection with the shortest distance is added. First of all, the floor reflection is added. This reflection does not have a devastating effect on the observed phase compared with the RSSI measurements of Figure 4.12. The RSSI shows strong fading effects and does not decrease monotonically any more. Next, a wall is modeled at a distance of two meters from the reader. In both simulations with reflections

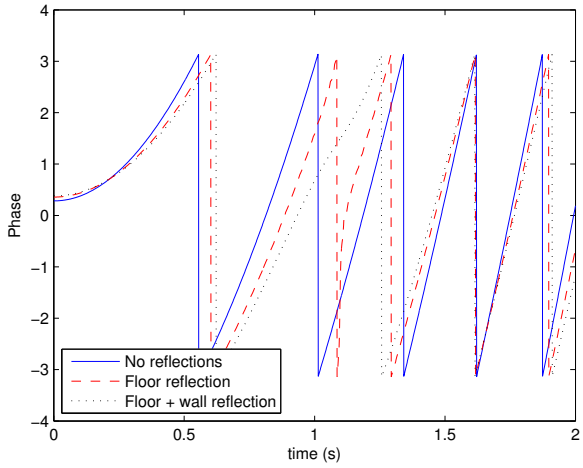

Figure 4.11 – Phase of a simulation of a tag moving away from reader.

the simulated phase still shows a parabolic shape. However, a change in the phase curves can be seen around the one second mark in the simulation with floor and wall reflections in Figure 4.11. The reflections have some effect on the observed phase, but the overall shape of the phase remains the same. Even with reflections the observed phase of received signal will decreases when it moves closer to the reader and the phase will increase when the tag moves away from the reader. This in contrast to the RSSI simulation where the original relation (decreasing RSSI for an increased distance) no longer holds. Furthermore, note that the rate of the phase change is a measure for the speed of the moving tag.

Nonuniform speed differences, a person never walks with a constant gait, increase the nonuniform sampling behavior already present due to the fact that the MAC protocol does not guarantee measurements regularly spaced in time. The protocol might be altered to sample at regularly spaced intervals, however the speed of a tag can (and will) differ in time. Therefore the movement detection algorithm should have some flexibility to detect the global shape of multiple measurements.

In the ideal case with only a direct path, the RSSI behaves parabolic. The RSSI simulations with multipath clearly show the strong influence of reflections. Because the reflections are expected to have little influence on the parabolic shape of the phase measurements, which have to be unwrapped (in contrast to the RSSI measurements), which have to be unwrapped, phase measurements could be used to detect movement of a tag. The parabolic shape (after unwrapping) of the observed phase in Figure 4.11 has to be detected. Furthermore, the direction of movement can be detected by observing the direction of the phase changes. The observed phase decreases when a tag gets closer to the reader. Before looking into detection

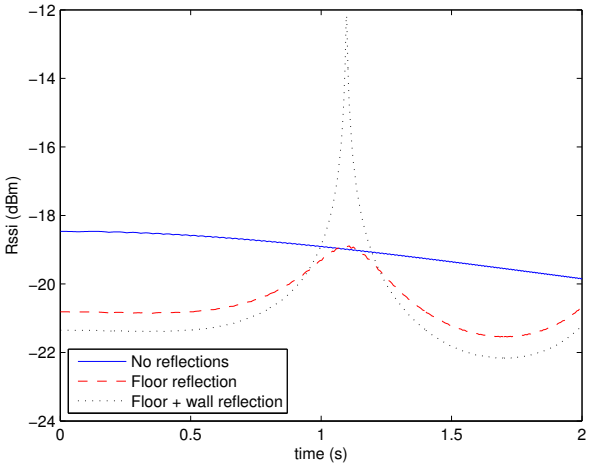

FIGURE 4.12 – RSSI of a simulation of a moving tag.

of moving tags some experiments are done to verify the approach.

4.5.2 EXPERIMENT

An antenna is fixed to the ceiling and connected to the same Impinj COTS reader as used in the localization experiments. A person walks underneath the antenna with a tag in ideal orientation. The person walks at a "normal" almost slow gait, which is about 1 m/s. In Figure 4.13 a typical measurement is shown and two passes can be seen. The person with the tag walks twice underneath the fixed antenna in reversed direction. From 0 to 2 seconds in the forward direction and from 6 to 8 seconds in the reversed direction.

Discussion of the Results

As expected, phase wraps can be observed in the phase measurement shown in the top part of Figure 4.13. The phase makes irregular jumps during the time the tag moves underneath the antenna, the first and last 2 seconds. A first attempt is done to solve the phase jumps as can be observed in the middle part, but a resolution problem can be seen when the tag is underneath the reader; the reader is unable to observe the moving tag fast enough to follow the exact phase trajectory.

Due to the MAC protocol, the phase measurements can be seen as irregularly sampled data points. As explained before, with the current setup we have no fine grained control on the moment a tag is read. Because the sampling is irregular, the measurements cannot be unwrapped and detecting the expected parabolic shape becomes difficult. Next, detection of a moving tag is investigated. The proposed detection is based on the variance of the phase of the signal and makes use of the

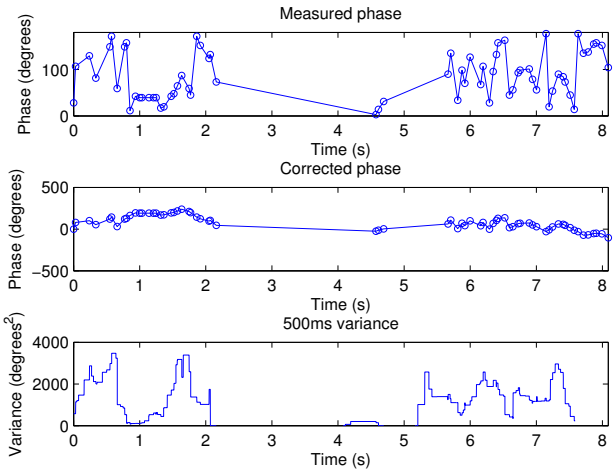

Figure 4.13 – Moving tag

fact that subsequent phase measurements change more than a phase measurements of a stationary tag. In a time invariant channel, subsequent phase measurements should be the same as there is no change. In the bottom part of Figure 4.13 the standard deviation over 500 ms of the unwrapped phase measurements is shown. The variance is calculated over all the samples taken the last 500 ms. And can be used to detect a moving tag based on multiple phase measurements.

Figure 4.14 shows a very slowly moving tag, firstly towards the portal, passing the portal and then leaving the portal. In this figure a parabolic shape is clearly present. The tag in Figure 4.14 moves about twice as slow compared to tag moving at 1 m/s shown by Figure 4.13. Because a person at 1 m/s can be tracked with the current read rate, to track a person moving at 2 m/s the reader has to be (at least) twice as fast. However, faster interrogation is not possible with EPC Generation 2 tags.

These results show that movement detection based on the phase measurements using the existing Impinj-based hardware setup is only possible at low moving speed due to the limited read speed. Recent research [80] shows that with help of a COTS reader placed on a cart, which moves slowly with 0.1 m/s perpendicular to a row of tagged books, a similar parabolic phase pattern can be measured for every tag. Based on this information the order of the books on the shelf is derived. Furthermore, very recent research [88] indicates that it is possible to detect movement, strictly following a model, of a carrier with multiple tags spaced centimeters apart and which is slowly moving (0.27 m/s). Using a Kalman filter the order of the tags on the carrier is determined.

There is no control at which moment a tag is read. The tag uses the MAC protocol described in Chapter 2 to select a slot randomly. An option to be investigated in the

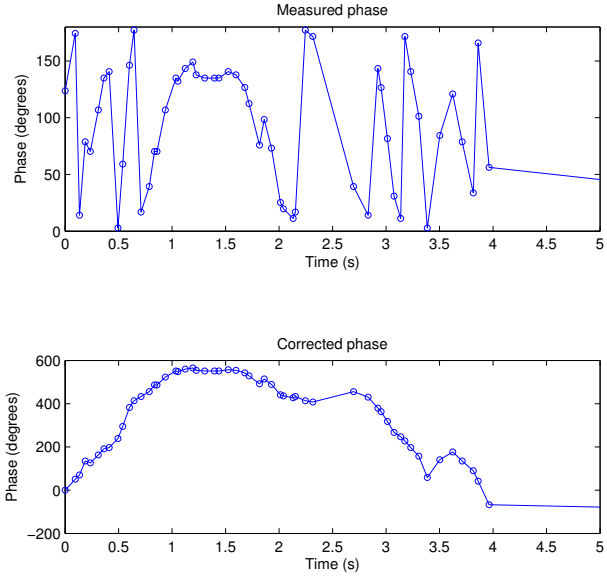

Figure 4.14 – Observed phase of a slowly moving tag

future is to query a tag multiple times, which is supported by the EPC Generation 2 standard, but not by the current reader firmware. By not sending a *QueryRep* command but reading some memory in the same tag, another phase measurement could be obtained without violating the EPC Generation 2 protocol. Furthermore, nearby (stationary) tags will also be read by a reader, further reducing the effective read rate as the time a reader spends on reading the tag we want to track is reduced. With clever use of session-flags this effect can be partially counteracted.

4.6 Conclusion

By using multiple frequencies and measuring the phase of the backscattered signal, a distance estimate between a tag and reader can be made. Even within a reflective environment (Figure 4.4) the phase-frequency relation is stable and can be used as measure for distance. In the experiments with EPC Generation 2 tags an average error of 0.42 m is made in an empty room, with a tag located 0.5 m to 2.2 m from the reader. The errors made during distance estimation directly influence the localization algorithm. Furthermore, the environment has a strong influence on the measurements, so the observation area should be densely populated with reference tags. A 2-dimensional localization experiment is done in a large room to avoid scatter. Based on the measured data, the KNN algorithm is able to estimate the location with a similar error with the help of phase measurements compared to RSSI measurements. An accuracy of 0.4 m is observed.

To discriminate between stationary and moving tags in a portal and detect whether tags are moving towards or away from the reader, the use of phase measurements is investigated. Measurements show that this is possible if tags are moving slowly. At higher speeds, the used COTS reader is unable to produce phase measurements of a tag fast enough due to the protocol and implementation choices made by the manufacturer. The EPC Generation 2 protocol was clearly never meant for localization purposes. With the current setup, detecting moving tags accurately is not possible. However, a possible solution is to implement a different tag reader protocol. If a single tag could be read more often, more phase measurements can be taken, which prevents phase ambiguity because phase wraps can be detected and therefore corrected. Experiments show that a doubling of sample rate makes phase reconstruction possible for tags moving at walking speed.

5 Near Field Localization

Abstract – *This chapter presents a near field localization system based on a phased array antenna system for reading UHF RFID tags. To estimate angle and range, the proposed system uses a two-dimensional MUSIC algorithm. A four-channel phased array antenna system is used to experimentally verify the estimation of angle and range for an EPC Generation 2 tag. The system is calibrated for phase offsets introduced by the analog reception hardware as simulations show the sensitivity to these offsets. The angle can be estimated with an average error of 3 to 4 degrees and range of 0.3 m. Results from an anechoic room show increased performance and the validity of using a near field model. A possible solution for the high error is researched, it is possible to calibrate the system for every angle to remove any instrument introduced error. This extensive calibration suffers from increased variance due to repeating steering vectors.*

5.1 Introduction

Localization systems based on distance, via RSSI or phase measurements, as discussed in the previous chapter prove to be inaccurate and require readers in physically separated locations. With the help of so-called phased array antenna systems, an extra parameter can be measured: the Direction of Arrival *(DOA)*. If also range can be estimated with a single array, 2D localization can be done from a single location. A reader and phased array can be combined in a single device to limit installation costs.

A well known technique to find the DOA of a signal is to use an array of antennas. In Chapter 3 some approaches described in literature were discussed.

Large parts of this chapter have been published in [JH:2].

In traditional array processing, the signal is assumed to originate from the far field and only a direction is estimated. Depending on the direction, every antenna receives the same signal with a (slight) time difference. By assuming a narrowband signal, similar to previous chapters (see Section 2.1.3) the time difference translates into a phase change. Based on this assumption, many algorithms to determine the DOA have been developed like MUSIC[78] and ESPRIT[76].

As explained in Chapter 3, the data signal transmitted by EPC Generation 2 tags can be treated as a narrowband signal. Furthermore, the distance over which UHF RFID operates is small compared to the size of the array when multiple antennas are used as a phased array. Therefore, the far field model cannot be completely justified. In this chapter we try to exploit the near field model in combination with a four channel phased array to estimate an angle and range of a nearby tag.

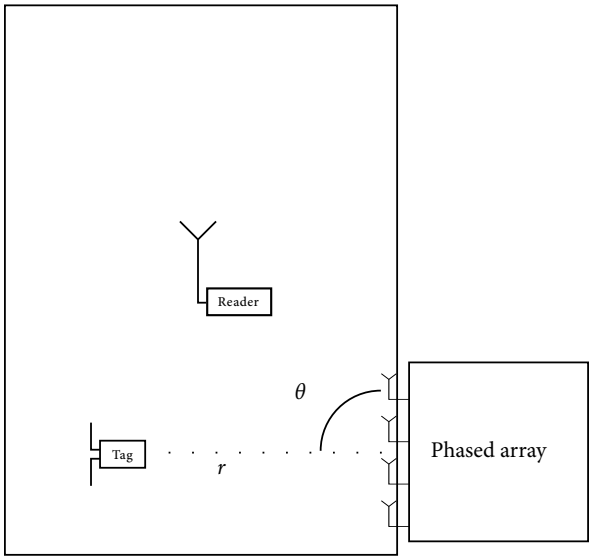

Figure 5.1 – Top view of single phased array, with four antennas, for estimation of angle θ and range r, showing a separate reader for reading the tag information.

In a conventional reader setup, the tag's backscatter is received by a single antenna which is also transmitting a continuous wave to power the tag. However, backscatter does not necessarily have to be received by the same antenna that transmits the continuous wave. In case it is the same antenna, it is known as a mono-static setup. In case of a separate antenna the setup is said to be bi-static. Of course the signal can be received by multiple antennas and in the setup presented in this chapter the signals are received by multiple antennas placed at regular intervals on a line to form a Uniform Linear Array *(ULA)*, as depicted in Figure 5.1. The Radio Frequency *(RF)* power that is needed to energize the tag is transmitted by a single separate reader.

5.2 Phased Array

Phased arrays can be used to estimate the angle of arrival of signals originating from RFID tags[12]. A common method is to use digital angle estimation algorithms to determine the DOA of the received signal. These algorithms make use of the fact that the signals propagating from the tag to the different antennas of the phased array, undergo a different propagation delay. By measuring this delay, the DOA can be estimated and because of the small bandwidth, this propagation delay translates into a phase difference between the receiving antennas, hence the name: phased array[85]. A major cost in terms of money and energy are the ADCs needed to convert the signals from the analog to the digital domain and the high-precision digital signal processing part. Since each element of the phased array contains a complete receiver, the total number of antennas is limited for practical applications.

To reduce cost, time-multiplexing of ADCs between antennas could be considered, but the signals received by all antennas in a single array need to be sampled at the same time to be able to estimate a direction of arrival. Time-multiplexing antennas and ADCs between arrays is only possible when there are no changes in the system, for example tag movement. This assumption is not guaranteed to be valid in our application domain. For that reason, in this thesis a setup with a separate receiver for each antenna is used.

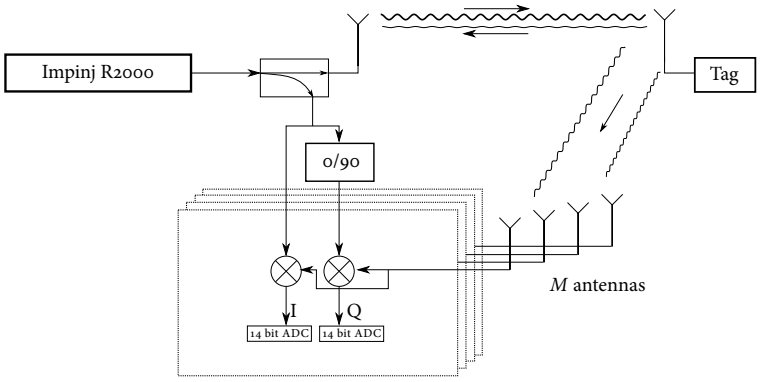

Figure 5.2 – Schematic overview

In Figure 5.2 an overview of the phased array hardware is given. A separate reader is used to energize nearby tags and interrogate a single tag. When a tag transmits information to the reader, the M antennas of the phased array intercept the same signal transmitted by the tag. At each antenna the tag signal is received with a phase shift depending on the angle and the distance between the tag and antenna.

In Figure 5.3 a more detailed overview of a traditional analog frontend including filtering and amplification is shown. This setup is known as a direction conversion

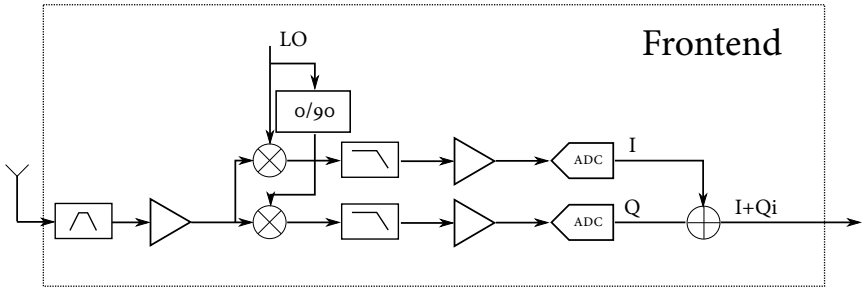

Figure 5.3 – Frontend

receiver[41]. Every channel is down-mixed by a mixer using an attenuated version of the transmitted carrier into an in-phase and quadrature baseband signal. This attenuated version of the transmitted carrier is tapped off with the help of a directional coupler as shown in Figure 5.2. During transmission of the continuous wave, this attenuated version is used for demodulation of the signal received by the array. Each baseband signal is sampled by two synchronized (sampled at the same time) ADCs, after which further processing is performed in the digital domain. For further processing the in-phase and quadrature signals from the ADCs are combined to form a single complex representation.

As described in Chapter 3, the use of phased arrays is proposed before to estimate an angle of arrival. For example [12] uses four phased array antenna systems consisting of three antennas each, located on corners of a square to localize tags within the square. A disadvantage of this technique is the requirement to use multiple antenna arrays. The system proposed in this chapter tries to use only a single antenna array. In [42] a circular, eight antenna array is used to estimate the angle of arrival in two dimensions using the MUSIC algorithm. In general, algorithms that estimate an angle of arrival assume far field conditions. However, in relation to the dimensions of the phased array, there is no clear separation between the near and far field. In the following section we validate the assumption of the use of a near field model with respect to the array; an assumption which allows estimation of range and angle with a single array.

5.3 Signal Model

In Figure 5.4, a schematic overview of the phased array setup is shown. In this figure, θ is the DOA that is to be estimated based on the signals received by the M antennas. The distance, d, between the antennas is equal to half the carrier wave length, $\frac{1}{2}\lambda$[85].

The signal backscattered by the tag, $s(t)$, can be seen as arriving from a certain angle, θ, at the array. The backscattered signal propagates along a sphere and is sampled by the array. If the tag is positioned within the near field of the array, com-

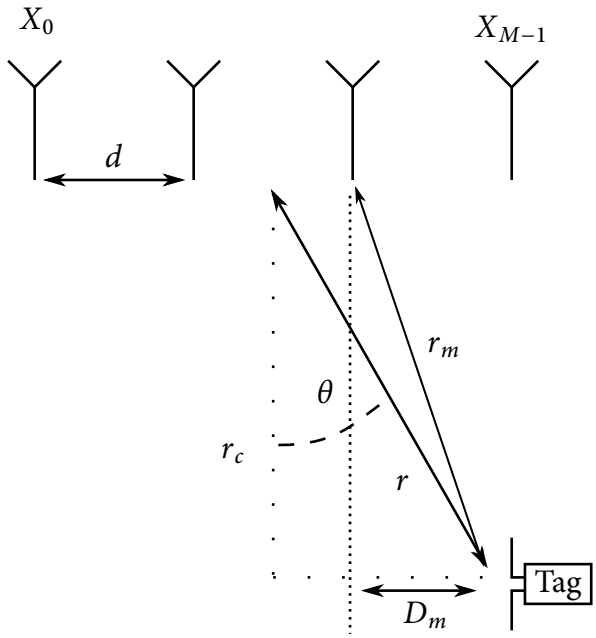

Figure 5.4 – Near field model

pared to the sampling of a plane wave, there is some additional phase difference depending on the range. Although there is a gradual transition between near and far field, a commonly used distance to separate the near and far field is the Fraunhofer distance $R_{farfield} = \frac{2D^2}{\lambda}$, whereby D is the largest dimension of the antenna and λ the wavelength[13]. An array of antennas can be seen as one antenna in this formula. Assuming four antennas spaced $\frac{1}{2}\lambda$ apart at UHF RFID frequencies, this near field range is about 1.5 meters. When the size of the array is increased to six antennas the near field extents to more than 4 meters.

The distance between a tag and an individual antenna of the array is modeled by Figure 5.4. Goniometric rules give the minimum distance between the array and the tag: $r_c = r\cos(\theta)$, where r is the distance to the centerpoint of the array. The parallel distance between a tag and the mth antenna is given by $D_m = r\sin(\theta) - \mu d$. Hereby m indicates the number of the antenna under consideration out of the M antennas and d resembles the spacing between the antennas. μ indicates the distance from the center of the array, when the antenna index m starts counting at 0, μ is defined as $(m - \frac{M-1}{2})$. Finally, the distance between the tag and the mth antenna is then expressed as

$$r_m = \sqrt{(r_c)^2 + (D_m)^2} \tag{5.1a}$$

$$r_m = \sqrt{(r\cos(\theta))^2 + (r\sin(\theta) - \mu d)^2} \tag{5.1b}$$

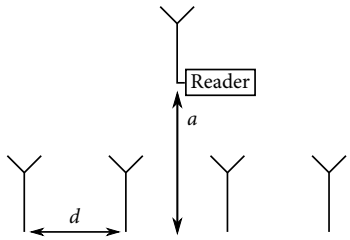

Figure 5.5 – Top view of model showing a separate reader antenna

$$r_m = \sqrt{r^2 + (\mu * d)^2 - 2 * \sin(\theta) * r * \mu * d} \tag{5.1c}$$

As explained before, the bandwidth of the information signal, with a maximum bandwidth of 250 kHz[31], modulated on a carrier of 865 MHz, gives a FB of less then 1%, which justifies the narrowband assumption. Therefore, the shift of the signal in time due to distance can be modeled as a phase shift[5]. Besides a phase shift, the distance between the tag and receiving antenna will influence the amplitude of the received signal. For now this dependence is not included in the model. So, we assume all antennas receive the same signal strength. For experiments shown in this chapter, all channels are normalized before DOA estimation. The signal $X_m(t)$ received by the mth antenna is modeled as:

$$X_m(t) = \sum_{i=1}^{N} s_i(t) * e^{j\frac{2\pi}{\lambda} * r_m} + n_m(t) \tag{5.2}$$

In this equation N denotes the number of signal sources $s_i(t)$ which arrive from different angles and ranges. For now we assume one signal because the MAC protocol prevents tags from simultaneous backscattering, therefore $N = 1$. In Equation 5.2, $n_m(t)$ denotes the additional white noise, r_m is the distance of the tag to antenna m, modeled by Equation 5.1. The wavelength is modeled by λ. In phased array literature the phase shifts modeled by Equation 5.2 for the m antennas are often described in a vector, the steering vector.

In addition to the distance between the receiving antennas and the tag, the distance between the antenna used for transmitting the carrier and the tag will have a phase changing effect. Because a tag reflects the wave transmitted by the separate reader antenna, the distance between the reader antenna and tag is fixed, therefore, the additional phase term is the same for all array antennas. In the experimental setup the reader antenna is placed in the center of the array with a distance of a from the centerline, an additional term is added to Equation 5.1: $\sqrt{a^2 + (r\cos(\theta))^2 + (r\sin(\theta))^2}$ Figure 5.5 gives a top view of the location of the separate reader antenna relative to the antenna array. Furthermore, Figure 5.13 shows a photograph of this setup.

With a far field model, only the DOA of the arriving signals can be estimated. Assuming near field conditions, not only the angle, but also the distance between the

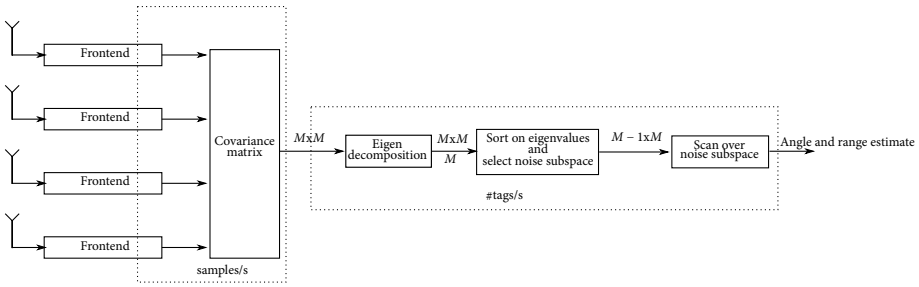

Figure 5.6 – Simplified block diagram of the MUSIC algorithm

tag and antenna array can be estimated. In this chapter the 2-dimensional variant of the MUSIC algorithm[78] will be used in simulations and experiments.

5.4 2D Range and DOA Estimation

Range and DOA estimation based on the near field assumption has received some interest. The traditional 1D (DOA) estimation techniques like MUSIC and ESPRIT have been transformed into 2D (range and DOA) variants. Although a 2D variant of the MUSIC algorithm is straight forward[44], it results in a computationally intensive 2D search. To enable fast computation, this search can be parallelized. The 2D variant of ESPRIT requires higher order statistics and is also computationally demanding but does not require a search[22]. Furthermore, computationally efficient algorithms have been derived[82], which can be less accurate and more susceptible to noise.

The MUSIC algorithm is known for its high resolution and robustness against phase deviations compared with for example the ESPRIT algorithm[76]. The high computational load is of less concern due to offline processing. The results of the 2D MUSIC algorithm will be compared with the results of the 2D ESPRIT algorithm.

5.4.1 MUSIC Algorithm

The one-dimensional MUSIC algorithm is based on the fact that the signal and noise subspaces are orthogonal[78]. Appendix A gives a short overview of the MUSIC algorithm, for more detail see [78] and [72].

The received signals are used to calculate a covariance matrix. Based on the eigenvectors the so called noise subspace is calculated. By scanning over this subspace with possible steering vectors, the orthogonality is tested. In Figure 5.6 a schematic overview of the MUSIC estimation system is shown. In a real-time system, samples are continuously taken by the M ADCs during the reception of data from a single tag. The covariance matrix has to be updated for every set of N samples.

The resulting covariance matrix is only processed once by the following blocks for every tag read. So, the covariance matrix calculations are executed at a speed proportional to the number of samples produced by the ADCs, and the MUSIC algorithm is executed at a speed proportional to the number of tag reads by the reader in a specific time frame. These blocks, operating at different computational speeds are indicated in Figure 5.6 as well.

5.4.2 ESPRIT Algorithm

Next to the MUSIC algorithm, the ESPRIT algorithm is often used to estimate DOAs with the help of a phased array[76]. The ESPRIT algorithm assumes two similar arrays with a known displacement. The elements of the arrays can overlap, something that is typically done to reduce the physical dimensions and number of antennas. Based on the two derived signal subspaces from both sub-arrays, the algorithm is able to determine a vector that rotates the first signal subspace into the second, from which the angle (and range) can be calculated. In Appendix B a more detailed overview of the ESPRIT algorithm is given together with a 2D variant, which was developed by [22]. In the following sections the 2D ESPRIT algorithm is used for comparison with the 2D MUSIC algorithm.

5.5 Simulations

Simulations are conducted to verify the ability of the 2D MUSIC algorithm to estimate angle and range and compare it with the results of the 2D ESPRIT algorithm. An Additive White Gaussian Noise *(AWGN)* channel is used for these simulations, with a resulting signal to noise ratio of 21 dB per communication channel, to simulate a realistic (RFID) environment[66]. Only four antennas are simulated because the intended hardware setup for experiments uses the same number of antennas. The number of samples used to calculate a single range estimation is chosen to be 2048, again simulating the proposed hardware.

In Figure 5.7 the simulation results of ranging estimates of a single tag using 2D MUSIC are shown. The tag signal is modeled to have a fixed angle of 5.75 degrees and the distance is varied as from 0 m to 1 m, which is well within the near field range of the array. It can be seen that the simulation results (labeled Simulation) match the signal model used to describe the true phase shifts (labeled Signal Model).

Every receiver chain is expected to have the same influence on the received signal. However, in a real system the analog filters and wires might introduce a different phase shift and attenuation. These phase and gain offsets, introduced by component tolerances, can add up and a simulation was done where the measured values concerning phase and gain offset per antenna from the used hardware platform are used (see Table 5.1). In Figure 5.7 it can be seen that (uncorrected) phase offsets introduce an error in the range estimation (labeled Simulation with offsets).

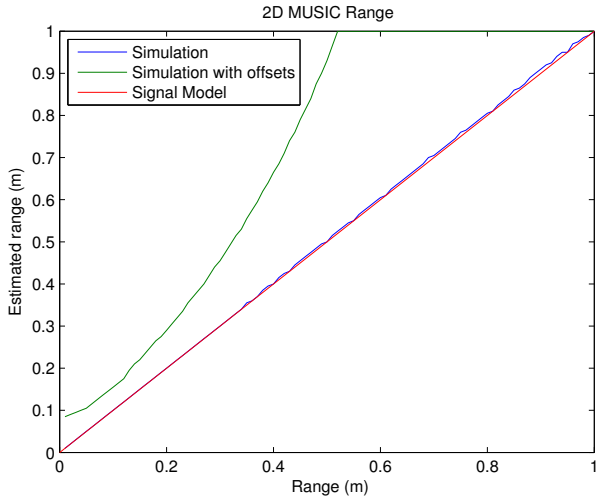

Figure 5.7 – Simulation results: 2D MUSIC range estimation

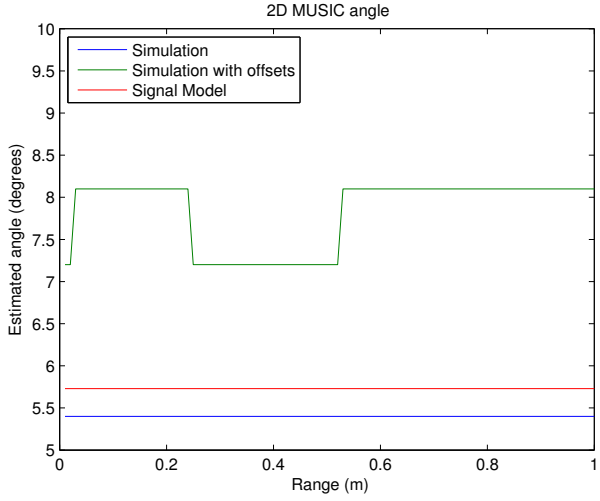

Figure 5.8 – Simulation results: 2D MUSIC angle estimation

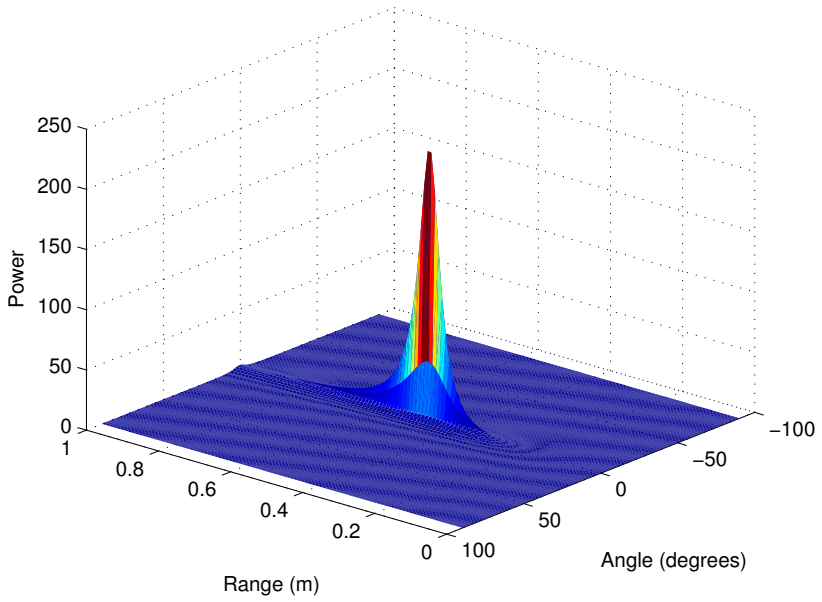

Figure 5.9 – Simulation results: 2D MUSIC pseudospectrum

In Figure 5.8 the simulation results for the angle estimation are shown. Note that the y axis shows angles between 5 and 10 degrees and the true angle is 5.75 degrees. For the angle simulation without offsets the estimated angle is constant, but a bit too low due to the step size used to scan the angle by the MUSIC algorithm (see Equation A.8). The step size is the difference between the angles that are used in evaluating expression A.8. For the simulation with offsets, the estimated angle toggles between two values. The difference between the two angle estimates corresponds to the step size.

A more precise estimation can be made by reducing the step size, thereby increasing computational load. Per application, the trade-off between step-size and computational load has to be made. For a real time system, this is significantly influenced by the rate, possibly hundreds of tags per second, at which tags might have to be localized. The complexity of the MUSIC algorithm increases linearly for every dimension.

These simulation results show that the 2D variant of the MUSIC algorithm is able to estimate the range and angle to a tag if the phase and gain offsets are known. In Figure 5.9 the resulting (pseudo) spectrum of the 2D MUSIC algorithm is shown with a peak in the center of the figure indicating the estimated range and angle of the simulated tag.

5.5.1 2D ESPRIT

In Figure 5.10, the simulation results of the 2D ESPRIT algorithm are shown. The top figure shows the estimated range for a simulation with changing range. The bottom figure shows the estimate angle while the range is changed. Similar observations as for the 2D MUSIC algorithm can be made. When offsets are introduced, the error increases significantly, indicating the need for a calibrated system.

Due to the second order approximation within the ESPRIT algorithm, used to model the expected phase shifts for a certain angle and range, the algorithm makes more errors in range estimation close to the array, shown by Figure 5.10. This is due to the fact that the signal model assumed by the algorithm, given by the second order approximation in Equation B.2, fits the simulated model less well. This also explains the large angle error for a small range. By decreasing the distance between the antennas, localization can be improved close to the array. In a real system however, the antennas have a certain size and a spacing smaller than $\frac{1}{2}\lambda$ might prove difficult.

5.5.2 Influence of Antenna Pattern

In traditional far field DOA estimation setups, the signal is assumed to arrive at the array as a plane wave. Every antenna receives the signal from the same angle. Therefore, if the antennas within the array have angle-dependent, but equal, phase shifts, this introduces no phase errors, as the phase shift can be assumed to be equal for every channel.

However, under near field conditions, the signal arrives at different antennas with a slightly different angle and this can result in a different phase shift. Figure 5.11 shows the measured antenna phase pattern for one of the antennas used for the experiments. Note that this pattern is measured for a single isolated antenna.

The result of the irregular antenna phase pattern is that for every angle there is a small phase difference, which can be included into simulations. Figure 5.12 shows the results of range estimation based on a model that is disturbed by an irregular radiation pattern (Simulation), shown in Figure 5.11, together with the ideal model (Signal Model). The angle is kept constant, at 6 degrees. It can be seen that the introduction of phase differences for every angle introduces additional errors. When the range becomes larger, the error becomes bigger due to the smaller phase differences that have to be detected which are easily distorted by the antenna pattern.

Angle-dependent phase behavior and the phase offset due to hardware imperfections described by Table 5.1, can be seen as instrumental effects. Together with other instrumental effects, like mutual coupling between antennas, these instrumental effects can be corrected based on the difference between expected and measured phases. To exclude unwanted environmental effects like reflections from the measured phases, the correction has to be based on measurements from an anechoic room.

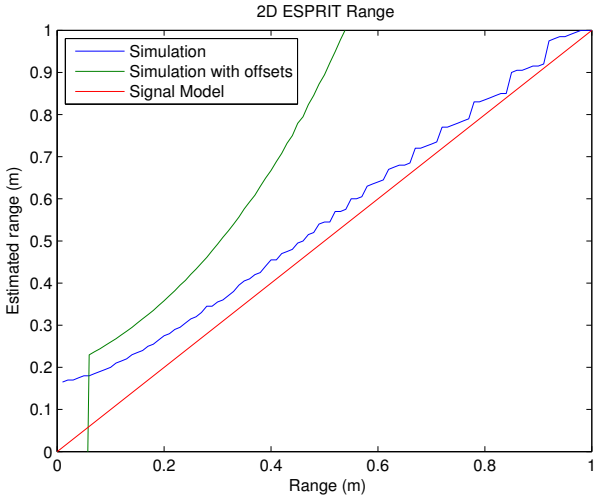

(a) Range

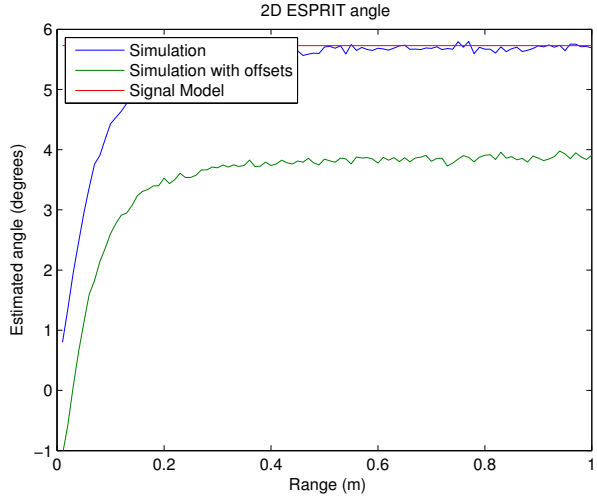

(b) Angle

Figure 5.10 – Simulation performance of 2D ESPRIT estimation.

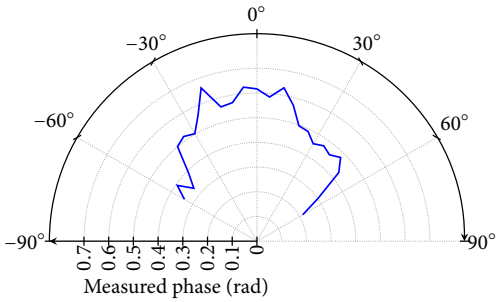

Figure 5.11 – Measured antenna phase pattern

To perform this correction, the steering vectors used in the MUSIC algorithm for a certain angle can be corrected by applying an expected phase shift due to the instrumental effects. This vector containing the phase corrections for a certain angle can be derived from previously measured phases for that angle in an anechoic room. The difference between the observed phases and expected phases of the steering vectors, can be measured and stored for every angle. During estimation in a different environment, the stored correction can be applied to the steering vectors. By using this approach, instrumental effects are calibrated out. This correction option is not available for the ESPRIT algorithm as the algorithm assumes that the antennas have a constant phase factor which is equal for all antennas.

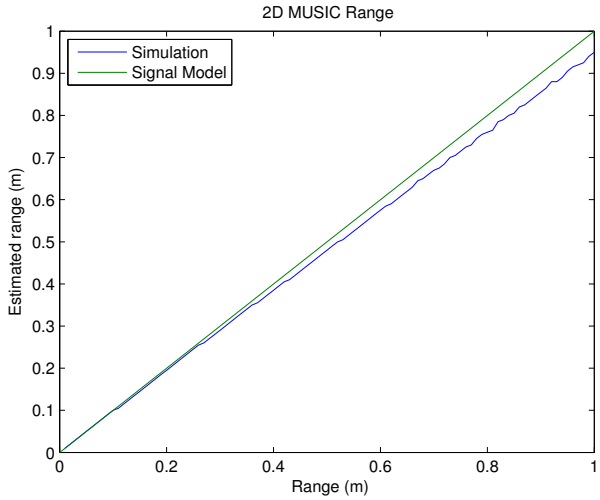

Figure 5.12 – Simulation with angle-dependent phase shifts introduced by the antenna pattern

5.6 Experiments

A four channel receive array is used for experiments. Each channel consists of a patch antenna, Low Noise Amplifier *(LNA)*, down-converter and 14-bit ADC. In correspondence with the simulations, the antennas are spaced $\frac{1}{2}\lambda$ apart. Furthermore, anti-aliasing filters are present in the receiver chains. The digital baseband information is fed into a Digital Signal Processor *(DSP)* board and recorded. The EPC Generation 2 tags need to be energized and an initialization sequence has to be transmitted before the tags start transmitting data, as described in Chapter 2. Therefore, a separate reader is used to communicate with the tag. To identify a tag, the reader has to decode the information. In parallel to this, with the help of a separate phased array, a DOA estimate is made. At a later stage this, estimate can be matched to an EPC reception by the reader to match a location to a specific tag. For these experiments the tags are exited by an Impinj R2000 based, off the shelf reader[47]. To prevent influence of the default hopping behavior, the R2000 is set to use a single frequency. The continuous wave transmitted by the R2000 during tag to reader communication is used by the down-converters of the four array reception channels. See Figure 5.13 for a photograph of the complete setup.

The sampling frequency of the ADCs is fixed at 1200 kHz. This sampling frequency is well beyond the Nyquist rate of the baseband signal. Furthermore, this frequency is chosen to limit the influence of nearby readers. If a nearby reader is using a different channel, it will have a strong carrier frequency which is down-converted together with the tag signal. This frequency component will show up as an alias somewhere in the baseband spectrum. Under ETSI regulations the channels are spaced 600 kHz apart and by selecting the sampling frequency to be twice the channel bandwidth, aliases can be placed out of band. Of every (successful) tag to reader communication period, 2048 stored samples are transfered to a computer for offline processing.

Every channel of the receiving array is designed equally. However, small deviations can add up and introduce phase and gain errors in the form of a bias. To calibrate the system, measurements with known distance and angle are used to calculate average phase and gain offsets for every channel. These offsets are shown in Table 5.1 and are assumed to be caused by component variations.

Table 5.1 – Phase and gain offsets due to hardware imperfections

Antenna	1	2	3	4
Phase offset (deg)	-17.2	-40.1	-22.9	0
Gain offset	1.4	1.6	0.9	1.0

5.6.1 Automated Test Setup

An EPC Generation 2 tag is placed on an automated test setup consisting of a computer controlled servo, aluminium track slider rail and non-conductive stand, as

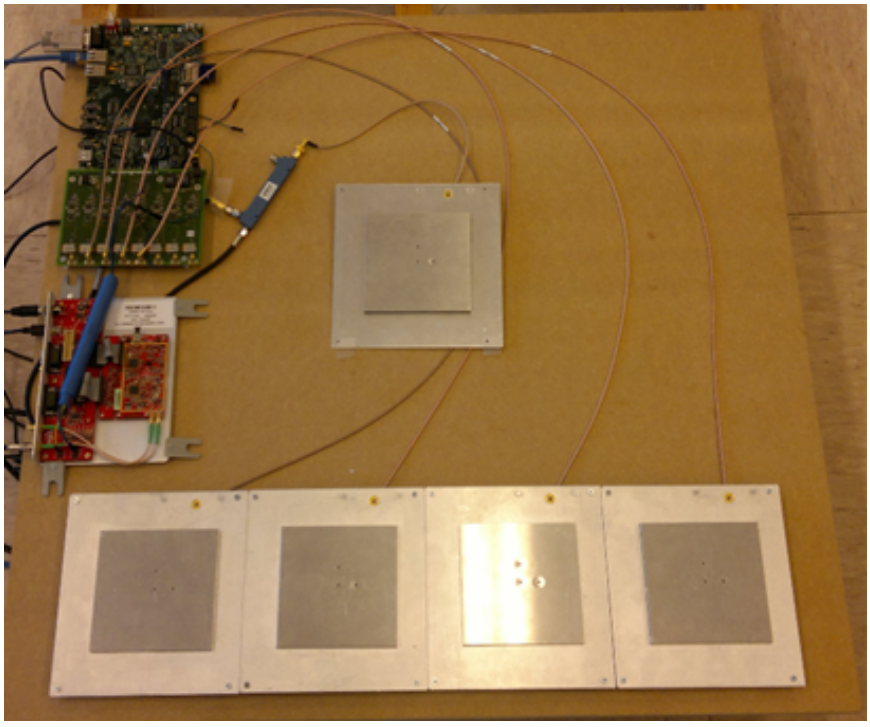

Figure 5.13 – EPC Generation 2 reader and four channel phased array hardware.

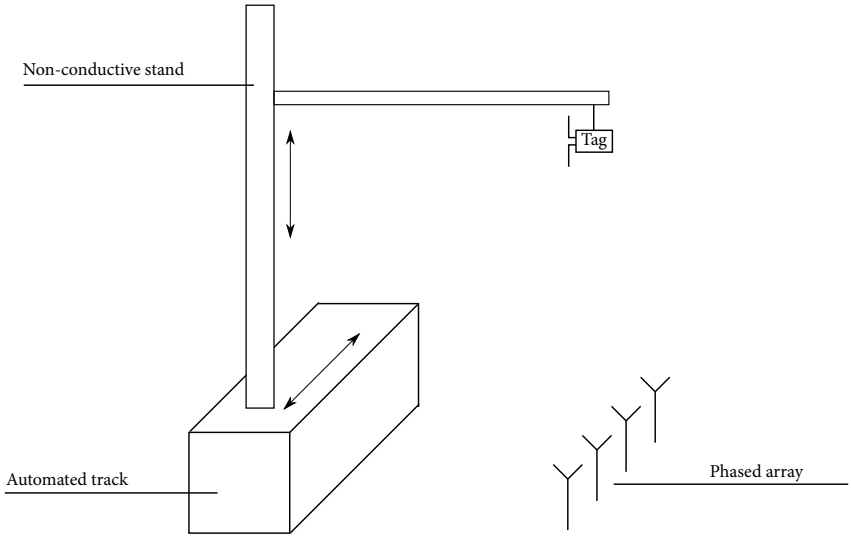

Figure 5.14 – Automated test setup

shown in Figure 5.14. The tag is moved horizontally in discrete steps by the servo. At every stop, the RFID reader starts interrogating the tag and ADC samples from 200 successful tag reads are stored. After a successful run of the servo over the entire horizontal range, the tag has to be manually moved in the vertical direction to measure at a different distance with respect to the array.

5.6.2 RMSE

In the following sections, the Root-Mean-Square-Error *(RMSE)* is used to describe the average error of the estimation algorithms. In general, the RMSE can be seen as the mean of the absolute error made in estimation. It is defined as:

$$RMSE = \sqrt{\frac{\sum_{n=1}^{N}\sum_{i=1}^{M_n}(m_{i,n} - \mu_n)^2}{\sum_{n=1}^{N} M_n}} \tag{5.3}$$

At N discrete steps, a number of estimations is made. The number of estimations or samples taken at every step (M_n) can differ. For example due to randomness in the protocol in experiments. Therefore, the number of samples taken at the nth step is defined as M_n. A single estimation is defined as $m_{i,n}$ and the (presumed) true location is defined as μ_n.

5.6.3 One- and Two-Dimensional MUSIC

DOA

To verify the experimental setup, the one-dimensional MUSIC algorithm is used to estimate the Direction of Arrival *(DOA)*. In Figure 5.15 the results on 1D DOA estimation are shown. This figure shows the average and standard deviation of a measurement run with a 0.75, 1.0 and 1.5 meter distance between the line over which the tag is moved which is parallel to the center line of the array (r_c in Figure 5.4 is kept constant and D_m is changed). Furthermore, it clearly shows the excellent relation between the average estimated angle and the expected angle.

Range

Besides estimating an angle, the 2D MUSIC algorithm is used to estimate a range, as done in the simulations. In Figure 5.16 a range estimation based on experimental data is shown for the same data of which angle estimates are shown in Figure 5.15. In this figure the estimate and expected range are shown. What immediately stands out is that the error is much larger and irregular compared to the DOA estimation. The figure shows that the 2D MUSIC algorithm introduces errors between -60% and +120% in room #1, the large empty office described in the previous chapter. Figure 5.17 shows the results for room #2, a typical office, and room #3, the anechoic

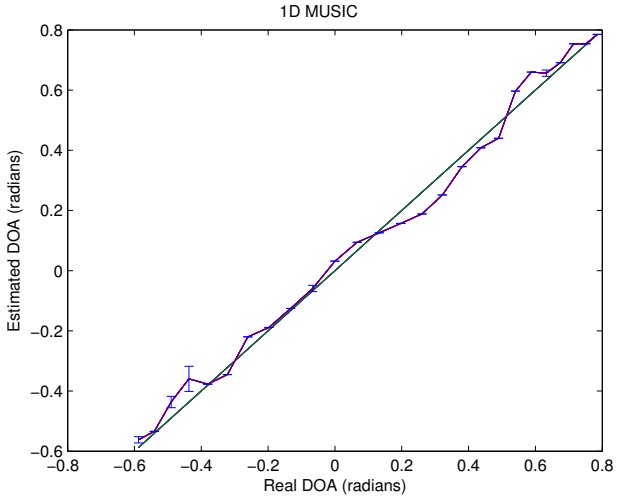

(a) 75 cm

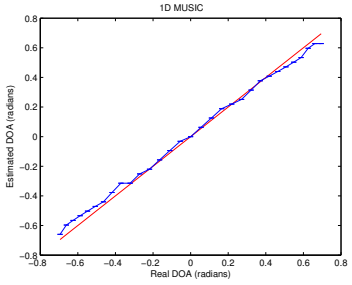

(b) 100 cm

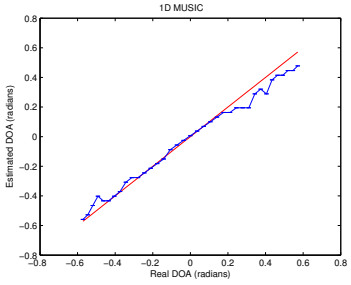

(c) 150 cm

Figure 5.15 – 1D MUSIC DOA estimation based on measurements at different distances in room #1.

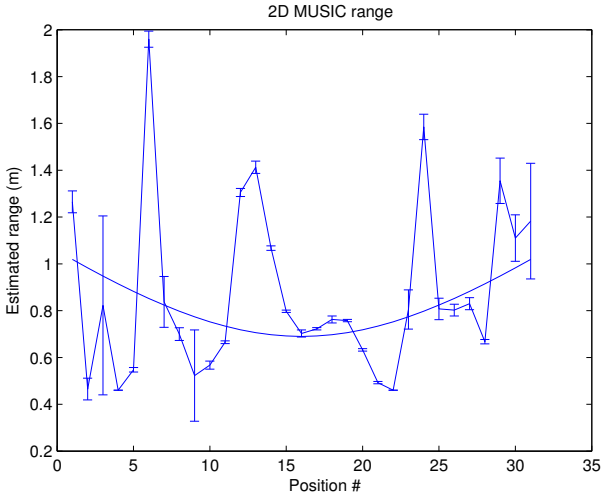

Figure 5.16 – Range estimation in room #1

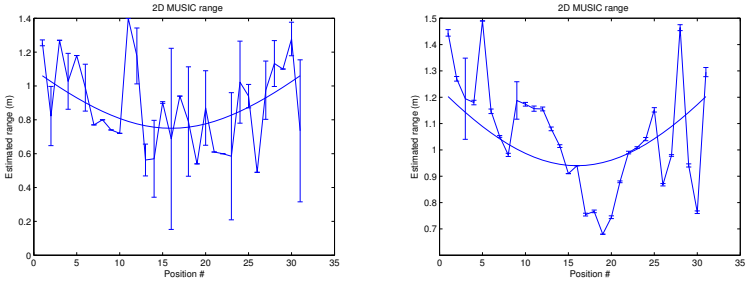

(a) Room #2 (b) Room #3

Figure 5.17 – Range estimation in room #2 and #3

room at Nedap. Furthermore, Table 5.2 shows the RMSE results over all angles for all three rooms. For a single measurement position of the tag, the deviations are small (the variance of the estimations is low) as shown by the error bars in Figure 5.16, for individual measurement positions. In room #2 the range estimates appear to have a larger variance, most likely due to reflections. Room #3 clearly shows that the measurements in an anechoic room are stable.

The table shows that the DOA estimates of a 1D MUSIC algorithm are comparable with the estimates of a 2D algorithm. This holds for the results of both normal rooms.

Table 5.2 – Root mean square error of estimated DOA and range using (2D) MUSIC.

	DOA (deg) 1D MUSIC	DOA (deg) 2D MUSIC	range (m) 2D MUSIC
Room #1 (empty)	3.31	3.05	0.30
Room #2 (office)	4.06	4.11	0.24
Room #3 (anechoic)	1.15	0.96	0.19

For comparison, the experiment is also done in an anechoic room (room #3) and results are presented in the third row of Table 5.2. These result show that the far field assumption made by the 1D MUSIC algorithm is indeed not completely valid. Indicated by the fact that the 2D MUSIC algorithm is able to estimate the angle with a smaller mean error than the 1D MUSIC algorithm in the anechoic room, the model mismatch increases the error for the 1D MUSIC algorithm. Furthermore, the anechoic room gives much better overall results, which gives a strong indication that the errors are caused by multipath effects. The algorithm is looking for the small phase difference between the far field and near field model, which is difficult in normal rooms, leading to a similar angle estimation for the far and near field model and large range estimation error.

Related literature gives comparable values. The average angle estimation error of 3.3 degrees (Table 5.2, first row, second column) is comparable with the reported 3.6 degrees by [54] based on DOA estimation of passive UHF RFID tags with the help of a three channel phase array. The authors of [43] achieve a mean error of 2.8 degrees with the help of an eight channel circular array and passive tags. Using active UWB tags and a phased array, the authors of [14] achieve a mean angle estimation error of 2.7 degrees.

The mean range estimation error of 0.30 m (Table 5.2, first row, fourth column) is 32% better than the range estimated based on phase measurements at multiple frequencies of 0.42 m in the previous chapter. In the anechoic room the range estimation is even better. However, for estimating range by a phased array, more hardware and computational complexity needs to be added to achieve this result compared to localization systems based on a single reader.

Results from the anechoic room show that multipath effects have a significant effect on the estimation results. However, the effect of the offsets introduced by hardware, like the angle-dependent phase shift, as explained in Section 5.5.2, is not taken into account. In the following section, calibration for this angle-dependent phase shift is elaborated.

5.6.4 Angle-Dependent Calibration

The received signals appear to be influenced by effects that are not modeled. To separate the environmental effects from instrumental effects we calibrate the system in the anechoic room and use these derived calibration values in room #1 and room #2.

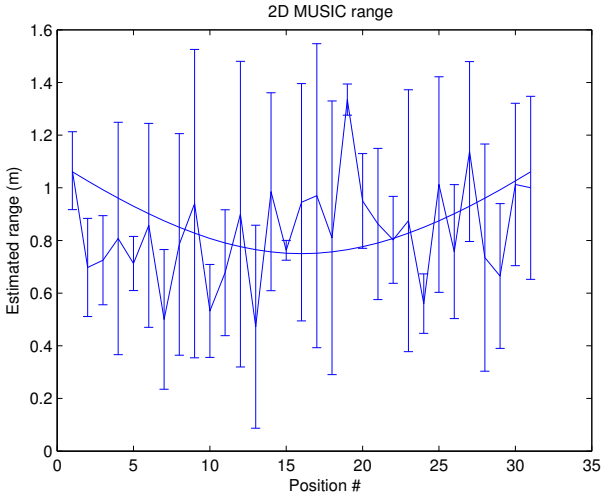

Figure 5.18 – Calibrated range in room #1

The first 20 samples of the 200 samples of every measurement position are used to calibrate the array.

The known angle is used to calculate a steering vector based on the ideal model. The difference between this modeled steering vector and the vector that is orthogonal to the experimental data, based on the null vector of the noise subspace, is stored as calibration vector for that angle. The result is calibration data that is different for every antenna and describes the phase shift for every angle.

During estimation in rooms #1 and #2, the steering vectors are again calculated based on the ideal model and subsequently changed, based on the stored calibration values. Intermittent values are interpolated. For the following results, the system uses this calibration as correction of the signal model.

As can be seen by the more closely matching curves in Figure 5.18, this system is able to determine the average range more accurately than the uncalibrated system, but there is a high standard deviation. Figure 5.19 shows the estimated angle. Due to the calibration, the system is unable to estimate the angle accurately. See the following subsection for an more detailed explanation. This can also be seen in Table 5.3. In this table the results from table 5.2 are repeated and extended with the 2D MUSIC angle and range estimates in case of calibration. The calibrated angle measurements for 2D MUSIC have a high average error, similar results are obtained for room #2 (graphs of range and DOA estimates are not shown here).

Note that calibration is only used for 2-dimensional estimation and therefore no results for the calibrated room are given for 1D MUSIC.

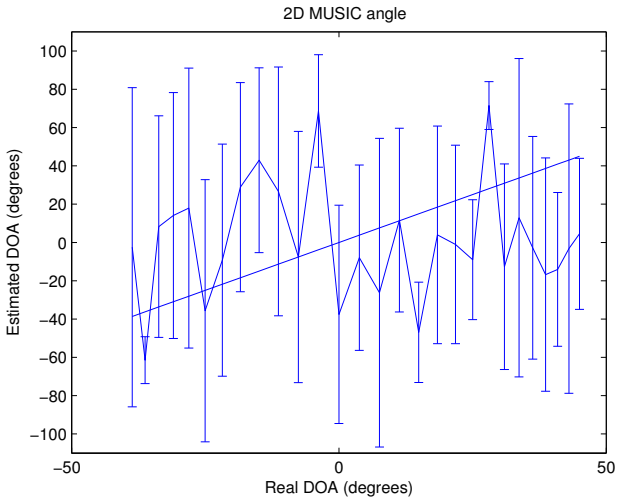

Figure 5.19 – Calibrated angle in room #1

Table 5.3 – Root mean square error of estimated DOA and range using (2D) MUSIC including calibration results.

	DOA (deg) 1D MUSIC	DOA (deg) 2D MUSIC	range (m) 2D MUSIC
Uncalibrated room #1 (empty)	3.31	3.05	0.30
Calibrated room #1 (empty)	-	39.84	0.22
Uncalibrated room #2 (office)	4.06	4.11	0.24
Calibrated room #2 (office)	-	49.10	0.27
Uncalibrated room #3 (anechoic)	1.15	0.96	0.19

Calibrated 2D DOA Estimation Performance

The results of DOA estimation based on the calibrated 2D MUSIC algorithm are unexpectedly worse than the uncalibrated case. The explanation is the irregular shape of the calibration function. The MUSIC algorithm scans the noise subspace with steering vectors looking for orthogonality. Wrong steering vectors produce an unwanted peak in the spectrum. An example of the MUSIC pseudospectrum produced by using the calibration values is shown in Figure 5.20, showing multiple peaks which introduces errors in the final estimation.

This error increasing effect can be illustrated by examining the effect of changing the steering vectors on angle estimation with calibration data. With the help of traditional beam-scanning, the angle of a signal arriving at an antenna array can be estimated, similar to MUSIC. This process is more intuitive than DOA estimation by means of MUSIC and therefore used for this analysis. Beam-scanning alters

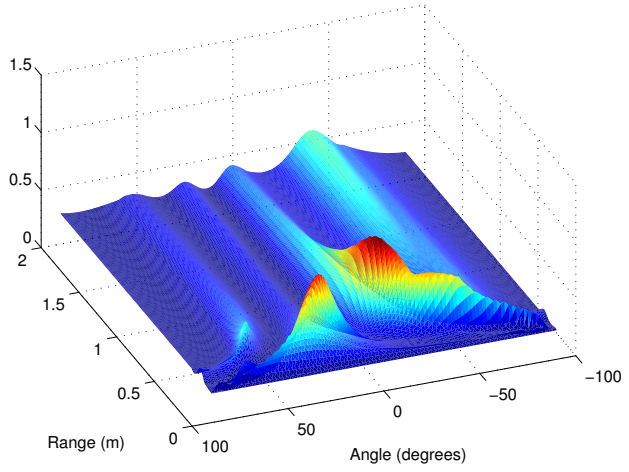

Figure 5.20 – 2D MUSIC pseudospectrum showing multiple peaks due to calibration.

the steering vectors for every possible angle and searches for the angle whereby the strongest signal is received. To calculate the power received by the array from a certain angle, the individual antenna signals are multiplied (phase shifted) with the elements of the steering vector. The resulting signals are summed and the power of the resulting signal is calculated as power from the angle belonging to the used steering vector. This process is also known as beamforming, as the phased array forms a beam into a certain direction[85].

The power for multiple angles can be plotted in a power-angle graph, called a beam pattern. The angle with the highest power is assumed to be the angle of the signal under investigation. Assume a noise-free situation and a four channel antenna array with a signal arriving at an angle of 0 degrees. Figure 5.21 shows the beam pattern in case steering vectors are based on an ideal model. The peak at 0 degrees clearly shows that the signal is arriving from this direction.

When the calibration values from the anechoic room are used to change the steering vectors, the beam pattern gets distorted and multiple peaks become visible, as can bee seen in Figure 5.22. The wrong angle estimate is made if the angle with the highest received power is chosen. This is the same process that creates multiple peaks in the 2D MUSIC spectrum and causes the increased error in the 2D MUSIC results based on calibration.

Concluding, using an angle-dependent calibration function derived from measured data introduces a large error in the DOA estimation and the range performance is not consistently improved. Using an irregularly shaped calibration vector is therefore not helpful to improve the accuracy of 2D estimation.

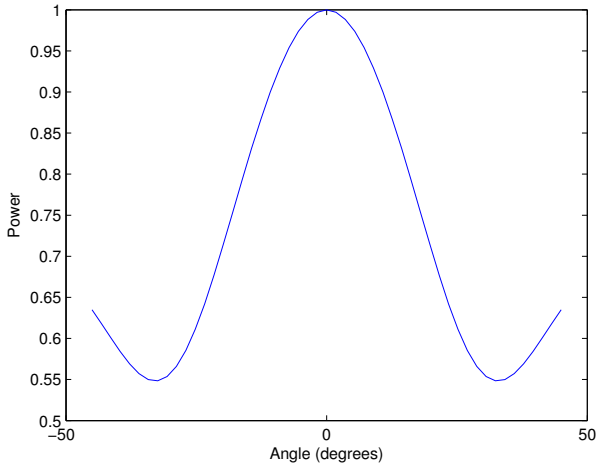

Figure 5.21 – Beam pattern without calibration

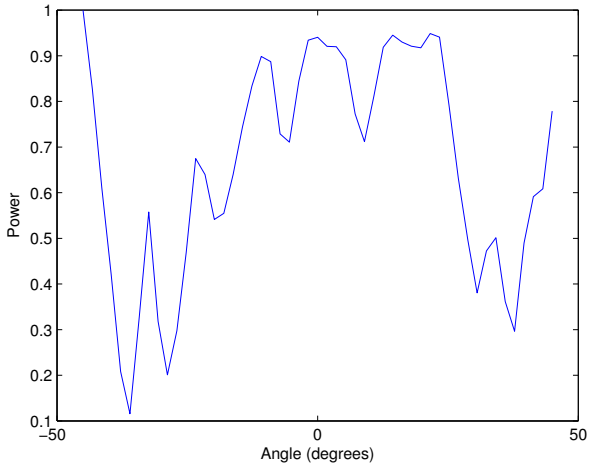

Figure 5.22 – Beam pattern with angle calibration

5.6.5 2D ESPRIT

The data is also processed by the 2D ESPRIT algorithm. In Table 5.4 the results are shown for the 2D ESPRIT algorithm and to facilitate easy comparison, the numbers for the uncalibrated 2D MUSIC algorithm from Table 5.2 are repeated. Note that the 2D ESPRIT does not scan over the possible angles, making it impossible to include angle-dependent calibration.

In Figure 5.23 the average range and angle estimations are shown for the measurements in room #1. It can be seen that near the edges of the array the 2D ESPRIT algorithm makes an unwanted jump in angle. This is due to the large spacing between the antennas as 2D ESPRIT needs $\frac{1}{4}\lambda$ spacing for unambiguous estimation[22]. In Table 5.4 the error is calculated for the part of the estimation graph without phase jumps. Based on the numbers given by the table, it can be concluded that the overall performance of 2D ESPRIT is worse compared to 2D MUSIC, except for the performance of the 2D ESPRIT angle estimation in the anechoic room. The RMSE of the 2D ESPRIT angle estimation for the anechoic room is 0.93 degree, compared to the 0.96 degrees for the 2D MUSIC algorithm. This 3% decrease can be explained by the fact that only the center part of the measurements is taken into account, the 2D MUSIC algorithm uses the complete range of angles. Near the edge of the array, DOA estimation is known to be problematic[85], making the comparison a bit unfair. Even by excluding the edges, the 2D ESPRIT algorithm performs worse in a realistic scenario based on the numbers shown in Table 5.4. The large estimation errors, especially in range, by the measurement in the second room are due to a strong outlying measurement with low variance. Excluding this outlier the average range error decreases to 1.68 m.

Table 5.4 – Root mean square error of estimated DOA and range. Note that 2D ESPRIT is only evaluated over part of the angle.

	DOA (deg) 2D ESPRIT	range (m) 2D ESPRIT	DOA (deg) 2D MUSIC	range (m) 2D MUSIC
Uncalibrated room #1	11.59	0.45	3.05	0.30
Uncalibrated room #2	14.91	19.33	4.11	0.24
Anechoic room #3	0.93	0.26	0.96	0.19

These experiments show that the 2D ESPRIT algorithm is able to estimate range and DOA in an environment with minimal reflections, at least over a part of the available angles. However, in a more challenging environment, the 2D MUSIC algorithm outperforms the 2D ESPRIT algorithm.

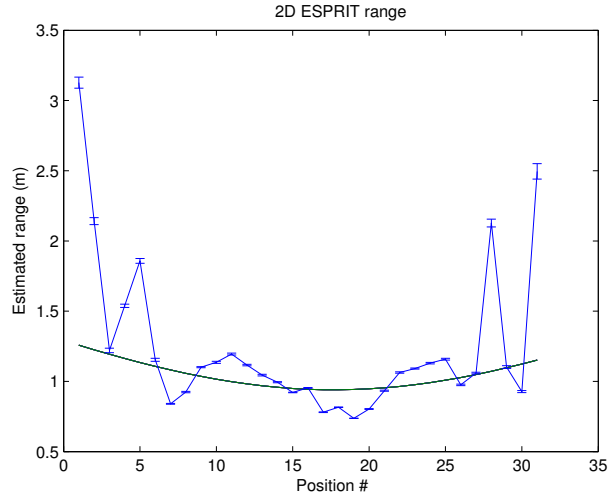

(a) Range

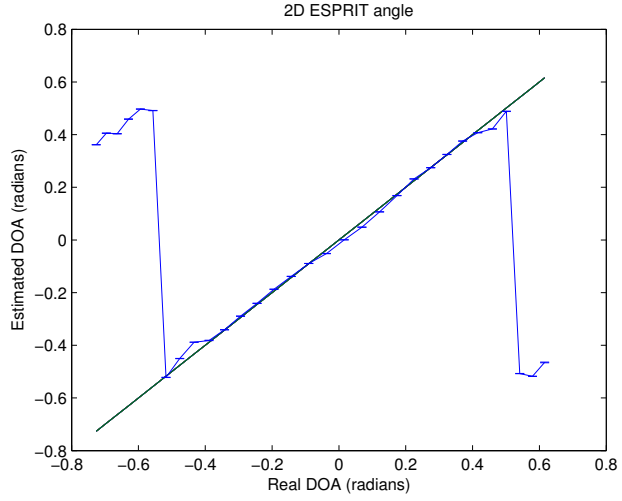

(b) Angle

FIGURE 5.23 – Experimental performance of 2D ESPRIT estimation in room #1.

5.7 Conclusion

In practical cases, the far field assumption is not always valid when a four channel phased array is used to interrogate EPC Generation 2 tags. This is certainly true when the range between the tag and array is small, for example in a portal setup: an antenna fixed to the wall or ceiling and a moving tag besides or underneath the antenna.

By using a four channel phased array antenna system, average DOA and range estimation errors are determined. Range estimation based on a 2D MUSIC or ESPRIT algorithm can introduce large errors. In general, an average angle error of 3 to 4 degrees and a range error in the order of 0.3 m is to be expected with the help of a 2D MUSIC algorithm, which is comparable to literature where range and angle are estimated separately. By calibrating the measured phases for every angle based on the first samples to calibrate for instrumental effects, experiments show that large errors are introduced in the angle estimation due to the irregular shape of the calibration. Furthermore, experiments in an anechoic room show the increased performance of 2-dimensional estimation in a near field scenario in a reflection-free environment. These experiments also indirectly indicate the presence of strong reflections in more realistic indoor environments.

Therefore, the main conclusion is that DOA estimation is the preferred method for localization, because range measurements give a large error, due to antenna patterns and reflections.

6

Using Phased Arrays with Low Resolution ADCs

Abstract – *In the previous chapter the results of range and DOA estimation in the near field are presented and the experiments indicate multipath effects in realistic environments. As an alternative, with the help of multiple phased arrays, a location can also be estimated. To save on hardware costs, which are significant for multiple arrays, in this chapter we explore the possibility of using single bit analog-to-digital converters and associated digital processing with matched precision for our four channel phased array setup. As DOA algorithms use the correlation coefficient between signals from different antennas and there is a direct relation between the correlation coefficient of quantized signals and unquantized signals, at the cost of additional signal power measurements, the error introduced by quantization can be corrected. The experimental results show that single bit quantization can be used for DOA estimation and the mean error increases only slightly. The proposed correction achieves minor improvements compared to uncorrected quantized estimation in realistic scenarios.*

In the previous chapter we showed that a phased array can be used to determine the DOA of a tag signal in the near field zone of a phased array. However, we also showed that, localizing the tag (not only determining the DOA, but also the exact position) within the near field using a single phased array gives range estimates with limited precision. To improve this precision, a standard localization technique is to use multiple phased arrays, each generating a DOA estimate[12]. These DOA estimates of the individual arrays can then be combined to obtain an estimate of the position of the tag. In Figure 6.1 an overview of the envisioned system is given.

Large parts of this chapter have been published in [JH:3].

Multiple phased arrays can be placed on the ceiling of a shop and are only used for localization of the tags using the DOA of all individual arrays. Communication with the tag to read the EPC is done with a separate reader. This reader is also used to energize the tag.

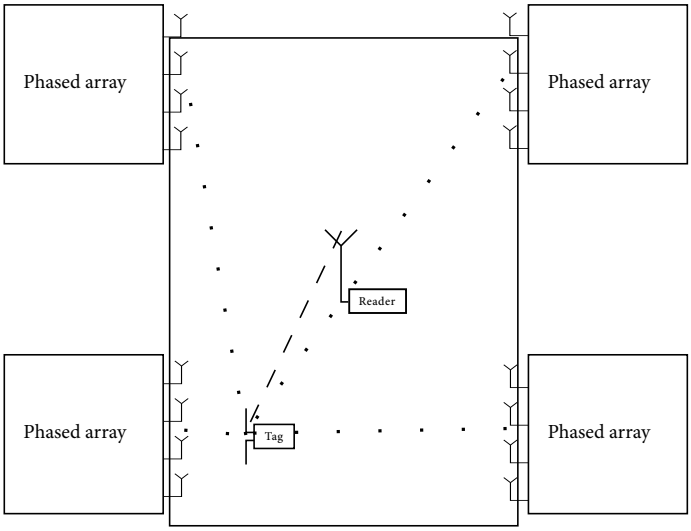

Figure 6.1 – Top view of multiple phased arrays, with four antennas each for localization and separate reader for communication.

Phased arrays currently used for DOA estimation use high precision receivers containing high resolution ADCs and high precision digital processing. This leads to high system costs and high computational complexity. Therefore, using multiple phased arrays could make this solution unattractive from a cost perspective.

To save processing power and system costs it is interesting to investigate whether it is possible to quantize the signal using only single bit analog to digital conversion and to process these signals in the digital domain with drastically reduced wordlengths. Normally phased arrays are used to increase the signal to noise ratio of an incoming signal[85]. This increase is generally referred to as array gain. However, the algorithms used to determine a DOA estimate exploit signal properties like the correlation between two received signals, and do not use the actual data contained in the received signal. Therefore, lowering the resolution of the ADCs might be a viable option to reduce processing power and cost. In the proposed system, within each receiver of a phased array, the signal from the tag is still split by a down-mixing modulator into an inphase and a quadrature component. These two signals are individually quantized into single bit signals which can be easily processed by a digital processing device, for example a Field-Programmable Gate Array *(FPGA)* or an Application Specific Integrated Circuit *(ASIC)*.

In this chapter we investigate the use of single-bit quantized signals to avoid the use of high resolution ADCs and high precision digital processing. After describing the proposed system in more detail, the effect of quantization is studied, after which a correction is derived to compensate for the effects of quantization. Besides simulations, our hardware setup, explained in Section 5.6, is used to verify DOA estimation using single-bit ADCs and the proposed correction with experiments.

6.1 System Decomposition

A localization system based on angle estimates from multiple phased arrays can be decomposed into three parts:

Covariance Matrix Calculation

As shown in Figure 5.6, for every antenna a frontend with two ADCs is used to sample the received signal. The covariance matrix is based on samples received by the antennas. For every phased array in the localization system, an estimate of this covariance matrix has to be derived. For each combination of antennas the dot product has to be calculated, and this part of the system has to operate at the sample rate of the ADCs.

Based on the 2048 samples taken by the ADCs in our current setup, about 131072 14-bit multiplications have to be performed to estimate a 4x4 covariance matrix. Since it is not an option to centralize the covariance matrix calculation (too much communication capacity would be required between the phased arrays and the centralized processor) this will be implemented within each array separately.

Angle Estimation

As angle estimation is done per tag-reading, it is executed at tag reading rate, in contrast to the covariance matrix calculations, which are at sample rate. The MUSIC algorithm described in Section 5.4.1 makes use of eigendecomposition to split the covariance matrix into a signal and noise subspace. To compute the eigenvectors and eigenvalues, in reference [68] a Digital Signal Processor *(DSP)* is used with the same architecture as the one used for experiments in this thesis. The authors implement a Cholesky algorithm to compute the eigenvectors of a 5x5 matrix and report the number of cycles needed. The used architecture can calculate four multiplications per cycle translating into about 8000 multiplications. The computation of the eigenvectors of a 4x4 matrix would require less computations as the matrix is smaller. Scanning over the noise space as within the MUSIC algorithm can be computationally expensive depending on the step size. With an angular step size of 1 degree, 180 steps would be needed. Note that in practice, due to antenna characteristics, the antennas will not receive usable signals when the angle is large i.e. a tag is almost in line with the array. So, a smaller number of steps will be used in practice. The MUSIC algorithm itself uses 36 complex multiplications

per step. Assuming 180 steps this gives 25920 normal multiplications for the complete pseudospectrum. Since the complexity of the angle estimation is high, the amount of data of the covariance matrix is low and angle estimation is done at tag reading rate, angle estimation can be executed by a centralized processor, where the covariance matrices are sent from the phased arrays to the central processor.

Localization

The angle estimations from the multiple phased arrays have to be combined into a location estimate. As angles are estimated per tag, localization has to be done at tag reading rate. This process has to combine the angle estimates from different phased arrays and therefore needs to be centralized. This thesis focuses on the calculation of the covariance matrix and angle estimation and will only cover basic localization in Section 6.8.

6.1.1 Proposed System

In Figure 6.1 a system consisting of four phased arrays is shown. To lower the computational burden on the individual arrays, in the proposed system the final angle estimation and localization are performed by a central processing unit. Figure 6.2 shows a system setup whereby individual phased arrays calculate the 4x4 covariance matrices each, which are then transmitted to a central processing unit to estimate the angles and combine these angle estimates into a location estimate.

In a commercial system, the frontend and covariance matrix calculation could be combined into a single ASIC to achieve major power and cost savings. No integrated solutions exist yet.

A large portion of the computational load of the DOA estimation algorithms based on the covariance matrix, is the calculation of the covariance matrix itself. To reduce power consumption and required chip area, it is interesting to investigate reduced precision ADCs in combination with matched precision covariance matrix calculation. In the extreme case, by using single bit ADCs, the multiplications used for the covariance matrix calculation become XOR operations, which would considerably simplify the 131072 multiplications in a four antenna phased array, processing a batch of 2048 samples. If the baseband amplifier is changed to act as a comparator, the signal can be directly sampled by the digital processing system, effectively removing the ADC. The removal of the ADCs reduces power usage and cost. The absolute cost reduction is dependent on the final implementation and the used architecture and is beyond the scope of this thesis.

By removing the ADC and multipliers, a small mixed-signal chip can be designed, containing the analog frontends (LNA, mixers, filters and amplifiers) and the covariance matrix calculations. Note that when using a single bit ADC, requirements concerning linearity and noise figure of the other components (LNA, mixer and amplifier) are more relaxed.

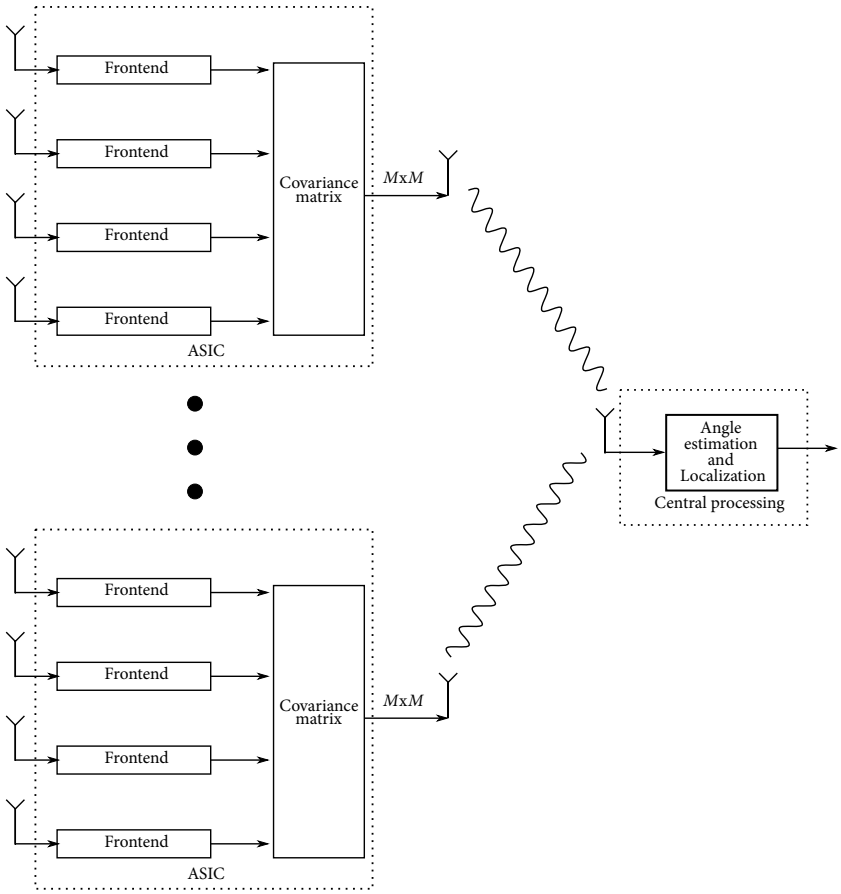

Figure 6.2 – Final system setup

6.2 Far Field Estimation and a Near Field Model

As shown in Chapter 5, when the RFID tags are close to the reader, the far field assumption does not hold. To get a better model of the signal propagation, we assume a near field signal model, like in Figure 5.4, whereby a single signal $X_m(t)$ is received by the mth antenna, which is modeled as:

$$X_m(t) = s(t) * e^{j\frac{2\pi}{\lambda} * r_m} + n_m(t) \tag{6.1}$$

In this equation, s is the signal transmitted by the tag and $X_m(t)$ is sampled by the ADCs. A phase shift is introduced depending on the distance between the mth receiving antenna and the tag (r_m). The wavelength λ of the carrier wave is used to translate from distance to a phase difference. Furthermore, for every channel, noise n_m is modeled.

Literature describes numerous far field DOA estimation algorithms such as MUSIC [78] and ESPRIT[76]. In contrast to the previous chapter, we use the ROOT-MUSIC algorithm to estimate the DOA in this chapter[78]. The ROOT-MUSIC algorithm does not yield a pseudospectrum whereby peaks indicate the DOA, but determines the DOAs analytically. ROOT-MUSIC is more computationally efficient than the normal MUSIC algorithm because it does not require an extensive search[73] for which a (variable) step size has to be selected. Furthermore, the overall performance difference is small[87].

If far field angle estimation algorithms are used, while this far field approximation does not hold, an error in the estimated DOA is made dependent on the angle and distance. There is no discrete boundary between far- and near field. In Figure 6.3 the error caused by using a far field DOA estimation algorithm, in this case ROOT-MUSIC, in a near field scenario is shown. Also the standard deviations are shown with error bars. The incoming signal is modeled to have a signal-to-noise ratio of 21 dB, similar to Section 5.5. For this simulation, the tag is moved along a line parallel to the centerline of the array and an angle estimation is made. Three fixed distances, between the line over which the tag is moved and the centerline of the array r_c, of 75, 100 and 150 cm are used. The estimation error is plotted for different angles, ranging from -90 degrees to 90 degrees. It can be seen that a signal originating near the middle of the array (θ = 0, broadside) or in line with the array (θ = ±90, end-fire) gives a small error. In between broadside and end-fire, the error is the largest, but still relatively small. If the distance from the centerline of the array becomes larger, the error made will become smaller, and vice versa. However, since the error remains small (< 1.5 degrees in the analysed cases) we conclude that far field DOA estimation algorithms give useful DOA estimates even in near field scenarios.

6.3 Correlation

In the proposed system, for each receiver within an individual array, in-phase and quadrature-phase signals are individually quantized into single bit signals which can very effectively be processed by a digital processing device.

Most DOA estimation algorithms are based on the correlation of received signals. The ROOT-MUSIC estimation algorithm uses the covariance matrix for its DOA estimations. This matrix is constructed out of the sampled signals received by the array antennas. The signal received by the mth antenna, $X_m(t)$, is sampled and per antenna, N samples are stored in a vector. This vector of samples is defined as:

$$\vec{X}_m = [X_m(1), X_m(2), ..., X_m(N)]^T \tag{6.2}$$

The vectors from all antennas are combined into a matrix:

$$\mathbf{X} = [\vec{X}_1, \vec{X}_2, ..., \vec{X}_M] \tag{6.3}$$

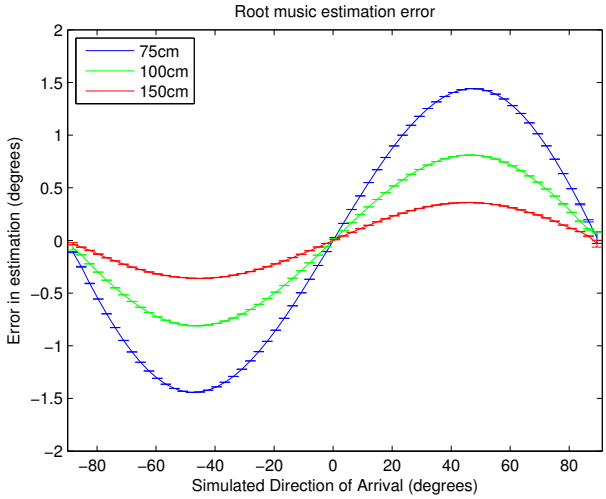

FIGURE 6.3 – Simulation: Error for near field scenario and far field MUSIC estimation.

This matrix is used to calculate the covariance matrix **R**, which is defined as:

$$\mathbf{R} = E[\mathbf{X}^H \cdot \mathbf{X}] \tag{6.4}$$

where $E[]$ indicates the expected value and ^{H} indicates the complex conjugate transpose.

Each element R_{pq} of this matrix is the covariance between two channels p, q. Every covariance R_{pq} is estimated from the sampled signals $\vec{X}_p$ and $\vec{X}_q$: $R_{pq} = \vec{X}_p^H \cdot \vec{X}_q$. These signals are complex, therefore this complex multiplication can be written as:

$$R_{pq} = (R_{pq}^{RR} + R_{pq}^{II}) + (R_{pq}^{RI} - R_{pq}^{IR}) \cdot j \tag{6.5}$$

where

$$R_{pq}^{RR} \triangleq Re(\vec{X}_p{}^H) \cdot Re(\vec{X}_q) \tag{6.6a}$$

$$R_{pq}^{II} \triangleq Im(\vec{X}_p{}^H) \cdot Im(\vec{X}_q) \tag{6.6b}$$

$$R_{pq}^{RI} \triangleq Re(\vec{X}_p{}^H) \cdot Im(\vec{X}_q) \tag{6.6c}$$

$$R_{pq}^{IR} \triangleq Im(\vec{X}_p{}^H) \cdot Re(\vec{X}_q) \tag{6.6d}$$

The covariances are related to the correlation coefficients of the signals. For two random variables, for example X and Y, the correlation coefficient ρ is defined in terms of the covariance R as $\rho_{XY} \triangleq \frac{R_{XY}}{\sigma_X \cdot \sigma_y}$. See for more information for example [41].

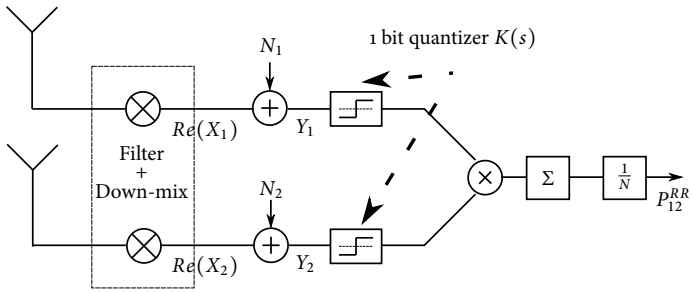

Figure 6.4 – Two channel correlation

Similarly, the covariance for R_{pq}^{RR} can be decomposed as follows:

$$R_{pq}^{RR} = \frac{R_{pq}^{RR}}{\sigma_{X_p}^R \cdot \sigma_{X_q}^R} \cdot \left(\sigma_{X_p}^R \cdot \sigma_{X_q}^R\right) = \rho_{pq}^{RR} \cdot \left(\sigma_{X_p}^R \cdot \sigma_{X_q}^R\right) \tag{6.7}$$

In this equation $\sigma_{X_k}^R$ is the standard deviation of $Re(X_k)$, the real part of the kth signal. Equation 6.7 is used to define the correlation coefficient ρ_{pq}^{RR}. Note that this correlation coefficient ρ_{pq}^{RR} is the correlation coefficient between ideal signals, without quantization. In case of single bit quantization we define this correlation coefficient as P_{pq}^{RR}. The correlation coefficients $\rho_{pq}^{IR}, \rho_{pq}^{RI}, \rho_{pq}^{II}$ and $P_{pq}^{IR}, P_{pq}^{RI}, P_{pq}^{II}$ are defined similarly.

In the following section, we define the relation between the correlation coefficients ρ and P, and we show how to partially correct the effect of quantization on the correlation coefficient.

6.4 Quantization

An error is introduced when the signals are quantized before calculating the correlation matrix. This effect can be explained by examining the correlation between two channels.

In Figure 6.4 a schematic overview of the calculation of the correlation coefficient between the real parts of two channels in case of single bit quantization is shown. The signals from two individual antennas are filtered and down-mixed to baseband. Independent white noise is added to the real parts of these baseband signals $Re(X_1)$ and $Re(X_2)$ to model receiver noise. The resulting signals are quantized by a single bit quantizer K where

$$K(s) = \begin{cases} 1, & \text{if } s > 0 \\ -1, & \text{if } s \leq 0 \end{cases} \tag{6.8a}$$

N samples of the quantized signals are correlated. Note that, because $|K(s)|=1$, no normalization is required to obtain the correlation coefficient P.

The correlation coefficients are then used for DOA estimation.

The correlation coefficient before quantization is defined as ρ_{pq}^{RR}, which is the correlation coefficient between Y_1 and Y_2 from Figure 6.4. The correlation coefficient before quantization ρ_{pq}^{RR} will differ from the correlation coefficient after quantization P_{pq}^{RR}. The same holds for the combinations $\rho_{pq}^{II} - P_{pq}^{II}$, $\rho_{pq}^{RI} - P_{pq}^{RI}$ and $\rho_{pq}^{IR} - P_{pq}^{IR}$. Because the correlation coefficients ρ_{pq}^{RR} and P_{pq}^{RR} are not equal, the resulting complex correlation coefficients ρ_{pq} and P_{pq} will differ, distorting the DOA estimation.

From literature it is known that there is a one-to-one relation between the unquantized and quantized correlation coefficient for sinusoidal signals[61]. However, the signals from a tag are not sinusoidal, more BPSK or square like. For these square waves, a different relation exists which is described in the following sections.

When the distortion introduced by the quantization is known, the correlation coefficients after quantization can be corrected for this effect and the correlation matrix can be corrected before DOA estimation.

6.5 Quantization of a Square Wave

As mentioned above, the signal received from an EPC Generation 2 tag is not sinusoidal, but can be more closely approximated by a BPSK modulated square wave.

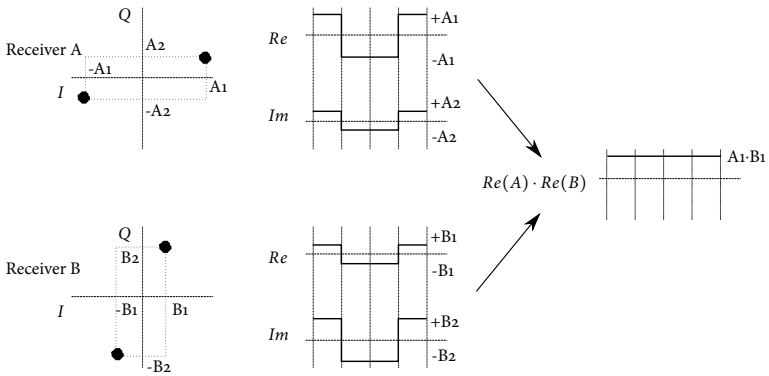

Figure 6.5 – Effect of phase rotation on baseband BPSK signal

Figure 6.5 shows the decomposed signal of two receivers that receive data from the same tag, note that in this model no noise is added. At baseband, data changes at (approximately) the same moment at the individual receivers. The phase difference is reflected in the ratio between the amplitudes of the real and imaginary parts. After correlation of the signals from two receivers, the effects of data changes

disappear and the same results are obtained as when constant signal levels are assumed. For example, when concentrating on the real parts in Figure 6.5, it is easily seen that $+A_1 \cdot +B_1 = -A_1 \cdot -B_1$. Under the assumption that the tag does not move during measurements, the correlation of $Re\{X_1\}$ and $Re\{X_2\}$ can be modeled to have a constant value and, in case of added noise, can be seen as a single random distribution.

The received signals in Figure 6.4, X_1 and X_2, are split into real and imaginary parts. As explained before, for every complex cross correlation, four correlation pairs (P_{12}^{RR},...,P_{12}^{II}) have to be calculated. For now, we concentrate on the real parts only. To $Re\{X_1\}$ and $Re\{X_2\}$ uncorrelated white Gaussian noise is added, modeled by N_1 and N_2. This results in Y_1 and Y_2, which are the signals right before quantization: $Y_1 = Re\{X_1\} + N_1$ and $Y_2 = Re\{X_2\} + N_2$ (see Figure 6.4). Because the signal levels can be assumed to be constant, for the input of the quantizer, this translates into a normal distribution of Y_1 and Y_2 with a mean of S_1 respectively S_2, and a standard deviation equal to the standard deviation of the noise. For example in the case of P_{12}^{RR} we can see from Figure 6.5 that S_1 equals A_1 and S_2 equals B_1.

After quantization, there are only two possible values left (1 and -1). Define U_1 as the probability that after quantization Y_1 is converted into a 1 and U_{-1} as the probability that Y_1 is converted into a −1. A schematic overview of this analysis for Y_1 is shown in Figure 6.6.

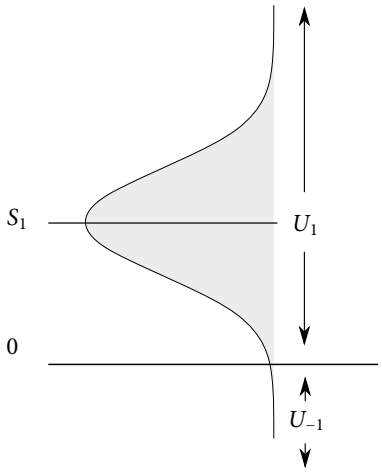

Figure 6.6 – Normal distribution with 0 as decision boundary

For the second channel with signal Y_2, similar random variables are defined: T_1 and T_{-1}.

Remember that the correlation coefficient is equal to the normalized covariance, which is an inner product of the two signals. Therefore, the expected value of the correlation coefficient $E[P]$ can be expressed in terms of the probabilities as follows:

$$E[P] = 1 \cdot (U_1 \cdot T_1 + U_{-1} \cdot T_{-1}) + -1 \cdot (U_1 \cdot T_{-1} + U_{-1} \cdot T_1) \tag{6.9}$$

From the normal distribution it can be seen that $U_{-1} = 1 - U_1$ and $T_{-1} = 1 - T_1$. With this we can rewrite Equation 6.9 to:

$$E[P] = (2 \cdot U_1 - 1)(2 \cdot T_1 - 1) \tag{6.10}$$

U_1 is the cumulative probability from zero to infinity. As said, the noise in the system is assumed to be Gaussian. Therefore, U_1 is the cumulative probability taken from of a Gaussian distribution with mean S_1 and a variance depending on the noise level.

This partial cumulative probability of a Gaussian distribution is also known as the Q-function, which is defined as:

$$Q(x) = \frac{1}{\sqrt{2\pi}} \int_x^\infty exp(-\frac{u^2}{2})du \tag{6.11}$$

Because $Q(x)$ is defined as the cumulative probability from x to infinity of a normal distributed variable with a zero mean and variance of 1, the argument of the Q-function has to be changed to include the mean and variance. It is well known that the resulting cumulative probability $F(x)$ for a distribution with mean μ and variance σ is a translation of $Q(x)$: $F(x) = Q(\frac{x-\mu}{\sigma})$[41]. In this case the means are S_1 and S_2, and the variances, σ, are assumed to be equal and the decision boundary is set to 0, therefore $x = 0$:

$$E[P] = (2 \cdot Q(\frac{-S_1}{\sigma}) - 1)(2 \cdot Q(\frac{-S_2}{\sigma}) - 1) \tag{6.12}$$

This correlation coefficient can be calculated for all four pairs that can be made out of the real and imaginary components of two complex signals.

From expression 6.12, it can be seen that, based on the signal-to-noise ratios $\frac{S_1}{\sigma}$ and $\frac{S_2}{\sigma}$, the correlation coefficient of single bit quantized signals can be determined. Our aim however, is to determine the correlation coefficient of the original, unquantized signals. In the next sections, we identify two cases where equation 6.12 reduces to an expression where the correlation coefficient only depends on a single SNR value. In those cases, 6.12 can be inverted and the SNR value can be determined based on the correlation coefficient of the quantized signals. Using this SNR value, the correlation coefficient of the unquantized signals can be determined. The result is an expression where the correlation coefficient of the unquantized signals is a function of the correlation coefficient of the quantized signals.

6.5.1 Different Phase

Due to different absolute phases of the two (complex) signals to be correlated, the mean (S_1 and S_2) of both signals Y_1 and Y_2 can differ. Because of circular symmetry we assume that the two received signals can always be rotated such that one of the signals has most power in the real (or imaginary) part[39]. Let us assume a high SNR, leading to the assumption that $U_1 \approx 1$ or $Q(\frac{-S_1}{\sigma}) \approx 1$. In Figure 6.7, this is graphically shown. The arrow indicates that the phase of one signal can change or, equivalently, we consider S_2 to be variable. Due to the assumption of high SNR, the distribution of Y_1 is narrow and therefore falls completely on one side of the decision boundary. The expected value of the correlation coefficient using Equation 6.12 then becomes:

$$E[P] = 1 \cdot \left(2 \cdot Q\left(\frac{-S_2}{\sigma}\right) - 1\right) \tag{6.13}$$

Expression 6.13 can be rewritten such that the signal-to-noise ratio of the receiver of Y_2, before quantization can be determined:

$$\frac{S_2}{\sigma} = -Q^{-1}(0.5 \cdot (E[P] + 1)) \tag{6.14}$$

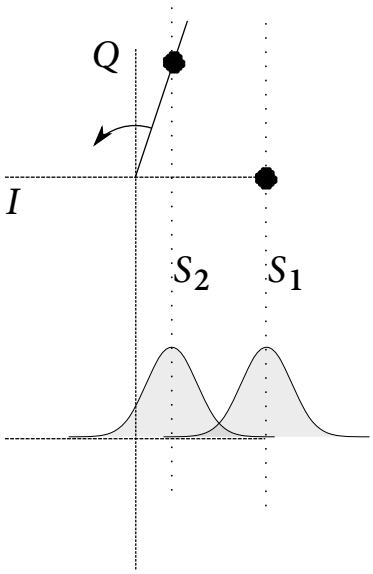

Figure 6.7 – Signals with different phase

6.5.2 Equal Phase

A similar derivation can be done for signals with equal phase. In Figure 6.8 again a graphical overview is shown. Equal phase leads to the assumption of an equal mean $S_1 = S_2 = S$, shown by the similar but independent distributions. By also assuming equal noise power, Equation 6.12 leads to:

$$E[P] = (2 \cdot Q\left(\frac{-S}{\sigma}\right) - 1)^2 \tag{6.15}$$

From this equation the signal-to-noise ratio before quantization $\frac{S}{\sigma}$ can be extracted:

$$\frac{S}{\sigma} = -Q^{-1}(0.5 \cdot (\sqrt{E[P]} + 1)) \tag{6.16}$$

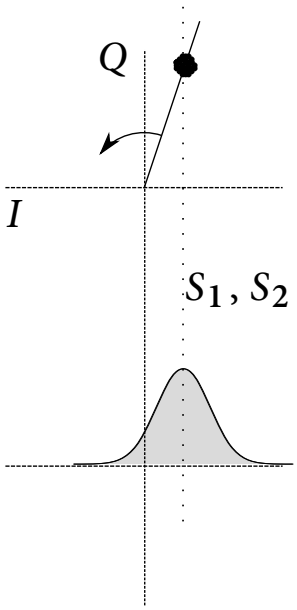

Figure 6.8 – Signals with equal phase

6.5.3 Relation to Correlation Coefficient

Based on the signal-to-noise ratios, expressed in Equation 6.14 and 6.16, the relation between the correlation coefficients with and without quantization (before and after quantization respectively) can be found.

In general the correlation coefficient ρ before quantization can be expressed in terms of the signal mean S and signal variance σ^2 [72]:

$$\rho = \frac{S^2/\sigma^2}{S^2/\sigma^2 + 1} \tag{6.17}$$

consequently:

$$\frac{S^2}{\sigma^2} = \frac{\rho}{1-\rho} \tag{6.18a}$$

$$\frac{S}{\sigma} = \sqrt{\frac{\rho}{1-\rho}} \tag{6.18b}$$

Using Equation 6.13, the relation between the quantized and unquantized correlation coefficient for the different phase situation can then be expressed analytically as:

$$E[P] = 2 \cdot Q(-\sqrt{\frac{\rho}{1-\rho}}) - 1 \tag{6.19}$$

and for the equal phase situation as

$$E[P] = (2 \cdot Q(-\sqrt{\frac{\rho}{1-\rho}}) - 1)^2 \tag{6.20}$$

based on Equation 6.13 and 6.15 respectively.

For two signals with equal and different phase, in Figure 6.9 the analytic relation between the correlation coefficient in case of quantization (y-axis) and the correlation coefficient in case of no quantization (x-axis) is shown. In the same figure simulation results, with 21 dB SNR, are shown, where $E[P]$ is approximated by the average correlation coefficient over a limited set of data points. Again, both cases are shown, whereby two simulated signals are quantized and correlated for both cases. It can be seen that the equations describing the relation between quantized and unquantized correlation values match the simulation. This figure also shows a black line, indicating the target correlation coefficients.

Both cases analysed above can be seen as corner cases. In reality the phases will never be equal, nor will one of the phases be exactly zero.

6.5.4 Correction

Despite the fact that the exact phase is not known, in the following section we examine the effect of both cases as if the phase is known. By rewriting expression 6.19, the correlation coefficient in case of no quantization as a function of the (measured) correlation coefficient after quantization can be determined:

$$\rho = \frac{Q^{-1}(0.5 \cdot (E[P]+1))^2}{Q^{-1}(0.5 \cdot (E[P]+1))^2 + 1} \tag{6.21}$$

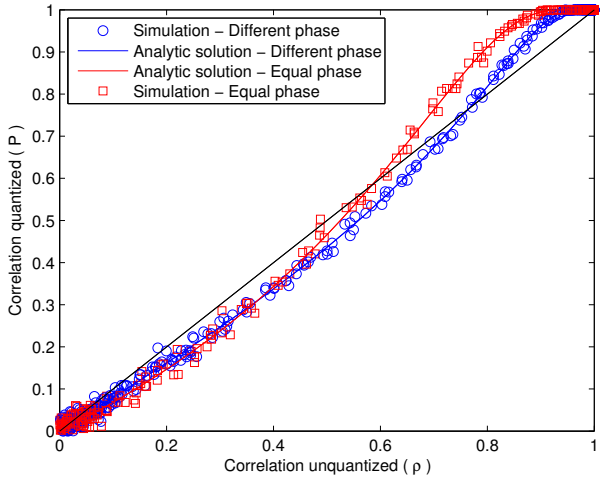

FIGURE 6.9 – Relation between correlation coefficients with and without quantization for equal and different phases in a simulation scenario

For $\rho_{pq}^{RR}, \rho_{pq}^{II}, \rho_{pq}^{RI}$ and ρ_{pq}^{IR} corresponding expressions can be given. Therefore, as already mentioned, by using expression 6.21 it is possible to correct the measured correlation matrix for the effects of quantization.

Within a real system, incorporating single bit quantization, the correlation coefficients P are measured and Equation 6.21 can be used to correct for the effects of quantization. Finally, Equation 6.7 is used to determine the covariances used to build the covariance matrix. Concentrating on the real components only, this leads to:

$$R_{pq}^{RR} = \frac{Q^{-1}(0.5 \cdot (P_{pq}^{RR} + 1))^2}{Q^{-1}(0.5 \cdot (P_{pq}^{RR} + 1))^2 + 1} \cdot (\sigma_{x_p}^R \cdot \sigma_{x_q}^R) \tag{6.22}$$

Note that for the last step, the standard deviations σ_{x_p} and σ_{x_q} need to be known. These can be measured by relatively simple power detectors.

For the equal phase scenario the result is similar:

$$R_{pq}^{RR} = \frac{Q^{-1}(0.5 \cdot (\sqrt{P_{pq}^{RR}} + 1))^2}{Q^{-1}(0.5 \cdot (\sqrt{P_{pq}^{RR}} + 1))^2 + 1} \cdot (\sigma_{x_p}^R \cdot \sigma_{x_q}^R) \tag{6.23}$$

The correction described above has to be performed on all correlation pairs separately, after which the covariance matrix from Equation 6.4 can be reconstructed. The DOA estimation algorithms can use this corrected covariance matrix as basis for estimation.

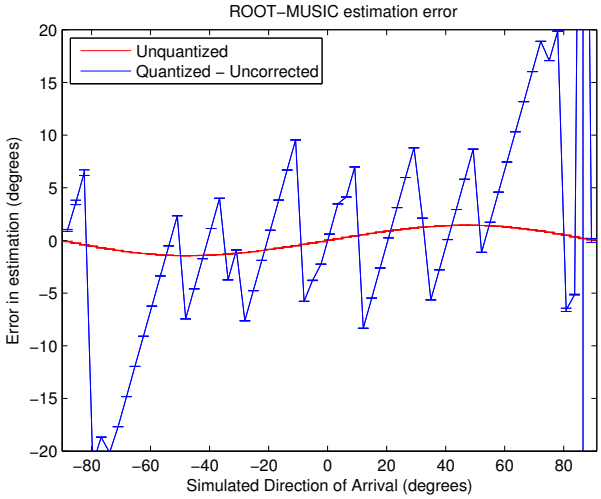

Figure 6.10 – Simulation: DOA error due to quantization - uncorrected

6.6 Simulation

Simulations are performed to investigate the effect of coarse quantization and the correction described above. Similar to the simulations in the previous chapter, noise is added leading to an SNR of 21 dB. The simulation settings are kept the same as in Figure 6.3 and a distance of 75 cm is used. The only change is the use of single bit quantization. In Figure 6.10 the error introduced by the quantization is shown together with the unquantized curve from Figure 6.3. Note that in this figure the scale of the y-axis is increased with a factor 10 compared to Figure 6.3. Compared to the unquantized system additional errors are introduced.

The results of correction, using the different phase model of the correlation coefficient can be seen in Figure 6.11. Note that the original scale of Figure 6.3 has been restored. Although this figure shows that the variance of the estimated angle increases due to the quantization, the mean estimation follows the expected error curve, which shows that the described correction is able to mitigate most effects introduced by quantizing.

6.7 Experiments

Besides simulations, experiments were done to verify the use of quantized data in a realistic scenario. The setup described in Chapter 5 is used to sample data from an EPC Generation 2 tag. For the following results, the same four channel array as shown in Figure 5.13 is used to intercept the communication between a tag and an off-the-shelf reader. Again, EPC Generation 2 tags need to be energized and

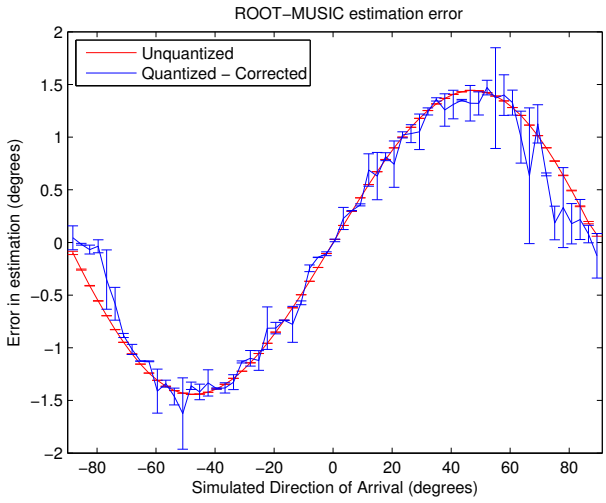

Figure 6.11 – Simulation: DOA error due to quantization - corrected

an initialization sequence needs to be transmitted before they start transmitting data, as described in Section 5.6 and Chapter 2. Therefore, a separate reader is used to stimulate a tag to transmit data. The four channels of the phased array are individually down-mixed into an inphase and quadrature phase baseband signal. After appropriate filtering, these baseband signals are sampled by a 14-bit ADC at a sampling rate of 1200kHz. With the help of post-processing, the signals are requantized to emulate the use of single bit ADCs and perform angle-estimation on the 14- and single bit quantized data. The tag was moved by a servo controlled support along the centerline of the array. For the results shown here, a height of 75cm was used (r_c from Figure 5.4).

In Figure 6.12 the correlation coefficients of the real parts of the single bit quantized signals are plotted against the coefficients of the real parts of the 14 bit signal. The 14 bit signal is considered as being unquantized. This figure has roughly the same shape as the analytical solutions from Figure 6.9. These figures are based on the signal from the two center antennas. Other signal pairs give similar results.

The goal of the proposed system is to estimate the DOA of the signal coming from the RFID tags. As is done in the simulations, the traditional DOA estimation algorithm ROOT-MUSIC is used to estimate the DOA of an RFID tag. In Figure 6.13(a) and Figure 6.13(b) the mean estimation and variance of this estimation are shown for multiple angles when the signals are unquantized and quantized without corrections respectively. Comparing the result, it can be seen that in case of quantization, the error in DOA estimates increases and the DOA estimate becomes less regular.

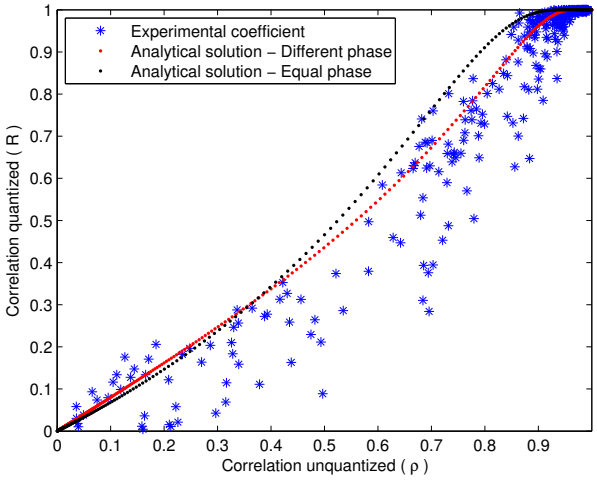

Figure 6.12 – Experimental: Quantized vs unquantized correlation coefficient

In Figure 6.13(c) and 6.13(d) the mean estimation and variance, when the signals are corrected after quantization, are shown. At first sight the results seem to have improved.

Discussion of the Results

To quantitatively compare the errors made by the original system and the quantized and corrected one, the Root-Mean-Square-Error *(RMSE)* is calculated over all the estimations shown in the figures. Per angle step, ranging from -45 to +45 degrees, 200 estimations are performed. Over all these estimations the RMSE and maximum error is calculated.

As the environment affects the estimation, the experiment is repeated in three different rooms, room #1 is a large and empty room with a ceiling of about 3 m, room #2 is a large empty office with a high ceiling (5 m) and an anechoic chamber, room #3. The results are presented in Table 6.1.

Quantization in rooms #1 and #2 degrades average performance by (5.48 - 5.0 =) 0.48 degrees and (5.94 - 3.36 =) 2.58 degrees which is 10% and 78% respectively. In the anechoic room the performance degrades (3.92 - 0.92 =) 3 degrees which is 325%.

DOA estimation experiments and cited literature in Chapter 5 indicate that an average error of about 3 degrees in the DOA estimation is achievable. The error due to quantization is double this figure for all measurements in rooms #1 and #2. The RMSE values based on corrected correlation values show that the correction algorithm is able to partially correct the errors made by quantization. In room #1 there

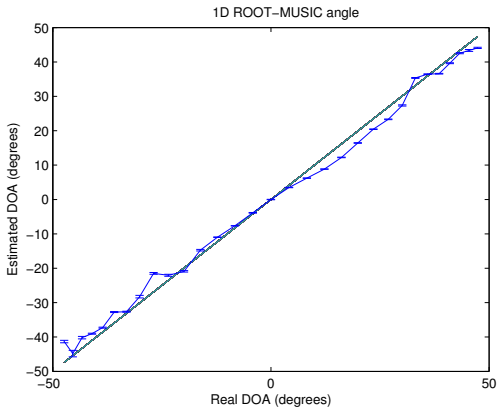

(a) Unquantized

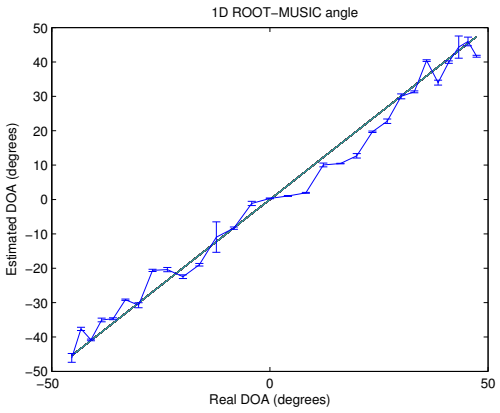

(b) Quantized and uncorrected

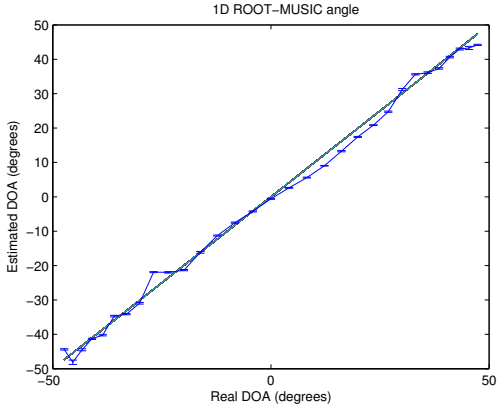

(c) Quantized and corrected with equal phase correction

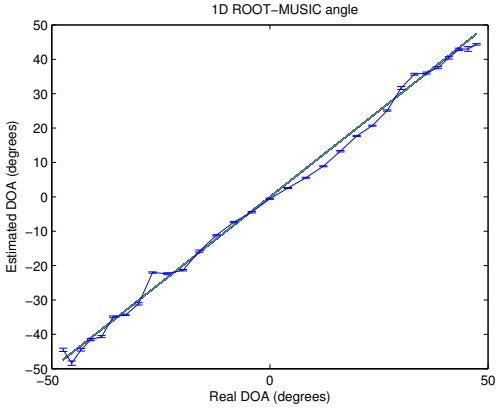

(d) Quantized and corrected with different phase correction

Figure 6.13 – Experimental: ROOT-MUSIC DOA estimation

Table 6.1 – Errors made in degrees of angle estimation

	Unquantized	Quantized	Corrected equal phase	Corrected different phase
RMSE room #1	5.00	5.48	5.24	5.13
Max room #1	10.59	14.22	10.94	14.43
RMSE room #2	3.36	5.94	3.38	3.39
Max room #2	4.91	12.46	6.45	6.49
RMSE anechoic room #3	0.92	3.92	1.07	1.07
Max anechoic room #3	2.13	7.86	2.59	2.52

is only a minor improvement possible by correction as the quantization makes only a 10% error. For the corrected cases the performance decreases by (5.24 - 5.00 =) 4.9% and (5.13 - 5.00 =) 2.7% respectively.

In room #2, the mean error in estimations based on quantized and corrected signals increases only (3.38 - 3.36 =) 0.02 degrees (which is 0.6%) indicating the effectiveness of the proposed correction. The error made by quantization increases slightly compared to room #1, This could be explained having more noise in room #2.

Room #3 is the anechoic chamber at Nedap. As can be seen, the mean error for all measurements decreases compared to room #1 and room #2, for the unquantized and corrected case even four times. This shows the effect of correction in a reflection free environment.

From the measurement results in the anechoic room it is concluded that reflections have a significant impact on the angle estimation. In the final application however, reflections will be present, causing an increased estimation error. Depending on the use of the DOA estimates, a trade-off has to be made whether the additional error made by quantization can be tolerated. In the following section the use of these quantized signals for 2D localization is investigated.

The calculation of the RMSE is described in Equation 5.3. This aggregated error value for all angles hides the fact that the DOA estimation algorithm introduces more errors when the angle is larger, for unquantized as well as quantized signals. In Table 6.2 an overview per angle is shown. It can be seen that in general the error increases for larger angles. Furthermore, irregularities can be seen whereby quantized or corrected values are smaller than the unquantized case, see for example at true angle -41 where the error in case of quantization is smaller than for the unquantized case. Due to reflections, the correlation of the quantized data does not follow the model, as can be seen in Figure 6.12. Any phase shift, in this case due to quantization, in the covariances of the covariance matrix used for DOA estimation has an influence on the final angle, similar to the distortion introduced by the calibrated steering vectors, described in the previous chapter. As the measurements have low variance, covariance estimations for a single angle have a stable error. Table 6.2 is given to indicate the estimation behavior of the angle estimation system in a specific room, with its own characteristics, and to show the effect of reflections on certain angle estimates.

Table 6.2 – RMSE made in degrees for different angle-estimations in room #1

True angle	Unquantized	Quantized	Corrected equal phase	Corrected different phase
-47.39	6.07	36.89	5.70	5.44
-45.41	1.11	1.44	1.33	1.49
-43.29	3.13	5.67	2.58	2.63
-41.01	1.98	0.30	1.21	1.10
-38.56	1.29	3.57	0.42	0.48
-35.93	3.18	1.28	3.44	3.25
-33.11	0.48	3.97	0.31	0.36
-30.10	1.87	0.97	1.16	0.83
-26.90	5.40	6.28	5.50	5.40
-23.50	1.47	3.17	1.26	0.87
-19.92	1.01	2.58	1.12	1.14
-16.16	1.43	2.85	1.54	1.92
-12.26	1.30	4.61	1.53	1.60
-8.25	0.59	0.35	0.85	1.03
-4.14	0.28	3.05	0.21	0.28
0	0.07	0.35	0.22	0.21
4.14	0.66	3.13	0.92	0.95
8.25	2.03	6.32	2.17	2.22
12.26	3.43	2.27	3.44	3.58
16.16	3.93	5.72	3.72	3.72
19.92	3.47	7.25	3.20	2.89
23.50	3.05	3.81	3.20	3.32
26.90	3.57	4.19	2.99	2.69
30.10	2.77	0.72	1.11	0.78
33.11	2.25	1.82	2.40	2.50
35.93	0.53	4.48	0.85	0.79
38.56	1.96	4.62	1.89	1.61
41.01	1.38	1.11	1.72	2.06
43.29	0.76	1.68	0.52	0.58
45.41	2.08	1.38	2.67	2.81
47.39	3.30	5.73	3.38	3.25

6.8 2D Localization

As suggested in Figure 6.1, with the help of multiple angle-estimations, the location of a tag can be determined. Literature describes several algorithms that can be used to determine the location of a tag by combining multiple angle measurements[11] [12] [54] .

However, the process of combining multiple angle measurements from different locations is non-trivial. In the case of UHF RFID, reference [54] uses a basic approach based on the centroid of intersecting angles. The same authors use different fusing methods in [11]. Similar problems have been addressed for acoustic localization. References [50] and [83] examine the placement of angle measurement sensors in more detail for general RF localization.

The simplest approach is to use two angle estimations, which is enough to estimate the location of a tag in a two dimensional plane. The intersection of the two angles can be seen as a location estimate. However, an error is made by estimating the DOAs with phased arrays, which will propagate to the location estimate.

It is beyond the scope of this thesis to analyse the error, but to gain some insight in the errors made by using the quantizing phased array system for two dimensional localization, first simulations are performed for a specific scenario and later on, localization within a plane is described . In this scenario two antenna arrays are modeled to observe a tag in a plane. The centers of the phased arrays are placed at $(0,0)$ and $(0,3)$ meter. The simulated tag position is defined by two coordinates, x_t and y_t, and is moved from $(x_t, y_t) = (1,1)$ to $(3,1)$ in steps of 10 cm. For every position simulations are performed at which every antenna array is used to estimate the angle. The estimated location (x_e, y_e) is determined by calculating the intersection point of the two estimated angles. See Figure 6.14 for an overview.

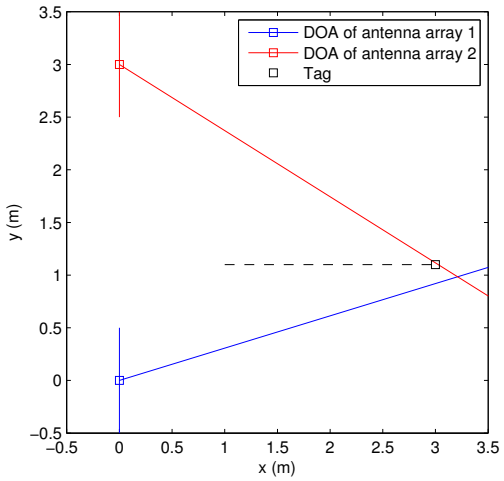

Figure 6.14 – Localization within a plane

In an ideal case, the measurements shown in Figure 6.13(b) can be used to gain insight in the errors introduced by real hardware. However, these measurements are done for tags at specific angles, which do not automatically match the angles needed for the described scenario. Therefore, the angle estimations from the previous section are used to determine the angle estimates for 'in-between' angles by means of curve fitting of the angle estimates in Figure 6.13(a) and Figure 6.13(b). Furthermore, the average standard deviation based on the observed errors is used as standard deviation of the estimated angles. From the previous section, the effect of applying the correction proved to be limited in practical cases. Therefore, for these simulations the unquantized case is compared with the uncorrected quantized case to give some insight in the introduced errors.

For every position, 100 simulations are performed. The estimated location (x_e, y_e) is determined by calculating the intersection point of the two estimated angles.

Table 6.3 – Errors made for localization (meters)

	Unquantized	Quantized
$m_x = E(\Delta x)$	0.20	0.31
$m_y = E(\Delta y)$	0.06	0.09
$m_D = E(\Delta D)$	0.21	0.33
$\sigma_x = \sqrt{E((\Delta x - m_x)^2)}$	0.12	0.25
$\sigma_y = \sqrt{E((\Delta y - m_y)^2)}$	0.03	0.07
$\sigma_D = \sqrt{E((\Delta D - m_D)^2)}$	0.11	0.25

Based on these simulations, a mean error and standard deviation for estimated coordinates x_e and y_e are determined and the results are presented in Table 6.3. The absolute distance difference between the estimation and true distance in both dimensions is indicated by $\Delta x = |x_e - x_t|$ and $\Delta y = |y_e - y_t|$. The combined distance error is defined as $\Delta D = \sqrt{\Delta x^2 + \Delta y^2}$. The means and standard deviations are given as m_x, m_y, m_D and σ_x, σ_y and σ_D respectively.

In case of quantization, both the error and the standard deviation of the estimated tag position increased compared to the unquantized case. In this specific case, the error, m_D, increased from 0.21 to 0.33 meter (approximately 65% increase) and the standard deviation σ_D is more than doubled. The error in the x direction perpendicular to the orientation of the antennas is larger (approximately a factor three) than the error in the y direction. To get a more uniform error spread in x and y direction, more antenna arrays have to be included as already shown by the planned system overview in Figure 6.1. An antenna perpendicular to the two current antennas will help to decreases the error in the x direction.

In Figure 6.15 the mean error in the quantized case, m_D, in a two dimensional plane is shown. As the DOA estimation results are not symmetrical with respect to the normal of the array (0°, see Figure 6.13(b)), the two dimensional localization error is neither. Furthermore, an accumulating pattern is visible in the estimation error due to the influence of a single array on the final estimation error. For some angles, both arrays produce large errors, resulting in a large error in the final location estimate. The influence of the angle estimates increases with distance, leading to the fact that the absolute errors in localization increase when the distances to the arrays increase.

6.9 Conclusion

To realize a more power- and cost effective system for accurate localization, this research investigates the use of single bit ADCs and digital processing with matched precision to estimate the DOA of EPC Generation 2 tags. The angle estimation algorithms make use of the covariance matrix, which is constructed of covariances between all individual antennas. Theoretically, there is a direct relation between the covariance between two unquantized signals and the covariance between two

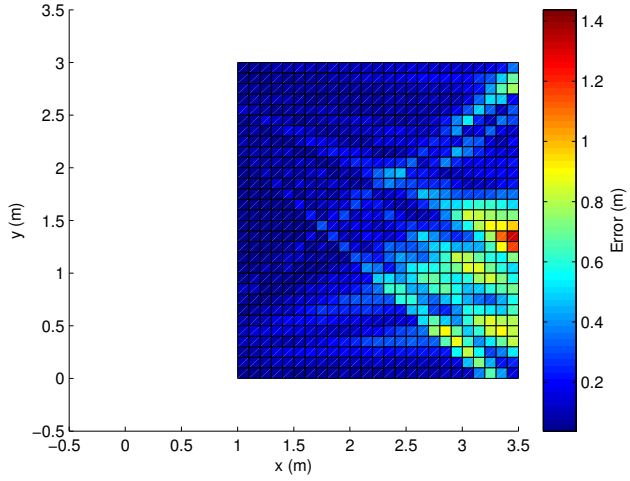

Figure 6.15 – Localization within a plane using DOA estimation based on quantized signals.

quantized versions of these signals. Therefore, it is possible to correct the covariances calculated from single bit quantized data. A phased array, consisting of four receiving elements is used to explore the use of single bit quantized signals. In simulation, correction of the angle estimation errors that are introduced by quantization, is effective and reduces the errors. Especially in the experimental results of measurements in the anechoic room the effect of correction can be seen. However, to calculate this correction, the system needs additional hardware to measure the signal power of the individual signals, which counteracts the cost effectiveness achievable by single bit quantization. Based on uncorrected quantized data, an average error of about 6 degrees is to be expected in a realistic environment compared to an average error of 4 degrees based on high resolution ADCs. By applying the correction, the errors caused by quantization can be corrected to values close to the unquantized case. Nevertheless, depending on the application, the additional error can be tolerated and using quantized, uncorrected signals might be suitable to decrease costs.

Simulations using two phased arrays to locate a tag indicate that errors in the DOA estimates translate to errors in the final estimated location of a tag. In case of quantization, both the mean error and standard deviation are larger compared to the unquantized case. The simulations with two phased arrays show that the overall error is larger in the direction perpendicular to the phased arrays. It is therefore recommended to analyse the extension of the configuration with a third phased array. Furthermore, the localization based on multiple angle estimates has to be investigated further.

7

Conclusion and Recommendations

Localization of objects in an indoor environment has been a kind of holy grail in literature for some time. Ideally, a localization system has to be accurate, reliable, cheap and give instant location estimates. Furthermore, such a system should operate within bandwidth and power limiting regulatory restrictions. Over the years, numerous systems have been developed, all with their own advantages and disadvantages.

In some environments, like retail or logistics, items are already tagged with Ultra High Frequency *(UHF)* band Radio Frequency Identification *(RFID)* tags to allow for tracking in a supply chain. The industry standard for these UHF tags are tags based on the EPCglobal Class 1 Generation 2 standard described in Chapter 2. The advantage of these tags is that they have a read range of several meters and can be passive at the same time.

Extensive literature exists on the topic of localization of EPC Generation 2 tags. Several different physical properties are exploited to derive a location estimate. In Chapter 3 an overview is given of known approaches to localization of EPC Generation 2 tags.

A general measure that is exploited for localization of wireless transceivers is the Received Signal Strength Indicator *(RSSI)*. By combining measurements of multiple readers, it is possible to derive a location estimate. Literature suggests the use of RSSI based methods in combination with reference tags on known locations. However, these methods do not give satisfactory results for EPC Generation 2 tags. Therefore, in Chapter 4, we present a multi reader localization setup based on phase measurements, taken at multiple frequencies, instead of RSSI measurements. EPC Generation 2 tags can be localized with an accuracy of about 0.4 m with the help of multiple readers and reference tags. Experiments in this chapter show that the proposed phase-based method achieves similar performance compared to a traditional RSSI-based system. Based on phase measurements from a

single reader, the range can be estimated with an accuracy of 0.42 m in an empty room. If a tag can be read fast enough by a reader, the observed phase of the received signal could be used to determine movement and whether a tag is moving towards or away from the reader.

The use of multiple readers in combination with reference tags requires extensive calibration. Furthermore, multiple readers require costly hardware, installation time and extensive cabling. In case a phased array receiver is used to receive the signals generated by a tag, tags operating in the UHF band are in many cases in the near field region of that phased array. Chapter 5 shows that then it is possible to estimate range and Direction of Arrival *(DOA)* of a tag. This technique improves the range estimate slightly to 0.3 m. The accuracy of the estimated angle, 4 degrees, is comparable to literature on separate DOA estimation. In an anechoic room the angle can be estimated with an accuracy of 1 degree and the range with an average error 0.2 m. Based on this, it is concluded that it is highly likely that multipath effects reduce range and angle estimation accuracy.

As an alternative, a known technique is to use DOA estimates from multiple phased arrays to estimate a location. In general, these arrays use high resolution and high speed Analog-to-Digital Converters *(ADCs)*, which leads to high power consumption, high system cost and high computational complexity, which in turn increases the overall cost. In Chapter 6 we show that it is possible to use single bit ADCs for DOA estimation. Quantization introduces some errors which can be (partially) corrected. However, even without correction the use of quantized signals only marginally increases the DOA estimation error in realistic environments. Therefore correction could be skipped to save on computational complexity. The average angle estimation error is 4 degrees in case of high resolution ADCs and increases to about 6 degrees in case of uncorrected single-bit quantization. By applying the suggested correction, the error is almost similar to the high resolution case. In the anechoic room, the effect of the correction can be seen more clearly; the uncorrected quantized average error decreases from 4 to 1 degree in case of corrected quantized signals.

This thesis focused on the design of a low-cost and bandwidth-limited localization system using Generation 2 tags. In Section 1.5 several requirements are mentioned. In case a phased array is used to localize tags, the location can be estimated based on a single transmission of a tag. Therefore, these systems are fast (R4). In Chapter 6 the use of single bit quantization is investigated to help fulfill the low-cost requirement (R3). Because the default EPC Generation 2 protocol is used, the proposed algorithms fulfill the bandwidth requirements (R5). The first two requirements are accuracy (R1) and reliability (R2). Localization within 50 cm is possible, however, the environment has a lot of influence on the final accuracy as shown by the anechoic room measurements. Every room has a different amount of reflections and will have different effects on the final localization accuracy. Dependent on the room and the application it has to be decided whether the proposed system is reliable and accurate enough.

7.1 Contributions

The main contributions of this thesis are:

- **Range estimation based on phase measurements at multiple frequencies to localize tags with multiple readers.** With the help of reference tags and multiple readers, EPC Generation 2 tags can be localized with an average error of 0.4 m in a 2 dimensional grid of reference tags spaced 0.3 m apart.
- The observation that EPC Generation 2 tags are in the **near field** region of a phased array makes it possible to estimate range and DOA with a single array with an average error of 4 degrees and 0.3 m.
- High resolution ADCs are not necessary to achieve reasonably accurate DOA estimations. **Single bit quantized** signals introduce an error in the calculation of the correlation coefficients, which can be corrected before estimating the DOA. However, even without correction, single bit quantized signals give reasonable results, the average error increases from 4 to 6 degrees.

7.2 Recommendations

The goal of this thesis was to find an accurate indoor localization system for EPC Generation 2 tags. Several solutions have been investigated by performing simulations and experiments. Recommendations for further analysis and experiments are given below.

The k-Nearest Neighbors *(KNN)* algorithm explored in this thesis is based on a static situation, a square grid with four readers. Furthermore, the measurements are taken separately per reader. By connecting the readers, measurements could be taken simultaneously. If more readers are available to cover a complete shop or warehouse, the measurements from all these readers could be combined in order to estimate a location.

The DOA algorithms based on quantized data as presented in Chapter 6 have to be tested with multiple phased arrays in a more realistic environment with characteristic properties like reflections and continuous changes of the channel.

By performing single bit quantization, the complexity of the ADC is drastically reduced and costs are decreased. However, more optimizations are possible. The intermediate frequency used to down convert the data is tapped off by a directional coupler and fed into a mixer. Not only the directional coupler increases cost, also the distribution of the carrier frequency is expensive, certainly in case of multiple distributed phased arrays. Because we are only interested in phase differences between antennas, the carrier could be generated locally per array. Another option is to skip the down-conversion step altogether and use sub-sampling as alternative. These approaches do have consequences for signal and (phase)noise levels and therefore need further research.

This thesis describes localization relatively close to the reader, mainly due to the fact that the phased array used for experiments is designed with fixed amplifiers and therefore not able to match the larger read range of Commercial Off-The-Shelf *(COTS)* readers. By using variable gain amplifiers, the array could be used for longer read ranges, giving insight in long range performance. The range might be even extended beyond the read range of the reader. It this case the tags can be powered by multiple readers and received with a limited number of arrays, something which could be interesting for warehouse applications.

The frontend used for the experiments is constructed of discrete components. The Low Noise Amplifier *(LNA)*, mixer and amplifier are power hungry and expensive. As the 868 MHz band is becoming more popular for consumer products, completely integrated solutions could possibly be used to improve efficiency.

Signal propagation in an indoor environment remains troublesome. As explained in Section 3.2.4, the use of a large bandwidth can resolve reflections. However, significant technology advancement is needed to include Ultra-WideBand *(UWB)* transmitters in a passive and low-cost tag. Current EPC Generation 2 tags have been shown to backscatter UWB transmissions, however, the signal level that needs to be transmitted by the readers, is above regulations. With the help of more sensitive hardware, the signal levels might be kept within reasonable range and prove to be a solution for resolving reflections.

A

(2D) MUSIC

The one-dimensional MUSIC algorithm is based on the fact that the signal and noise subspaces are orthogonal[78]. This appendix gives a short overview of the MUSIC algorithm, for more detail see [78] and [72]. In traditional MUSIC the far field model is used, therefor the following equations describe the reception of signals by an antenna array in a far field situation, whereby every antenna receives the signal with a small phase difference depending on the angle, θ. In a far field situation only the angle introduces a phase shift, in contrast to Equation 5.2 which also depend on range. Remember that there are M antennas and N signal sources. The system takes D samples from the signals it receives by the M antennas. Based on [84] and [72], the received signal matrix can be modeled as:

$$\mathbf{X} = \sum_{n=1}^{N} \mathbf{a}(\theta_N)\mathbf{s}_n + \mathbf{n} \tag{A.1a}$$

$$\mathbf{X} = \mathbf{AS} + \mathbf{n} \tag{A.1b}$$

Hereby $\mathbf{A}$ is a matrix of MxN steering vectors.

$$\mathbf{A} = [\mathbf{a}(\theta_1)\ \mathbf{a}(\theta_2)\ ...\ \mathbf{a}(\theta_\mathbf{N})] \tag{A.2}$$

And $\mathbf{S}$ is a matrix of NxD samples containing samples of the transmitted signal.

$$\mathbf{S} = [\mathbf{s}_1\ \mathbf{s}_2\ ...\ \mathbf{s}_N]^T \tag{A.3}$$

The matrix of received signals, $\mathbf{X}$, is of size MxD and is used to calculate a covariance matrix $\mathbf{R}$:

$$\mathbf{R} = E[\mathbf{X}\mathbf{X}^H] \tag{A.4a}$$

$$\mathbf{R} = E[\mathbf{A}\mathbf{S}\mathbf{S}^H\mathbf{A}^H] + E[\mathbf{n}\mathbf{n}^H] \tag{A.4b}$$

$$\mathbf{R} = \mathbf{A}\mathbf{Z}\mathbf{A}^H + \sigma^2\mathbf{I} \tag{A.4c}$$

$$\mathbf{R} = \mathbf{R}_\mathbf{s} + \sigma^2\mathbf{I} \tag{A.4d}$$

In this equation σ represents the noise variance and $\mathbf{I}$ the identity matrix. Subsequently, the signal covariance matrix, R_s, is defined as:

$$\mathbf{R_s} = \mathbf{AZA}^H \tag{A.5a}$$

$$\mathbf{Z} = \begin{bmatrix} E[|\mathbf{s}|^2] & 0 & \cdots & 0 \\ 0 & E[|\mathbf{s}|_2^2] & \cdots & 0 \\ 0 & 0 & \cdots & E[|\mathbf{s}|_N^2] \end{bmatrix} \tag{A.5b}$$

The dimensions of the (signal) covariance matrix are MxM and the rank is equal to the number of signals, N. $\mathbf{R}_s$ therefore contains $M - N$ eigenvectors with a zero eigenvalue.

The eigenvectors with the zero eigenvalue have to be orthogonal to an eigenvector describing the received signal. Let $\mathbf{e}_n$ be such an orthogonal eigenvector, it can then be proven that[78]:

$$\mathbf{A}^H\mathbf{e}_n = 0 \tag{A.6}$$

This implies that all $M - N$ eigenvectors with a zero eigenvalue are orthogonal to all N signal steering vectors. The eigenvectors with a zero eigenvalue, $\mathbf{E}_n$, are part of the noise subspace. The other eigenvectors describe the received signals and are said to span the signal subspace, $\mathbf{E}_s$.

The MUSIC algorithm is based on the noise subspace, $\mathbf{E}_n$, and scans over these eigenvectors with all possible steering vectors, looking for the occurrence of orthogonality. In case an orthogonal steering vector is found, the signal is known to be originating from the angle described by this steering vector. In a practical situation the signal covariance matrix is unknown. However, an estimate of this matrix can be used instead.

The number of signals N is often known beforehand, in the case described in this thesis only a single signal is received $N = 1$. If the number of signals is unknown, techniques exist to estimate the number of signals[49].

The MUSIC algorithm can be split into multiple steps:

1. Estimate the covariance matrix $\mathbf{R}$.
2. Find the eigenvectors and eigenvalues: $\mathbf{R} = \mathbf{E}\Lambda\mathbf{E}^H$
3. Partition the eigenvectors to obtain $\mathbf{E}_n$, based on the eigenvectors belonging to the $M - N$ smallest eigenvectors.
4. Scan over all possible angles θ and store the product between the steering vector and the noise subspace.
5. Select the N largest peaks of these stored values as the steering vectors belonging to the angle of the received signals.

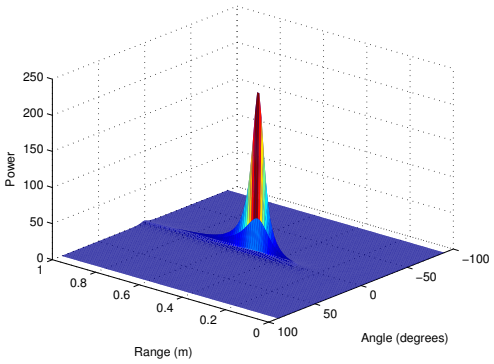

Figure A.1 – Example of a 2D MUSIC pseudospectrum.

A.1 Scanning over the Noise Subspace

The (estimated) covariance matrix is split into signal and noise subspaces by means of an eigen decomposition. In the theory the eigenvectors with an eigenvalue of zero belong to the noise subspace and are exactly orthogonal. In practice the eigenvectors with the smallest eigenvalue are grouped in the noise subspace and Equation A.6 is not exactly zero. Therefor the algorithm scans in steps over all possible steering vectors and selects the most orthogonal one.

The algorithm searches through all possible steering vectors, $\mathbf{a}(\theta)$ for a far field model. The algorithm tries to find the steering vector(s) that are most orthogonal to the noise subspace. For the far field model this leads to

$$\theta_{est} = \max_{\theta} \frac{1}{\mathbf{a}(\theta)^H \mathbf{E}_n \mathbf{E}_n^H \mathbf{a}(\theta)} \tag{A.7}$$

The Euclidean distance between two vectors is zero if they are orthogonal. Calculating the squared Euclidean distance $\mathbf{a}(\theta)^H \mathbf{E}_n \mathbf{E}_n^H \mathbf{a}(\theta)$ for a range of angles gives a small outcome when the steering vector $a(\theta)$ is orthogonal to the noise subspace. The MUSIC pseudospectrum is defined as the inverse of this search, see Equation A.7, giving large, sharp (theoretically infinitively high) peaks for steering vectors orthogonal to the noise subspace.

To estimate not only the angle but also the range, the steering vector is changed to $\mathbf{a}(\theta, r)$, based on the near field model described in Section 5.3. A two dimensional search is then used to estimate the angle and range.

$$(\theta_{est}, r_{est}) = \max_{\theta, r} \left(\frac{1}{\mathbf{a}(\theta, r)^H \mathbf{E}_n \mathbf{E}_n^H \mathbf{a}(\theta, r)} \right) \tag{A.8}$$

In Figure A.1 the resulting pseudospectrum of a 2D MUSIC algorithm is shown with a peak in the center of the figure indicating the estimated range and angle of the simulated tag at angle 0° and range 0.5 m.

B

(2D) ESPRIT

As said in Chapter 5, the ESPRIT algorithm is based on the signal subspace $\mathbf{E_s}$, also described in Appendix A. In a noiseless case with a single signal, the signal subspace would be equal to the matrix **A** with a single steering vector. However, with multiple signals it is only known that the rank between the signal matrix **A** and signal subspace $\mathbf{E_s}$ is equal. Therefore, there exists a matrix **T** in such a way that $\mathbf{E_s} = \mathbf{AT}$. A second, displaced, array results in a second signal subspace, $\mathbf{E_{s2}}$, which adds an additional term which contains the phase shift due to the displacement between the arrays, Φ.

$$\begin{bmatrix} \mathbf{E_{s1}} \\ \mathbf{E_{s2}} \end{bmatrix} = \begin{bmatrix} \mathbf{AT} \\ \mathbf{A\Phi T} \end{bmatrix} \tag{B.1}$$

These two equations can be used to derive an expression for Φ. Based on Φ, the final angle estimates can be derived[76].

The ESPRIT algorithm is known to be more computationally efficient than the MUSIC algorithm. However, the ESPRIT algorithm is easily affected by distortions in the received signal[69] [76].

2D ESPRIT

A two-dimensional version has been developed by the authors of [22]. The 2D ESPRIT algorithm makes use of cumulants to derive a third relation, $\mathbf{E_{s3}}$, which describes the extra phase shift due to range, observed by a third array. The signal model described in Equation 5.2 is approximated by a second order model and changed into:

$$X_m(t) = \sum_{i=1}^{N} s_i(t) * e^{j[\phi_i m + \omega_i m^2]} + n_m(t) \tag{B.2}$$

whereby

$$\phi_i = -2 \cdot \frac{d}{\lambda} \sin(\theta_i), \qquad \omega_i = \pi \frac{d^2}{\lambda r_i} \cos^2(\theta_i) \tag{B.3}$$

Based on three displaced sub-arrays, leading to three signal subspaces, the algorithm is able to estimate range and angle.

$$\begin{bmatrix} \mathbf{E_{s1}} \\ \mathbf{E_{s2}} \\ \mathbf{E_{s3}} \end{bmatrix} = \begin{bmatrix} \mathbf{AT} \\ \mathbf{A\Phi T} \\ \mathbf{A\Omega T} \end{bmatrix} \tag{B.4}$$

First $\mathbf{E_{s1}}$ and $\mathbf{E_{s2}}$ are used to estimate Φ and thus the angles, θ_i. Furthermore, it is possible to use $\mathbf{E_{s1}}$ and $\mathbf{E_{s3}}$ to derive Ω. With the help of the previously estimated angles it is then possible to derive a range estimate, r_i.

Acronyms

A	ADC	Analog-to-Digital Converter
	ASIC	Application Specific Integrated Circuit
	AWGN	Additive White Gaussian Noise
B	BER	Bit Error Rate
	BLF	Backscatter Link Frequency
	BPSK	Binary Phase Shift Keying
C	COTS	Commercial Off-The-Shelf
	CRC	Cyclic Redundancy Check
D	DC	Direct Current
	DOA	Direction of Arrival
	DSP	Digital Signal Processor
	DSSS	Direct Sequence Spread Spectrum
E	EPC	Electronic Product Code
	ERP	Effective Radiated Power
	ETSI	European Telecommunications Standards Institute
F	FB	Fractional Bandwidth
	FCC	Federal Communications Commission
	FHSS	Frequency-Hopping Spread Spectrum
	FMCW	Frequency-Modulated Continuous-Wave
	FPGA	Field-Programmable Gate Array
G	GPS	Global Positioning System
H	HF	High Frequency
I	IC	Integrated Circuit
	IFF	Identification Friend or Foe
	IR	Infrared
K	KNN	*k*-Nearest Neighbors
L	LF	Low Frequency
	LNA	Low Noise Amplifier
M	MAC	Medium Access Control
	MAE	Mean Absolute Error
	MMS	Miller-Modulated Subcarrier

P	PIE	Pulse-Interval-Encoded
	PW	Pulsewidth
R	RF	Radio Frequency
	RFID	Radio Frequency Identification
	RMSE	Root-Mean-Square-Error
	RSSI	Received Signal Strength Indicator
	RTLS	Real-Time Location System
S	SAR	Synthetic Aperture Radar
	SNR	Signal-to-Noise Ratio
T	Tari	Type A Reference Interval
U	UHF	Ultra High Frequency
	ULA	Uniform Linear Array
	UWB	Ultra-WideBand
V	VNA	Vector Network Analyzer

Bibliography

[1] Atlas RFID store. https://www.atlasrfidstore.com/tageos-eos-110-r6-rfid-paper-tag-monza-r6/. Accessed: 2016-07-20. (Cited on page 2).

[2] *RFID Systems: Research Trends and Challenges*. John Wiley & Sons, Ltd, 2010. ISBN 9780470665251. doi: 10.1002/9780470665251. (Cited on page 47).

[3] Agentschap Telecom. Frequentieregister. URL http://nfr.agentschaptelecom.nl/. Accessed: 2016-05-17. (Cited on pages 10 and 26).

[4] F. Ali, A. Urban, and M. Vossiek. A High Resolution 2D Omnidirectional Synthetic Aperture Radar Scanner at K Band . In *2010 European Radar Conference (EuRAD)*, pages 503–506, Sept 2010. (Cited on page 29).

[5] B. Allen and M. Ghavami. *Adaptive Array Systems, Fundamentals and Applications*. John Wiley & Sons, 2005. (Cited on pages 13 and 60).

[6] D. Arnitz, U. Muehlmann, T. Gigl, and K. Witrisal. Wideband System-Level Simulator for Passive UHF RFID. In *2009 IEEE International Conference on RFID*, pages 28–33, April 2009. doi: 10.1109/RFID.2009.4911189. (Cited on page 26).

[7] D. Arnitz, U. Muehlmann, and K. Witrisal. UWB ranging in passive UHF RFID: proof of concept. *Electronics Letters*, 46(20):1401–1402, September 2010. ISSN 0013-5194. doi: 10.1049/el.2010.1703. (Cited on pages 5, 26, and 37).

[8] D. Arnitz, U. Muehlmann, and K. Witrisal. Wideband Characterization of Backscatter Channels: Derivations and Theoretical Background. *IEEE Transactions on Antennas and Propagation*, 60(1):257–266, Jan 2012. ISSN 0018-926X. doi: 10.1109/TAP.2011.2167923. (Cited on page 26).

[9] D. Arnitz, U. Muehlmann, and K. Witrisal. Characterization and Modeling of UHF RFID Channels for Ranging and Localization. *IEEE Transactions on Antennas and Propagation*, 60(5):2491–2501, May 2012. ISSN 0018-926X. doi: 10.1109/TAP.2012.2189705. (Cited on pages 19 and 26).

[10] H. Arthaber, T. Faseth, and F. Galler. Spread-Spectrum Based Ranging of Passive UHF EPC RFID Tags. *IEEE Communications Letters*, 19(10):1734–1737, Oct 2015. ISSN 1089-7798. doi: 10.1109/LCOMM.2015.2469664. (Cited on page 25).

[11] S. Azzouzi, M. Cremer, U. Dettmar, T. Knie, and R. Kronberger. Improved AoA Based Localization of UHF RFID Tags Using Spatial Diversity. In *2011 IEEE International Conference on RFID-Technologies and Applications (RFID-TA)*, pages 174–180, Sept 2011. doi: 10.1109/RFID-TA.2011.6068634. (Cited on pages 5, 28, and 101).

[12] S. Azzouzi, M. Cremer, U. Dettmar, R. Kronberger, and T. Knie. New Measurement Results for the Localization of UHF RFID Transponders Using an Angle of Arrival (AoA) Approach. In *2011 IEEE International Conference on RFID (RFID)*, pages 91–97, April 2011. (Cited on pages 57, 58, 81, and 101).

[13] C. A. Balanis. *Antenna Theory: Analysis and Design*. Newnes, 1997. (Cited on page 59).

[14] M. D. Blech, M. O. Benzinge, and T. F. Eibert. 2-Dimensional Ultra-Wideband Monopulse Based Direction Finding. In *2008 IEEE MTT-S International Microwave Symposium Digest*, pages 1159–1162, June 2008. doi: 10.1109/MWSYM.2008.4633263. (Cited on page 73).

[15] R. W. Bohannon. Comfortable and maximum walking speed of adults aged 20-79 years: reference values and determinants. *Age and Ageing*, 26(1):15–19, 1997. doi: 10.1093/ageing/26.1.15. (Cited on page 47).

[16] M. Bouet and A. L. dos Santos. RFID Tags: Positioning Principles and Localization Techniques. In *2008 1st IFIP Wireless Days*, pages 1–5, Nov 2008. doi: 10.1109/WD.2008.4812905. (Cited on page 33).

[17] L. Bowden. The story of IFF (Identification Friend or Foe). *IEE Proceedings A - Physical Science, Measurement and Instrumentation, Management and Education - Reviews*, 132(6):435–437, October 1985. ISSN 0143-702X. doi: 10.1049/ip-a-1.1985.0079. (Cited on page 3).

[18] W. D. Boyer. A Diplex, Doppler Phase Comparison Radar. *IEEE Transactions on Aerospace and Navigational Electronics*, ANE-10(1):27–33, March 1963. ISSN 0096-1957. doi: 10.1109/TANE.1963.4502075. (Cited on page 23).

[19] A. Buffi and P. Nepa. A phase-based technique for discriminating tagged items moving through a UHF-RFID gate. In *2014 IEEE RFID Technology and Applications Conference (RFID-TA)*, pages 155–158, Sept 2014. doi: 10.1109/RFID-TA.2014.6934219. (Cited on page 24).

[20] A. Buffi, P. Nepa, and F. Lombardini. A Phase-Based Technique for Localization of UHF-RFID Tags Moving on a Conveyor Belt: Performance Analysis and Test-Case Measurements. *IEEE Sensors Journal*, 15(1):387–396, Jan 2015. ISSN 1530-437X. doi: 10.1109/JSEN.2014.2344713. (Cited on pages 24 and 28).

[21] M. Burmester, B. de Medeiros, J. Munilla, and A. Peinado. Secure EPC Gen2 Compliant Radio Frequency Identification. In P. M. Ruiz and J. J. Garcia-Luna-Aceves, editors, *Ad-Hoc, Mobile and Wireless Networks: 8th International Conference, ADHOC-NOW 2009, Murcia, Spain, September 22-25, 2009 Proceedings*, pages 227–240, Berlin, Heidelberg, 2009. Springer Berlin Heidelberg. ISBN 978-3-642-04383-3. doi: 10.1007/978-3-642-04383-3_17. URL `http://dx.doi.org/10.1007/978-3-642-04383-3_17`. (Cited on page 22).

[22] R. Challa and S. Shamsunder. High-Order Subspace-Based Algorithms for Passive Localization of Near-Field Sources. In *Signals, Systems and Computers, 1995. 1995 Conference Record of the Twenty-Ninth Asilomar Conference on*, volume 2, pages 777–781 vol.2, Oct 1995. (Cited on pages 61, 62, 78, and 113).

[23] K. Chawla, G. Robins, and L. Zhang. Object Localization Using RFID. In *2010 5th IEEE International Symposium on Wireless Pervasive Computing (ISWPC)*, pages 301–306, May 2010. doi: 10.1109/ISWPC.2010.5483750. (Cited on page 22).

[24] V. Chawla and D. S. Ha. An Overview of Passive RFID. *IEEE Communications Magazine*, 45(9):11–17, September 2007. ISSN 0163-6804. doi: 10.1109/MCOM.2007.4342873. (Cited on pages 3 and 4).

[25] X. Chen, L. Xie, C. Wang, and S. Lu. Adaptive Accurate Indoor-Localization Using Passive RFID. In *2013 International Conference on Parallel and Distributed Systems (ICPADS)*, pages 249–256, Dec 2013. doi: 10.1109/ICPADS.2013.44. (Cited on pages 5 and 22).

[26] J. S. Choi, H. Lee, R. Elmasri, and D. W. Engels. Localization Systems Using Passive UHF RFID. In *Fifth International Joint Conference on INC, IMS and IDC, 2009. NCM '09.*, pages 1727–1732, Aug 2009. doi: 10.1109/NCM.2009.198. (Cited on pages 30, 44, and 47).

[27] J. S. Choi, H. Lee, D. W. Engels, and R. Elmasri. Passive UHF RFID-Based Localization Using Detection of Tag Interference on Smart Shelf. *IEEE Transactions on Systems, Man, and Cybernetics, Part C (Applications and Reviews)*, 42(2):268–275, March 2012. ISSN 1094-6977. doi: 10.1109/TSMCC.2011.2119312. (Cited on page 47).

[28] M. Cremer, A. Pervez, U. Dettmar, T. Knie, and R. Kronberger. Improved UHF RFID Localization Accuracy Using Circularly Polarized Antennas. In *2014 IEEE RFID Technology and Applications Conference (RFID-TA)*, pages 175–180, Sept 2014. doi: 10.1109/RFID-TA.2014.6934223. (Cited on page 28).

[29] M. Cremer, A. Pervez, U. Dettmar, C. Hudasch, T. Knie, R. Kronberger, and R. Lerche. Transmit Beamforming for Angle-of-Activation (AoAct) Estimation in Passive UHF RFID Systems. In *2015 IEEE International Conference on RFID Technology and Applications (RFID-TA)*, pages 1–7, Sept 2015. doi: 10.1109/RFID-TA.2015.7379790. (Cited on page 28).

[30] T. Deyle, H. Nguyen, M. Reynolds, and C. C. Kemp. RF Vision: RFID Receive Signal Strength Indicator (RSSI) Images for Sensor Fusion and Mobile Manipulation. In *2009 IEEE/RSJ International Conference on Intelligent Robots and Systems*, pages 5553–5560, Oct 2009. doi: 10.1109/IROS.2009.5354047. (Cited on pages 22 and 23).

[31] D. M. Dobkin. *The RF in RFID: Passive UHF RFID in Practice*. Newnes, 2008. (Cited on pages 18 and 60).

[32] Electromagnetic compatibility and Radio spectrum Matters (ERM); Radio Frequency Identification Equipment operating in the band 865 MHz to 868 MHz with power levels up to 2 W; Part 1: Technical requirements and methods of measurement. V1.4.1. Standard, 2011. (Cited on pages 11 and 17).

[33] M. Fantuzzi, D. Masotti, and A. Costanzo. A Novel Integrated UWB UHF One-Port Antenna for Localization and Energy Harvesting. *IEEE Transactions on Antennas and Propagation*, 63(9):3839–3848, Sept 2015. ISSN 0018-926X. doi: 10.1109/TAP.2015.2452969. (Cited on page 26).

[34] M. U. Farooq, M. Asif, S. W. Nabi, and M. A. Qureshi. Optimal Adjustment Parameters for EPC Global RFID Anti-collision Q-Algorithm in Different Traffic Scenarios. In *2012 10th International Conference on Frontiers of Information Technology (FIT)*, pages 302–305, Dec 2012. doi: 10.1109/FIT.2012.61. (Cited on page 14).

[35] T. Faseth, M. Winkler, H. Arthaber, and G. Magerl. The Influence of Multipath Propagation on Phase-Based Narrowband Positioning Principles in UHF RFID. In *2011 IEEE-APS Topical Conference on Antennas and Propagation in Wireless Communications (APWC)*, pages 1144–1147, Sept 2011. doi: 10.1109/APWC.2011.6046829. (Cited on page 37).

[36] C. Floerkemeier and S. Sarma. An Overview of RFID System Interfaces and Reader Protocols. In *2008 IEEE International Conference on RFID*, pages 232–240, April 2008. doi: 10.1109/RFID.2008.4519372. (Cited on page 4).

[37] F. Galler, T. Faseth, and H. Arthaber. SDR based EPC UHF RFID Reader DS-SS Localization Testbed . In *2015 IEEE 16th Annual Wireless and Microwave Technology Conference (WAMICON)*, pages 1–4, April 2015. doi: 10.1109/WAMICON.2015.7120382. (Cited on page 25).

[38] J. D. Griffin and G. D. Durgin. Complete Link Budgets for Backscatter-Radio and RFID Systems. *IEEE Antennas and Propagation Magazine*, 51(2):11–25, April 2009. ISSN 1045-9243. doi: 10.1109/MAP.2009.5162013. (Cited on page 19).

[39] C. Gwinn. Correlation Statistics of Quantized Noiselike Signals. *Publications of the Astronomical Society of the Pacific*, 116(815):84, 2004. URL `http://stacks.iop.org/1538-3873/116/i=815/a=84`. (Cited on page 92).

[40] J. Han, Y. Zhao, Y. S. Cheng, T. L. Wong, and C. H. Wong. Improving Accuracy for 3D RFID Localization. *International Journal of Distributed Sensor Networks*, 2012, 2012. doi: 10.1155/2012/865184. (Cited on page 30).

[41] S. Haykin. *Digital Communication Systems*. John Wiley & Sons, 2014. (Cited on pages 13, 58, 87, and 91).

[42] G. Hislop and C. Craeye. Spatial smoothing for 2D direction finding with passive RFID tags. In *Antennas Propagation Conference, 2009. LAPC 2009. Loughborough*, pages 701–704, Nov 2009. doi: 10.1109/LAPC.2009.5352444. (Cited on pages 28 and 58).

[43] G. Hislop, D. Lekime, M. Drouguet, and C. Craeye. A prototype 2D direction finding system with passive RFID tags. In *Proceedings of the Fourth European Conference on Antennas and Propagation*, pages 1–5, April 2010. (Cited on pages 28 and 73).

[44] Y.-D. Huang and M. Barkat. Near-Field Multiple Source Localization by Passive Sensor Array. *IEEE Transactions on Antennas and Propagation*, 39(7):968–975, Jul 1991. ISSN 0018-926X. (Cited on page 61).

[45] *Monza 3 Tag Chip Datasheet*. Impinj, 6 2010. Rev. 3.0. (Cited on page 14).

[46] *Monza 6 Tag Chip Datasheet*. Impinj, 12 2014. Rev. 3.0. (Cited on page 19).

[47] *Electrical, Mechanical & Thermal Specification*. Impinj, 7 2015. Rev. 2.0. (Cited on pages 17, 22, 39, and 68).

[48] ISO/IEC 18000-6C (EPCglobal Class-1 Gen-2). version 1.0.9. Standard, 2004. (Cited on page 10).

[49] J.-S. Jiang and M. A. Ingram. Robust Detection of Number of Sources Using the Transformed Rotational Matrix. In *2004 IEEE Wireless Communications and Networking Conference (IEEE Cat. No.04TH8733)*, volume 1, pages 501–506 Vol.1, March 2004. doi: 10.1109/WCNC.2004.1311595. (Cited on page 110).

[50] L. M. Kaplan, Q. Le, and N. Molnar. Maximum likelihood methods for bearings-only target localization. In *2001 IEEE International Conference on Acoustics, Speech, and Signal Processing. Proceedings (Cat. No.01CH37221)*, volume 5, pages 3001–3004 vol.5, 2001. doi: 10.1109/ICASSP.2001.940281. (Cited on page 101).

[51] M. Khan and V. Antiwal. Location Estimation Technique using Extended 3-D LANDMARC Algorithm for Passive RFID Tag. In *IEEE International Advance Computing Conference*, pages 249 –253, march 2009. doi: 10.1109/IADCC.2009.4809016. (Cited on page 30).

[52] M. Kim and N. Y. Chong. Direction Sensing RFID Reader for Mobile Robot Navigation. *IEEE Transactions on Automation Science and Engineering*, 6(1):44–54, Jan 2009. ISSN 1545-5955. doi: 10.1109/TASE.2008.2006858. (Cited on page 23).

[53] N. S. Kodippili and D. Dias. Integration of Fingerprinting and Trilateration Techniques for Improved Indoor Localization. In *2010 Seventh International Conference on Wireless and Optical Communications Networks - (WOCN)*, pages 1–6, Sept 2010. doi: 10.1109/WOCN.2010.5587342. (Cited on page 35).

[54] R. Kronberger, T. Knie, R. Leonardi, U. Dettmar, M. Cremer, and S. Azzouzi. UHF RFID Localization System Based on a Phased Array Antenna. In *2011 IEEE International Symposium on Antennas and Propagation (APSURSI)*, pages 525–528, July 2011. doi: 10.1109/APS.2011.5996761. (Cited on pages 28, 73, and 101).

[55] G. La Scalia, G. Aiello, R. Micale, and M. Enea. Coverage analysis of RFID indoor localization system for refrigerated warehouses based on 2D-ray tracing. *International Journal of RF Technologies*, 3(2):85–99, 2012. doi: 10.3233/RFT-2012-018. (Cited on page 19).

[56] J. Landt. The history of RFID. *IEEE Potentials*, 24(4):8–11, Oct 2005. ISSN 0278-6648. doi: 10.1109/MP.2005.1549751. (Cited on page 4).

[57] G. Li, D. Arnitz, R. Ebelt, U. Muehlmann, K. Witrisal, and M. Vossiek. Bandwidth Dependence of CW Ranging to UHF RFID Tags in Severe Multipath Environments. In *2011 IEEE International Conference on RFID*, pages 19–25, April 2011. doi: 10.1109/RFID.2011.5764631. (Cited on page 25).

[58] Y. Liu and Y. Qiu. An Indoor Localization of UHF RFID Using a hybrid Approach. In *2012 2nd International Conference on Consumer Electronics, Communications and Networks (CECNet)*, pages 1653–1656, April 2012. doi: 10.1109/CECNet.2012.6201426. (Cited on pages 5 and 27).

[59] F. Lombardini, F. Viviani, P. Nepa, and A. Buffi. Robust Coherent Localization of Moving UHF-RFID Tags by a SAR-Like Approach. In *Proceedings of EUSAR 2014; 10th European Conference on Synthetic Aperture Radar*, pages 1–4, June 2014. (Cited on page 29).

[60] Y. Maguire and R. Pappu. An Optimal Q-Algorithm for the ISO 18000-6C RFID Protocol. *IEEE Transactions on Automation Science and Engineering*, 6(1):16–24, Jan 2009. ISSN 1545-5955. doi: 10.1109/TASE.2008.2007266. (Cited on page 14).

[61] J. McFadden. The Correlation Function of a Sine Wave Plus Noise after Extreme Clippings. *IRE Transactions on Information Theory*, 2(2):82–83, June 1956. ISSN 0096-1000. doi: 10.1109/TIT.1956.1056789. (Cited on page 89).

[62] R. Miesen, F. Kirsch, and M. Vossiek. Holographic Localization of Passive UHF RFID Transponders. In *2011 IEEE International Conference on RFID*, pages 32–37, April 2011. doi: 10.1109/RFID.2011.5764633. (Cited on page 29).

[63] R. Miesen, F. Kirsch, and M. Vossiek. UHF RFID Localization Based on Synthetic Apertures. *IEEE Transactions on Automation Science and Engineering*, 10(3):807–815, July 2013. ISSN 1545-5955. doi: 10.1109/TASE.2012.2224656. (Cited on page 29).

[64] L. M. Ni, Y. Liu, Y. C. Lau, and A. P. Patil. LANDMARC: Indoor Location Sensing Using Active RFID. In *Proceedings of the First IEEE International Conference on Pervasive Computing and Communications, 2003. (PerCom 2003)*, pages 407–415, March 2003. doi: 10.1109/PERCOM.2003.1192765. (Cited on pages 29, 33, 34, 37, and 38).

[65] T. Nick, J. Götze, W. John, and G. Stoenner. Localization of UHF RFID labels with reference tags and Unscented Kalman Filter. In *2011 IEEE International Conference on RFID-Technologies and Applications (RFID-TA)*, pages 168–173, Sept 2011. doi: 10.1109/RFID-TA.2011.6068633. (Cited on pages 30 and 47).

[66] P. Nikitin and K. Rao. Antennas and Propagation in UHF RFID Systems. In *2008 IEEE International Conference on RFID*, pages 277–288, April 2008. (Cited on page 62).

[67] P. V. Nikitin, R. Martinez, S. Ramamurthy, H. Leland, G. Spiess, and K. V. S. Rao. Phase Based Spatial Identification of UHF RFID Tags. In *2010 IEEE International Conference on RFID (IEEE RFID 2010)*, pages 102–109, April 2010. doi: 10.1109/RFID.2010.5467253. (Cited on pages 23 and 47).

[68] Z. Nikolić, H. T. Nguyen, and G. Frantz. Design and Implementation of Numerical Linear Algebra Algorithms on Fixed Point DSPs. *EURASIP Journal on Advances in Signal Processing*, 2007(1):087046, 2007. ISSN 1687-6180. doi: 10.1155/2007/87046. URL `http://dx.doi.org/10.1155/2007/87046`. (Cited on page 83).

[69] O. A. Oumar, M. F. Siyau, and T. P. Sattar. Comparison between MUSIC and ESPRIT Direction of Arrival Estimation Algorithms for Wireless Communication Systems. In *The First International Conference on Future Generation Communication Technologies*, pages 99–103, Dec 2012. doi: 10.1109/FGCT.2012.6476563. (Cited on page 113).

[70] A. Parr, R. Miesen, and M. Vossiek. Inverse SAR Approach for Localization of Moving RFID Tags. In *2013 IEEE International Conference on RFID (RFID)*, pages 104–109, April 2013. doi: 10.1109/RFID.2013.6548142. (Cited on page 29).

[71] A. Povalac and J. Sebesta. Phase Difference of Arrival Distance Estimation for RFID Tags in Frequency Domain. In *IEEE International Conference on RFID-Technologies and Applications*, pages 188 –193, sept. 2011. doi: 10.1109/RFID-TA.2011.6068636. (Cited on pages 25, 39, and 44).

[72] J. G. Proakis and D. K. Manolakis. *Digital Signal Processing (4th Edition)*. Prentice-Hall, Inc., Upper Saddle River, NJ, USA, 2006. ISBN 0131873741. (Cited on pages 61, 94, and 109).

[73] B. D. Rao and K. V. S. Hari. Performance analysis of Root-Music. *IEEE Transactions on Acoustics, Speech, and Signal Processing*, 37(12):1939–1949, Dec 1989. ISSN 0096-3518. doi: 10.1109/29.45540. (Cited on page 86).

[74] K. V. S. Rao. An overview of backscattered radio frequency identification system (RFID). In *1999 Asia Pacific Microwave Conference*, volume 3, pages 746–749 vol.3, 1999. doi: 10.1109/APMC.1999.833700. (Cited on page 4).

[75] K. V. S. Rao, P. V. Nikitin, and S. F. Lam. Antenna Design for UHF RFID Tags: A Review and a Practical Application. *IEEE Transactions on Antennas and Propagation*, 53(12):3870–3876, Dec 2005. ISSN 0018-926X. doi: 10.1109/TAP.2005.859919. (Cited on page 17).

[76] R. Roy and T. Kailath. ESPRIT - Estimation of Signal Parameters Via Rotational Invariance Techniques. *IEEE Transactions on Acoustics, Speech and Signal Processing*, 37(7):984–995, Jul 1989. ISSN 0096-3518. (Cited on pages 56, 61, 62, 86, and 113).

[77] S. Sarkka, V. V. Viikari, M. Huusko, and K. Jaakkola. Phase-Based UHF RFID Tracking With Nonlinear Kalman Filtering and Smoothing. *IEEE Sensors Journal*, 12(5): 904–910, May 2012. ISSN 1530-437X. doi: 10.1109/JSEN.2011.2164062. (Cited on pages 30, 35, and 39).

[78] R. Schmidt. Multiple Emitter Location and Signal Parameter Estimation. *IEEE Transactions on Antennas and Propagation*, 34(3):276–280, Mar 1986. ISSN 0018-926X. (Cited on pages 28, 56, 61, 86, 109, and 110).

[79] S. Y. Seidel and T. S. Rappaport. 914 MHz Path Loss Prediction Models for Indoor Wireless Communications in Multifloored Buildings. *IEEE Transactions on Antennas and Propagation*, 40(2):207–217, Feb 1992. ISSN 0018-926X. doi: 10.1109/8.127405. (Cited on page 42).

[80] L. Shangguan, Z. Yang, A. X. Liu, Z. Zhou, and Y. Liu. Relative Localization of RFID Tags using Spatial-Temporal Phase Profiling. In *12th USENIX Symposium on Networked Systems Design and Implementation (NSDI 15)*, pages 251–263, Oakland, CA, 2015. USENIX Association. ISBN 978-1-931971-218. (Cited on page 51).

[81] A. Sheinker, B. Ginzburg, N. Salomonski, L. Frumkis, and B. Z. Kaplan. Localization in 3-D Using Beacons of Low Frequency Magnetic Field. *IEEE Transactions on Instrumentation and Measurement*, 62(12):3194–3201, Dec 2013. ISSN 0018-9456. doi: 10.1109/TIM.2013.2270919. (Cited on page 4).

[82] N. Tayem, C. Attanaayake, and A. Abatan. Range and Bearing Estimation for Near-Field Sources. In *2010 IEEE 72nd Vehicular Technology Conference Fall (VTC 2010-Fall)*, pages 1–5, Sept 2010. (Cited on page 61).

[83] O. Tekdas and V. Isler. Sensor Placement for Triangulation-Based Localization. *IEEE Transactions on Automation Science and Engineering*, 7(3):681–685, July 2010. ISSN 1545-5955. doi: 10.1109/TASE.2009.2037135. (Cited on page 101).

[84] A.-J. van der Veen and G. Leus. *Signal Processing for Communications*. Delft University of Technology, 2005. (Cited on page 109).

[85] H. L. Van Trees. *Optimum Array Processing*. John Wiley & Sons, Inc., 2002. ISBN 9780471221104. (Cited on pages 57, 58, 76, 78, and 82).

[86] J. Vongkulbhisal and Y. Zhao. An RFID-Based Indoor Localization System Using Antenna Beam Scanning. In *2012 9th International Conference on Electrical Engineering/Electronics, Computer, Telecommunications and Information Technology (ECTI-CON)*, pages 1–4, May 2012. doi: 10.1109/ECTICon.2012.6254175. (Cited on page 27).

[87] N. P. Waweru, D. B. O. Konditi, and P. K. Langat. Performance Analysis of MUSIC, Root-MUSIC and ESPRIT DOA Estimation Algorithm. *International Journal of Electrical, Computer, Energetic, Electronic and Communication Engineering*, 8(1):209 – 216, 2014. ISSN PISSN:2010-376X, EISSN:2010-3778. URL `http://waset.org/Publications?p=85`. (Cited on page 86).

[88] M. Wegener, D. Froß, M. Rößler, C. Drechsler, C. Pätz, and U. Heinkel. Relative localisation of passive UHF-tags by phase tracking. In *2016 13th International Multi-Conference on Systems, Signals Devices (SSD)*, pages 503–506, March 2016. doi: 10.1109/SSD.2016.7473683. (Cited on page 51).

[89] P. Wilson, D. Prashanth, and H. Aghajan. Utilizing RFID Signaling Scheme for Localization of Stationary Objects and Speed Estimation of Mobile Objects. In *2007 IEEE International Conference on RFID*, pages 94–99, March 2007. doi: 10.1109/RFID.2007.346155. (Cited on page 33).

[90] Y. Zhao, Y. Liu, and L. M. Ni. VIRE: Active RFID-based Localization Using Virtual Reference Elimination. In *2007 International Conference on Parallel Processing (ICPP 2007)*, pages 56–56, Sept 2007. doi: 10.1109/ICPP.2007.84. (Cited on page 30).

[91] C. Zhou and J. D. Griffin. Accurate Phase-Based Ranging Measurements for Backscatter RFID Tags. *IEEE Antennas and Wireless Propagation Letters*, 11:152–155, 2012. ISSN 1536-1225. doi: 10.1109/LAWP.2012.2186110. (Cited on pages 5, 23, and 37).

List of Publications

[JH:1] J. Huiting, H. Flisijn, A. B. J. Kokkeler, and G. J. M. Smit. Exploiting phase measurements of EPC Gen2 RFID tags. In *2013 IEEE International Conference onRFID-Technologies and Applications (RFID-TA)*, pages 1–6, Sept 2013. doi: 10.1109/RFID-TA.2013.6694503.

[JH:2] J. Huiting, A. B. J. Kokkeler, and G. J. M. Smit. Near field phased array DOA and range estimation of UHF RFID tags. In *RFID Technology (EURFID), 2015 International EURASIP Workshop on*, pages 103–107, Oct 2015. doi: 10.1109/EURFID.2015.7332393. (Best paper award).

[JH:3] J. Huiting, A. B. J. Kokkeler, and G. J. M. Smit. The effects of single bit quantization on direction of arrival estimation of UHF RFID tags. In *2016 IEEE International Conference on RFID-Technologies and Applications (RFID-TA)*, pages 55–60, Sept 2016. doi: 10.1109/RFID-TA.2016.7750731. (Best paper award).

This thesis

```
@phdthesis{huiting2017:thesis,
    author={Huiting, Jordy},
    title={Indoor Localization of UHF RFID Tags},
    school={University of Twente},
    address={PO Box 217, 7500 AE  Enschede, The Netherlands},
    year={2017},
    month=jun,
    day={30},
    number={CTIT Ph.D. Thesis Series No. 16-412},
    issn={1381-3617},
    isbn={978-90-365-4250-0},
    doi={10.3990/1.9789036542500}
}
```

BibTeX of this thesis

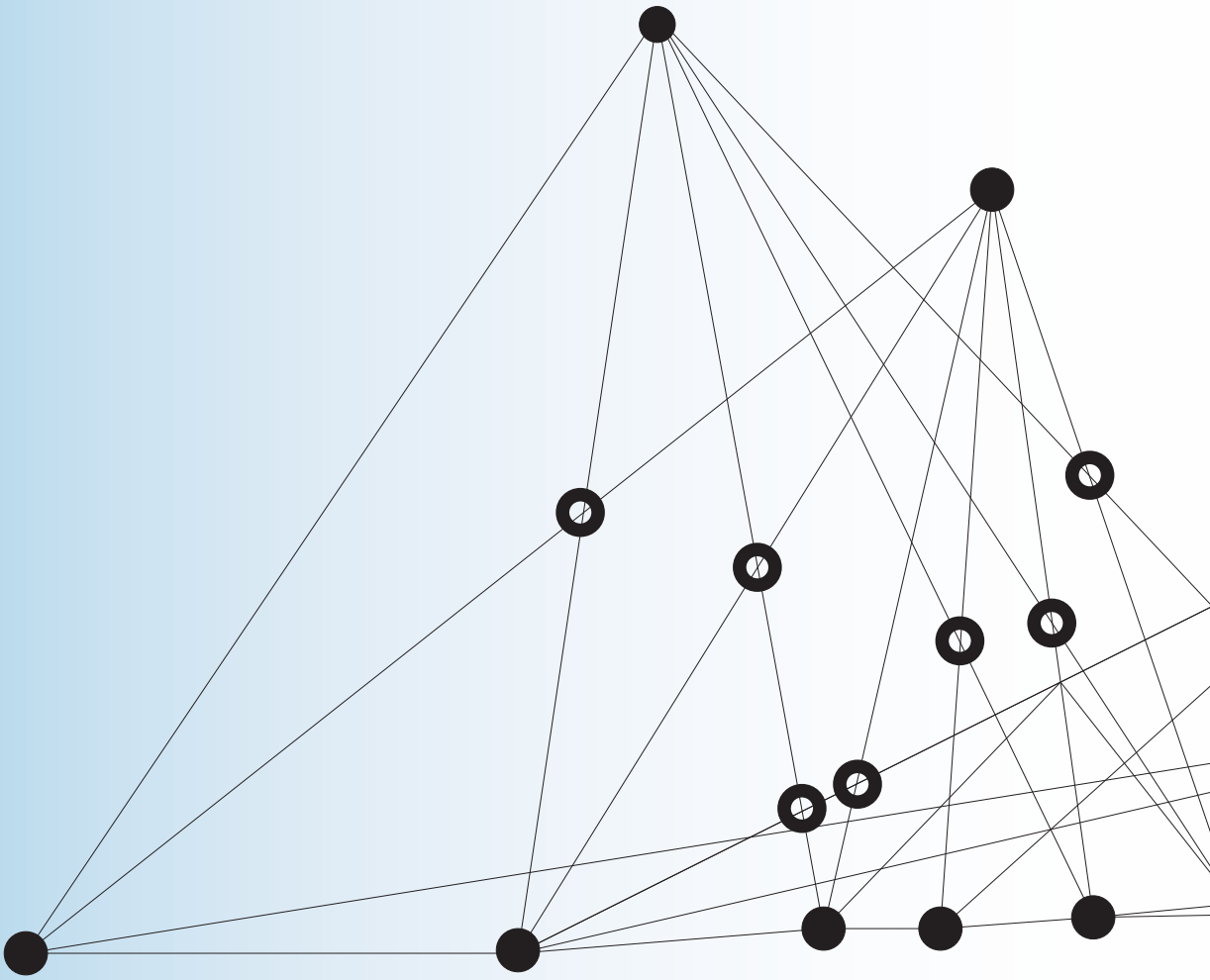

ISBN 978-90-365-4250-0

Stellingen

behorende bij het proefschrift

Indoor Localization of UHF RFID Tags

door Jordy Huiting,
te verdedigen op vrijdag 30 juni 2017

1 — De huidige passieve UHF RFID tags zijn nooit bedoeld voor lokalisatie en zullen een lokalisatiesysteem met beperkte nauwkeurigheid opleveren. *(Dit proefschrift)*

2 — In het nabije veld van een antenne array speelt het hoekafhankelijke fasegedrag van de antennes een rol, echter antenne ontwikkelaars houden hier geen rekening mee. *(Hoofdstuk 5)*

3 — De extra afwijking die geintroduceerd wordt in de hoekschatting door gebruik van de sterk gekwantiseerde signalen staat niet in verhouding tot de kosten om de afwijking te voorkomen. *(Hoofdstuk 6)*

4 — Goedkope en simpele antenne arrays kunnen gebruikt worden om vanuit meerdere posities hoekschattingen te doen. Op deze manier kunnen fouten in de uiteindelijke lokalisatie worden uitgemiddeld. *(Hoofdstuk 6)*

5 — Zelflerende algoritmes leveren commercieel werkbare resultaten op, maar leiden niet tot wetenschappelijke inzichten in de onderliggende mechanismen.

6 — De populariteit van de vrij te gebruiken 860 MHz ISM band gaat de komende jaren voor capaciteitsproblemen zorgen.

7 — De kwaliteit van een conferentie valt niet af te leiden uit de naam van de organiserende partij.

8 — In de wetenschap worden experimenten erg gewaardeerd, behalve wanneer de resultaten tegenvallen.

9 — De computer ondersteunt het denkproces van studenten, maar stimuleert het echter niet.

10 — Van boven opgelegde maatregelen in het wetenschappelijk onderwijs bedoeld om doorstroom van studenten te bevorderen, leiden tot slimme innovaties in het beoordelen van studenten door docenten om de doorstroom daadwerkelijk te bevorderen.